EXECUTIVE SUMMARY

Badlands Bombing Range, South Dakota

ESTCP Project MM-0210

JULY 2007

Approved for public release; distribution unlimited.

Environmental Security Technology
Certification Program

Report Documentation Page

Form Approved
OMB No. 0704-0188

1. REPORT DATE	2. REPORT TYPE	3. DATES COVERED
01 JUL 2007	**N/A**	**-**

4. TITLE AND SUBTITLE	5a. CONTRACT NUMBER
Badlands Bombing Range, South Dakota	5b. GRANT NUMBER
	5c. PROGRAM ELEMENT NUMBER
6. AUTHOR(S)	5d. PROJECT NUMBER
	5e. TASK NUMBER
	5f. WORK UNIT NUMBER
7. PERFORMING ORGANIZATION NAME(S) AND ADDRESS(ES) **Science Applications International Corporation 120 Quade Dr. Cary, NC 27513**	8. PERFORMING ORGANIZATION REPORT NUMBER
9. SPONSORING/MONITORING AGENCY NAME(S) AND ADDRESS(ES)	10. SPONSOR/MONITOR'S ACRONYM(S)
	11. SPONSOR/MONITOR'S REPORT NUMBER(S)

12. DISTRIBUTION/AVAILABILITY STATEMENT
Approved for public release, distribution unlimited

13. SUPPLEMENTARY NOTES
The original document contains color images.

14. ABSTRACT

15. SUBJECT TERMS

16. SECURITY CLASSIFICATION OF:			17. LIMITATION OF ABSTRACT	18. NUMBER OF PAGES	19a. NAME OF RESPONSIBLE PERSON
a. REPORT	b. ABSTRACT	c. THIS PAGE			
unclassified	**unclassified**	**unclassified**	**UU**	**97**	

Table of Contents

Lists of Figures

Lists of Tables

Acknowledgements

Contributors to this demonstration include SAIC (formerly AETC Incorporated) and Duke University under funding from the Environmental Security Technology Certification Program Office.

Abstract

The objective of this demonstration was to compare the discrimination potential of three dynamic surveys among themselves and with static grid data over common targets at the CT-3A Bombing target, Former Badlands Bombing Range, South Dakota. This demonstration leveraged an ordnance and explosive removal action funded by the Corps of Engineers, whose objective was to remove all items larger than a 40mm projectile. We analyzed data from part of the bombing target with the goal of identifying particular targets of interest that could be discriminated from the plethora of munitions debris that is present at this locale. Recovered targets of interest were unfortunately few in number, but include (i) four 20mm projectiles, (ii) six 2.25inch aluminum sub-caliber aircraft rocket warheads, and (iii) one ferrous 2.75inch folding-fin aircraft rocket warhead.

Data from multiple geophysical systems were analyzed using UX-Analyze. The data sets include (i) electromagnetic survey data acquired using a man-portable litter configuration and a vehicle-towed array, (ii) electromagnetic data acquired in a grid over individual targets, and (iii) magnetic data acquired using a man-portable two-sensor system. UX-Analyze provides the necessary infrastructure to systematically identify and extract anomalies from the dataset, execute the characterization routines, and perform target classification. It is integrated into Oasis montaj™, a commercial data processing and visualization software suite. The inversion routines within UX-Analyze assume a dipolar source and derive the best set of induced dipole model parameters that account for the spatial variation of the signal as the sensor is moved over the object.

Discriminating the 20mm projectiles and 2.25inch aluminum warheads from the plethora of munitions debris responses based on their inverted shape parameters proved challenging. Even though the litter-based EMI sensor was carried along transects spaced 0.5m apart, many signatures were spatially limited and observed on only a single profile. Additionally, as measured by the dynamic survey platforms, the anomalies could not be well represented by a dipole model. The mean fit error is 33% (standard deviation of 27.3) for the litter-carried data and 30% (standard deviation of 17.5) for the towed array data. We anticipated that the limited spatial views of individual targets, small spatial footprint, and low-amplitude signatures hindered the EMI characterization routines' ability to estimate accurate size, shape, and depth estimates.

In stark comparison to the litter-carried and towed-array EMI data, the gridded EMI data acquired in a cued fashion was well represented by a dipole model. For commonly selected targets, the mean dipole fit error was 5% for the cued system compared to ≥23% for the dynamic surveys. Additionally, with the exception of one horizontal 37mm buried at 30cm, the inverted shape parameters for symmetric targets in the geophysical prove out appear symmetric.

Although the target population is, as a rule, too small to be properly characterized by inverting individual signatures as measured by a dynamic platform, a significant number of the munitions debris items can be screened by setting appropriate thresholds if specific goals are established for the site. Ninety seven percent of the anomalies, for example, possess peak responses that are less than 0.8 times that of the 2.75inch ferrous warhead. Approximately thirty percent of the

anomalies possess amplitudes that are less than 0.5 times that measured for the 2.25inch aluminum warheads. Using a less conservative threshold of 0.8 times that of the 2.25inch warhead, we find that sixty percent of the anomalies could be classified as too small.

Badlands Bombing Range, South Dakota

1. Introduction

1.1 Background

The objective of this ESTCP project is to further feature-based discrimination approaches through demonstrations at live sites and by embedding analysis routines into a commercial software package for use by others. Major tasks include (i) transitioning target characterization and classification algorithms for magnetic and electromagnetic data to a commercial product, and (ii) establishing the efficacy and cost effectiveness of the decision-making approach through demonstrations at sites with varying site conditions and survey goals.

Feature-based characterization and classification schemes have improved discrimination performance in some demonstrations. These algorithms, however, are not readily available to the user community and have had limited exposure to data acquired under 'production-imposed' constraints. This program is designed to address the availability problem as well as further test the ability to improve decisions using features - or model parameters - derived from field data.

Our technical approach promotes the selection of potential UXO targets using quantitative evaluation criteria and transparent decision-making processes. As such, we developed an analysis framework within Oasis montaj™ and embedded previously developed analysis algorithms. The analysis algorithms provide quantitative evaluation criteria; namely, target characterization followed by statistical classification. Transparency is achieved by leveraging the professional, flexible, and visual computing environment inherent in Oasis montaj™, a commercial geophysical data processing and visualization package.

This demonstration leveraged an ongoing OE removal action at the Badlands Bombing Range (BBR) in order to evaluate the merits of using quantitative, physics-based decision criteria encoded in UX-Analyze™ for the purpose of anomaly discrimination. Documented ordnance items found at the site include 20mm projectiles, 2.25 inch rockets, 2.75 inch rockets, 40mm anti-aircraft projectiles, 75mm projectiles, 60mm mortars, incendiary bomblets, 100lb practice bombs and 250lb and 500lb bombs (Parsons, 2004).

1.2 Objectives of the Demonstration

This demonstration has two primary objectives, (i) compare and contrast the discrimination potential of three productions surveys over common targets (two EMI and one magnetic survey), and (ii) investigate effects of data quality on inverted fit results by comparing data acquired in a gridded, cued mode to standard dynamic survey modes.

1.3 Regulatory Drivers

The Senate Report (Report 106-50), pages 291–293, accompanying the *National Defense Authorization Act for Fiscal Year 2000* (Public Law 106-65), included a provision entitled "Research and development to support unexploded ordnance clearance, active range unexploded ordnance clearance, and explosive ordnance disposal." This provision requires the Secretary of Defense to submit to the Congressional defense committees a report that gives a complete estimate of the current and projected costs, to include funding shortfalls, for UXO response at active facilities, installations subject to base realignment and closure (BRAC), and formerly used defense sites (FUDS).

The following statements are taken verbatim out of the DoDs 2001 Report to Congress:

> *"Decades of military training, exercises, and testing of weapons systems has required that we begin to focus our response on the challenges of UXO. Land acreage potentially containing UXO has grown to include active military sites and land transferring or transferred for private use, such as Base Realignment and Closure (BRAC) sites and Formerly Used Defense Sites (FUDS). DoD responsibilities include protecting personnel and the public from explosive safety hazards; UXO site cleanup project management; ensuring compliance with federal, state, and local laws and environmental regulations; assumption of liability; and appropriate interactions with the public.*
>
> *…Through limited experience gained in executing these activities, it has become increasingly clear that the full size and extent of the impact of sites containing UXO is yet to be realized. … DoD has completed an initial baseline estimate for UXO remediation cost. This report provides a UXO response estimate in a range between $106.9 billion and $391 billion in current year [2001] dollars. …Technology discovery, development, and commercialization offers some hope that the cost range can be decreased. …*
>
> *… **Objective**: **Develop standards and protocols** for navigation, geo-location, data acquisition and **processing**, and performance of UXO technologies.*
> - *Standard, high quality archived data are needed for optimal data processing of geophysical data, re-acquisition for response activities, quality assurance, quality control, and review by all stakeholders. In addition standards and protocols are required for evaluating UXO technology performance to aid in selecting the most effective technologies for individual sites.*
> - ***Standard software and visualization tools are needed to provide regulatory and public visibility to and understanding of the analysis and decision process made in response activities**."*

1.4 Stakeholder/End-User Issues

The stakeholders and end-users of this data processing and analysis technology include private contractors that conduct geophysical investigations in support of UXO clean up programs and governmental employees that provide technical oversight. This demonstration introduces the stakeholders and end-users to data products associated with this analysis approach and to the inherent transparency of the decision-making process.

2. Technology Description

2.1 Technology Developments and Application

2.1.1 Data Acquisition System Hardware

Data from four geophysical systems were analyzed. AETC personnel acquired EM61 MkII data using a man-portable litter configuration for the CT-3A bombing target field survey and a cued configuration for individual targets. For the field survey, the sensor were carried in a litter mode and augmented with an inertial navigation unit and RTK DGPS sensors (Figure 1). Magnetic data were acquired using NRLs man-portable magnetic adjunct. This system consists of two cesium-vapor magnetometers mounted on either side of wheeled assemblage. It integrates with RTK DGPS for spatial registration.

Figure 1. Magnetometer (left) and EMI (right) systems.

Cued EM61 MKII data were acquired over twenty individual targets using a 6x5 point rectangle grid (nodes separated by 20.3cm and 40.6cm respectively resulting in a 1.0x1.6 m area). The

grid was elevated 20 cm above the ground, and the EM61 was positioned directly on the grid, without wheels. Sensor location was established by lining up cross hairs on the EM61 bottom coil with grid line intersections (Figure 2).

Figure 2. EM61 sensor during cued data collection.

Parsons also acquired EM61 MkII data using a three-coil towed array. The coils are spaced 0.91m (three feet) apart (Figure 3).

Figure 3. Parsons three-coil EM61 array deployed at the Badlands Bombing Range.

2.1.2 UX-Analyze Software

The anomaly characterization algorithms used here assume a dipolar source and derive the best set of induced dipole model parameters that account for the spatial variation of the signal as the sensor is moved over the object. The model parameters are target X,Y location and depth, three dipole response coefficients corresponding to the principle axes of the target (EMI only), and the three angles that describe the orientation of the target. The size of the target can be estimated using empirical relationships between either the dipole moment for magnetic data or the sum of the targets' response coefficients. Cylindrical objects like most UXO have one large coefficient and two smaller, equal coefficients. Plate-like objects nominally have two large and one small coefficient.

UX-Analyze was developed to facilitate efficient UXO data analysis within the Oasis montaj™ environment. It consists of multiple databases, custom graphical interfaces, and data visualizations. UX-Analyze provides the infrastructure to systematically identify and extract anomalies from the dataset, call the characterization routines, store the fitted source parameters for each anomaly, perform target classification, and document the analysis. Once the analysis is complete, individual images for each anomaly can be automatically produced for documentation purposes.

2.2 Previous Testing of the Technology

We have performed preliminary tests of the Demonstration data analysis and classification technology during algorithm development. A number of the user graphical interfaces and dialogue boxes are briefly described below. Each of these capabilities was tested prior to the demonstration.

2.2.1 UX-Analyze

UX-Analyze allows users to systematically identify, extract, edit, and store data around individual anomalies. It provides efficient data structures and access for the analysis algorithms, stores the fitted parameters, and allows for multiple data types and surveys. This module is the interface between Oasis montaj and the demonstration analysis software (Figure 4).

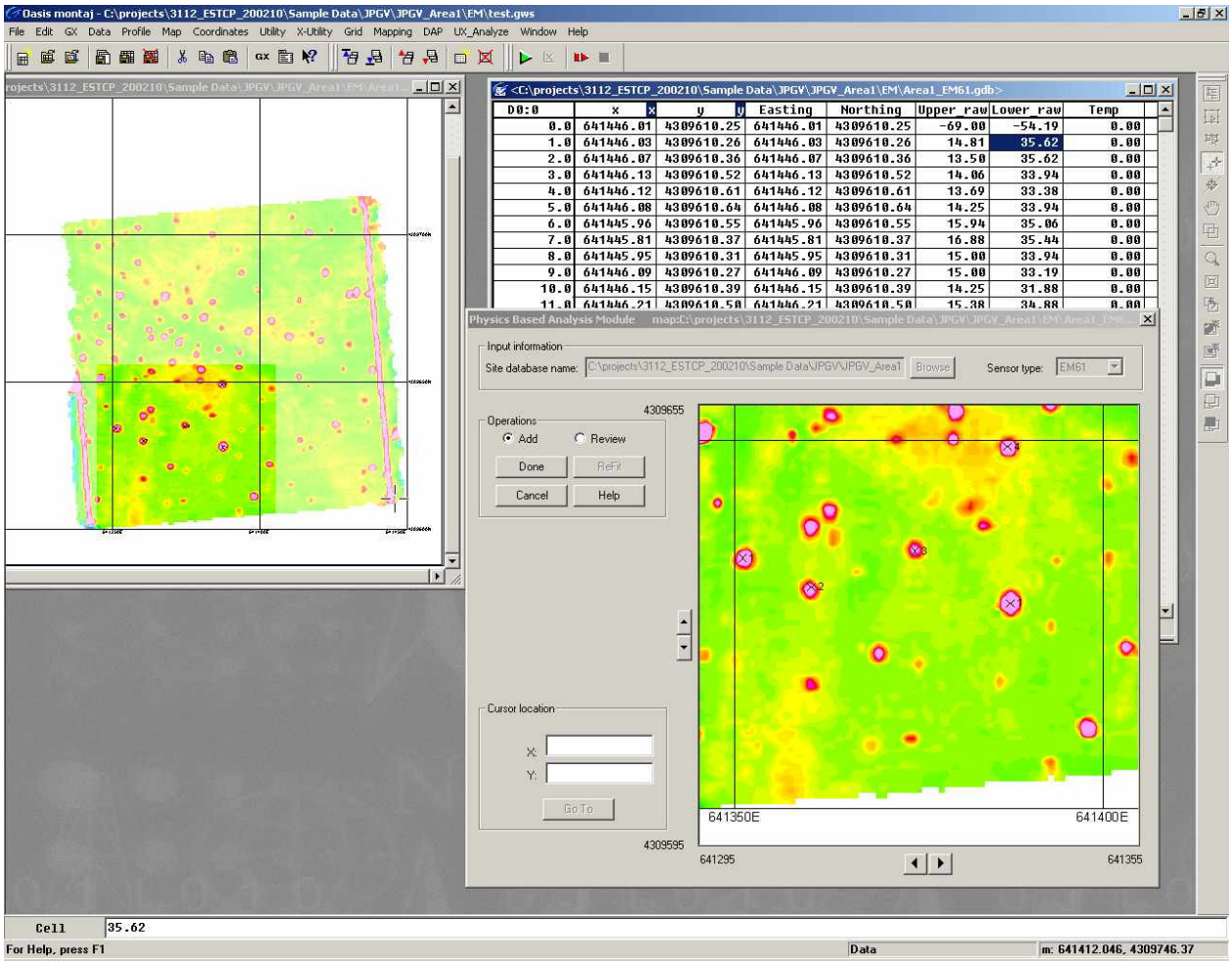

Figure 4. Screen snapshots showing the UX-Analyze interface.

2.2.2 Characterization Modules

Characterization routines for magnetic and EMI data have been integrated with UX-Analyze framework. These 3-D routines include graphic displays and controls that allow the user to manually select, filter, and invert each anomaly individually (Figure 5) or in batch. The derived model parameters are stored in a master target database. The inversion routines were previously developed by AETC Incorporated for the *MTADS* Data Analysis System (DAS) under funding from ESTCP and SERDP (Barrow and Nelson, 1998; ESTCP Report 199526). The MTADS DAS codes were prototyped using the Interactive Development Language (IDL).

Algorithm equivalency tests were conducted to verify that the C-based inversion routines embedded in Oasis montaj produce identical performances as the prototyped IDL formulations. Magnetic and EMI data were synthesized for forty-nine sources that have a unique combination of inclination and declination but constant moment and depth of burial. To ensure that each routine received the exact same input for each anomaly, we extracted data samples around each

anomaly individually once and then used the extracted data subsets as input for both. The data sets were inverted using both codes and compared. No significant differences were observed.

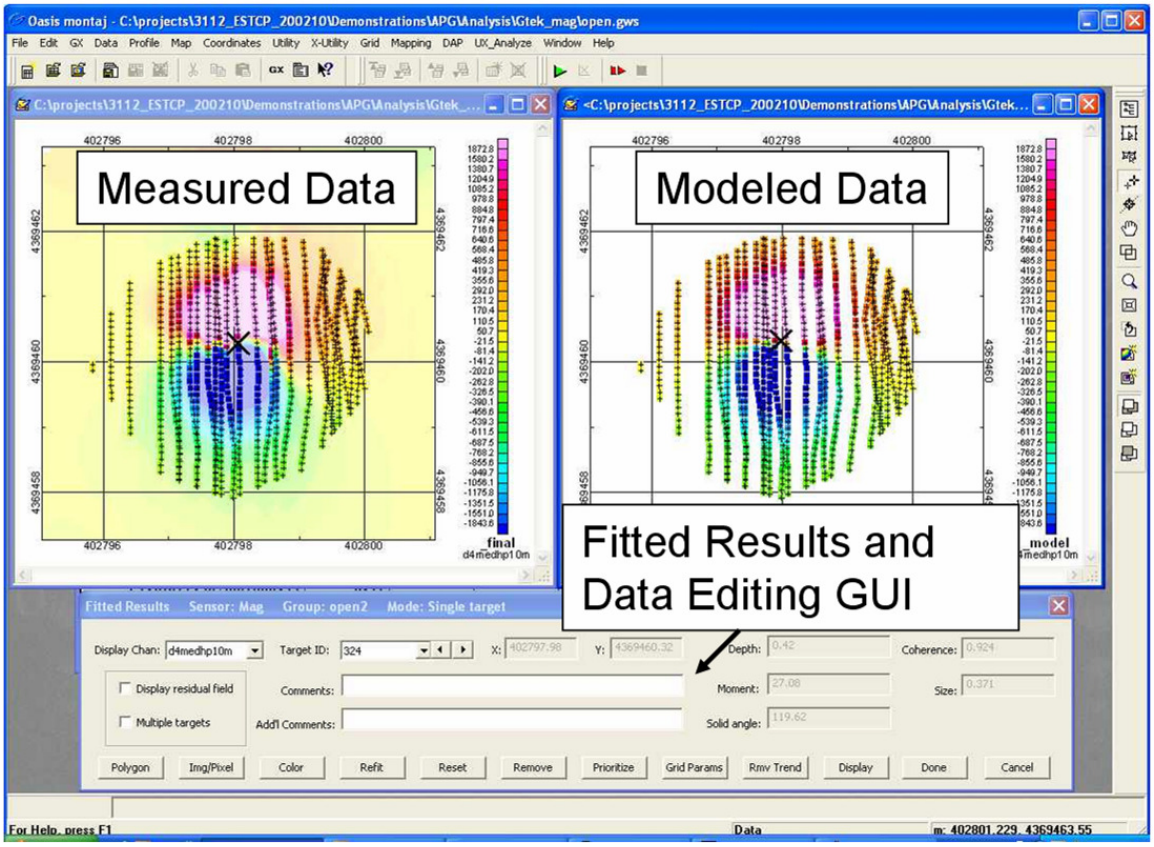

Figure 5. Screen snapshots showing the user interface during data inversion. In this figure, the measured data is shown in the upper left map, the model parameters (fitted results) are displayed in the lower center window, and the forward model generated using the model parameters is shown in the upper right map.

2.2.3 Classification Module

Classifying objects as UXO or non-UXO based on inverted target features is challenging due to imperfect, non-unique feature estimates and potentially non-separable feature classes. The imperfect and non-unique feature estimates result largely from distortions in the spatial distribution of the anomaly. The distortions in turn are commonly caused by (i) errors in the spatial registration of the measured data samples, and/or (ii) nearby geologic or environmental signatures not associated with the source in question. As a result, separating the fitted parameters into distinct and disparate classes is non-trivial. For this demonstration, we utilized the generalized likelihood ratio test (GLRT) - a statistical classification method that has proved promising during the recent past (Figure 6).

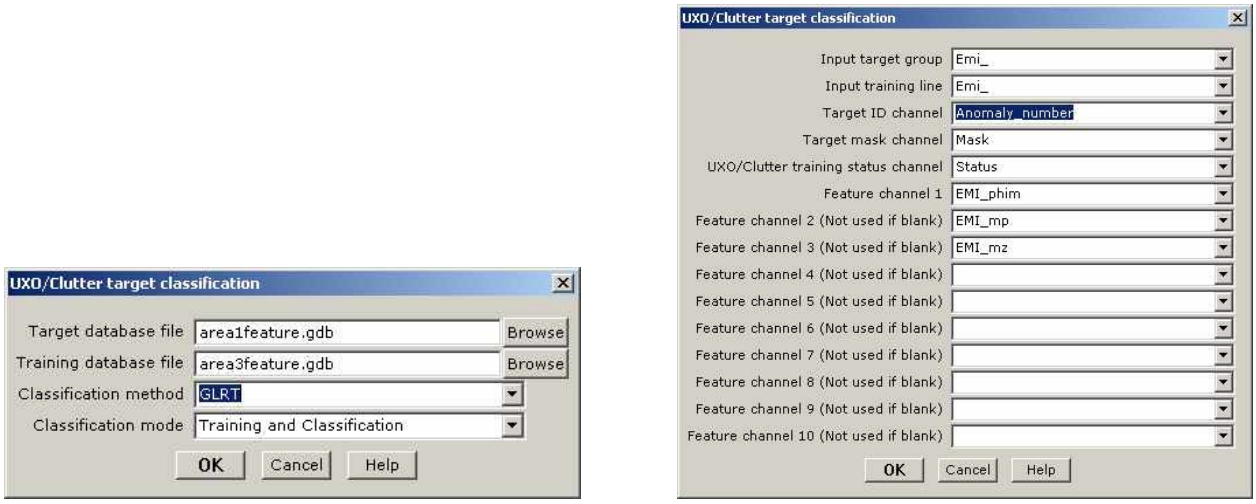

Figure 6. Screen snapshots showing the user dialogue interfaces that call the classification routines.

2.2.4 Data Analysis Documentation

UX-Analyze produces individualized anomaly reports, one for each anomaly, to document the decision process for each anomaly (Figure 7). In each plot, the measured data is graphically displayed next to the modeled data. The model parameters are listed in the middle of each page, and a profile extracted along the transect that passes closest to the dipoles location – as estimated by the inversion routine – is located at the bottom. The positions of individual measurements are superimposed on the maps.

Essentially, the anomaly plots graphically provide an intuitive confidence measure. If the measured and modeled data are indistinguishable, the reviewer can have confidence that the estimated source parameters are approximately correct. If the two maps are do not resemble each other, however, it tells us that the source in question (i) cannot be represented well using a point dipole source, (ii) is not isolated, (iii) does not have sufficient signal-to-noise ratio, or (iv) was not properly sampled (spatially or temporally). In any case, if the two maps are dissimilar the inverted model parameters are most likely not correct.

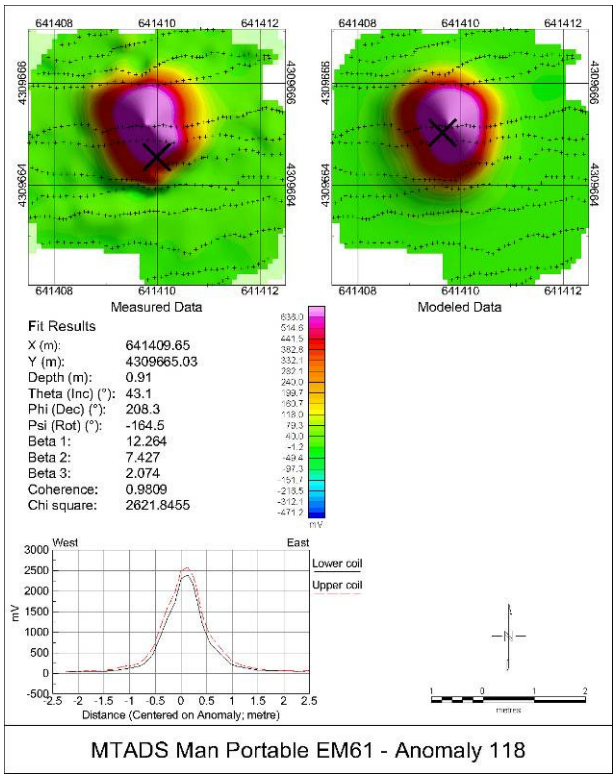

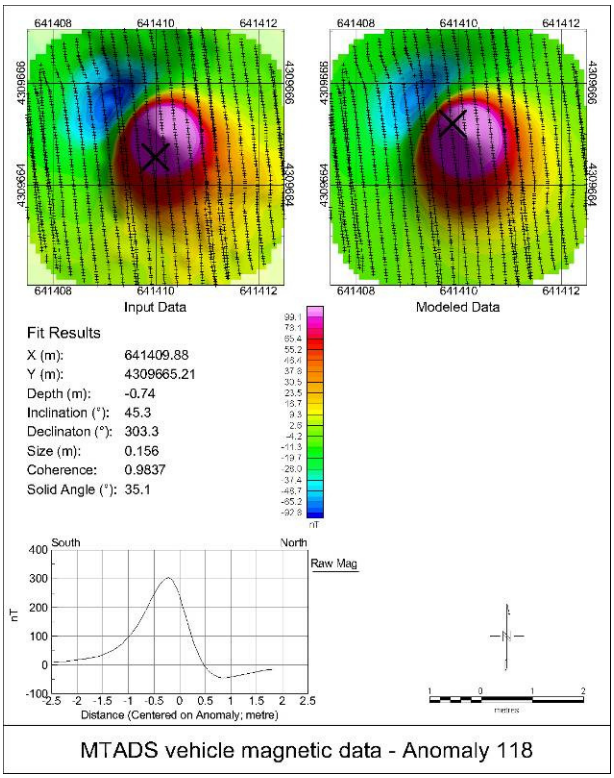

Figure 7. To document the analysis, UX-Analyze generates a one-page summary for each anomaly. In the anomaly summaries shown above, the measured data is shown in the upper left hand corner, the inverted model parameters in the middle left, the forward model in the upper rights, and a profile in the lower left corner. This layout was selected to provide insight into the confidence of the analysis and conclusions. EMI data for the anomaly are shown in the left summary, and magnetic data on the right.

2.3 Factors Affecting Cost and Performance

The analysis approach adopted here utilizes the spatial distribution of the measured magnetic or EMI signatures. As such, it requires high signal-to-noise data that possess a high degree of spatial precision across the footprint of the anomaly. The costs to acquire data that will support discrimination decisions are higher than that required if the goal is only to detect the presence of an object. The analysis costs are also higher if attempts are made to quantitatively discriminate relative than only to detect.

The factors affecting acquisition costs relate to particulars of the sensing system, spatial registration system, the target objectives, and the site environment. Although these costs are not the focus of this demonstration, they are very important to the ultimate transferability of this approach.

The factors affecting analysis time include are significantly affected by (i) the degree to which the anomalies are spatially separated, (ii) the number of anomalies, and (iii) the amount of geologic-related signatures that possess similar wavelengths as the targeted signatures. The data density is also a factor, but only marginally so compared to the factors listed above.

Discrimination performance is measured by our ability to characterize and classify one object from another. The factors that affect performance, therefore, relate to the similarity (in feature space) between the sought-after object versus the clutter, our ability to accurately measure the responses, the presence of signatures that spatially interfere or otherwise compete with the UXOs response, as well as our ability to quantitatively characterize and classify the source objects. Many of these factors are not under our direct control.

2.4 Advantages and Limitations of the Technology

This analysis approach uses spatially referenced geophysical data to estimate target parameters for each anomaly. This has an inherent advantage over ancillary analysis methods that are commonly used. Due to a lack of analysis routines available, many contractors make UXO and non-UXO declarations based on anomaly amplitude, half width, spatial footprint, or overall 'look'. These characterization methods are sensitive to the targets' orientation and depth of burial (or distance from the sensor). The methodology demonstrated here separates the measured signatures into that which is inherent to the target, and that which is related to the geometry of the problem (such as distance to sensor and orientation). The fitted parameters that are inherent to the target itself are used to classify the unknown object.

The primary advantage, therefore, is the potential for discriminating between UXO and non UXO-like objects based upon geophysical survey data. This is in contrast to simply identifying the location of anomalies from the geophysical survey data. Results from past demonstration have shown that that some discrimination is possible using magnetic and electromagnetic data (Robitaille et al., 1999). Magnetic discrimination is based primarily on the apparent fitted dipole size (or scaled dipole moment). Using EMI data, increased discrimination performance can sometimes be achieved by utilizing estimated shape information. If successful discrimination capabilities can be achieved, significant excavation savings can be realized by leaving the non-hazard clutter items unearthed.

This is not to say, however, that the data analysis technology being demonstrated will solve the UXO characterization and classification problems. Even with optimal data quality, the estimated fit parameters cannot always be separated into distinct, non-overlapping classes of UXO and non UXO-like objects. In fact, none of the fit parameters are actually unique to UXO items. Because of this, clutter items that physically resemble UXO will probably be misclassified. Additionally, if the data quality is not optimal the fitted parameters cannot be trusted.

3. Demonstration Design

3.1 Performance Objectives

Table 1. Performance Objectives

Type of Performance Objective	Primary Performance Criteria	Expected Performance (metric)
Qualitative	Ease of use	Minimal training required for data processor experienced in Oasis montaj™
	Robustness	Analysis flow not seriously interrupted by bugs
Quantitative	Analysis time	<5 min/anomaly characterization; 0.5 min/anomaly document
	False Positive Rejection Ratio	0.8
	Location Accuracy	0.3m
	Depth Accuracy	0.3m

3.2 Selecting Test Sites

We selected the Former Badlands Bombing Range because (i) we wanted to leverage the ongoing removal action funded by the Corps of Engineers, (ii) the contractors, Corps, and regulatory personnel conducting the remedial action were cooperative and supportive, and (iii) the site presents a geophysically hospitable environment in terms spatial registration issues because of its wide-open nature and rolling terrain. All in all, the site provided a realistic challenge, has an existing infrastructure, and has willing collaborators conducting the OE removal action.

3.3 Test Site History/Characteristics

The Former Badlands Bombing Range is located within the Oglala Sioux Pine Ridge Reservation, South Dakota and occupies approximately 341,725 acres (Figure 8). Portions of the Badlands National Park lie within the former Badlands Bombing Range.

Ownership and control of land within the boundary of the Former Badlands Bombing Range is highly complex. To simplify, the land is essentially owned by the Oglala Sioux Tribe or individual Native Americans. Some of these lands are leased to local ranchers or commercial farmers. Portions of the Badlands National Park that fall within the boundary of the former Range are owned by the Oglala Sioux Tribe but managed by the National Park Service. Right-of-entry access to land within the boundary of the range is typically through the Oglala Sioux Tribe and/or Bureau of Indian Affairs (BIA). In some instances, access can be granted by individual landowners.

The following site history information was summarized from the Archives Search Report and extracted verbatim from Parson's Final Removal Action Work Plan dated April 2004 (Parsons 2004).

"In 1942, the Rapid City Army Air Field (currently known as Ellsworth Air Base) established a bombing and aerial gunnery range for the purpose of training B-17 combat crews. The land utilized for the range was within the boundaries of the Oglala Sioux Pine Ridge Reservation. The land was acquired by four means: purchase or condemnation of privately owned land, condemnation lease of land owned by the Oglala Sioux Tribe, a revocable permit obtained from the BIA, and special use permit obtained from the National Park Service.

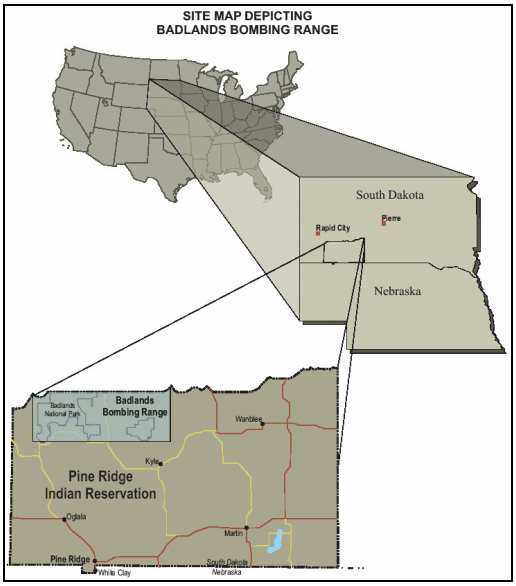

Figure 8. Site map for the Former Badlands Bombing Range.

By 1947, a variety of different aircraft, including B-29 and B-36 bombers, were using the range for bombing practice. In addition, fighter aircraft were using the site for air-to-air gunnery, air-to-ground gunnery, and dive-bombing practice. At this time, radar bombing targets were also located on the site. In 1958, the Air Force stopped using the site for aerial gunnery and bombing, but bombing practice continued using radar scoring. However, the western portion of the site was retained by the regular Army and the South Dakota Army National Guard for use as an impact area and maneuver area between 1954 and 1963.

In 1963, the Air Force declared most of the site as excess, but two parcels of land were retained: one for radar reflector targets and one for a proposed fighter weapons range. As a result of being declared excess, two range clearances were conducted: one in 1963 and another in 1964. The first clearance involved the land leased from the Oglala Sioux Tribe. The second involved the remainder of the land. These clearance actions are thought to have been only surface clearances.

The parcel retained as a fighter weapons range was used as an artillery range by the South Dakota National Guard from about 1960 to 1975. This range had defined impact and buffer areas. The parcel retained for radar reflector targets (commonly referred to as Reflector City) was used primarily for radar bomb scoring. The National Guard also established firing points for artillery within this range, and projectiles were fired into a defined impact area.

Training activities on the site ceased and the artillery range was swept in 1975. The Department of Defense transferred all of the property back to the Oglala Sioux Tribe and the National Park Service, with the exception of the impact area of the artillery range. Ellsworth Air Force Base currently controls the impact area, also known as the High Impact Area.

Known ordnance used on the range includes 100- to 500-pound sand-filled bombs; live 100- to 500-lb bombs; 100-lb magnesium-filled photo-flash bombs; 2.25 inch sub-caliber aircraft rockets; 2.75-in folding-fin aircraft rockets; 20- and 75-millimeter ammunition; .50-caliber ammunition; 3.5-inch anti-tank rockets; and 105-mm and 8-inch howitzer projectiles."

3.4 Present Operations

Parsons is conducting a multi-year OE removal action at the BBR under contract to the USACE-Omaha District. Their objectives are to remove OE in several areas including: existing homesteads/working structures and access roads, 400 and 500-ft buffers around four bombing targets on Cuny Table, and a 500 acre area in the northern part of Cuny Table known as Gallegos table (Figure 9). During the 2005 field season, they acquired and interpreted EM61 MkII data over approximately 80+ acres, using a 3m-wide vehicle-towed array, at the CT-1, CT-3 and CT-3A bombing targets.

This demonstration leverages Parsons' work at the CT-3A bombing target. Removing OE from this target is a multi-year task. The general distribution of targets at the CT-3A target is evident the EM61 MkII data presented in Figure 10. In this figure, the data at the center of the site (within the large black square) were acquired in 2004. This demonstration leveraged two grids, each 61x61m (200x200 feet), directly north of the bulls-eye approximately 240m. Target selection criteria included availability, target density, and degree of overlapping signatures.

The landscape in the vicinity of the bombing target is rolling prairie (Figure 11).

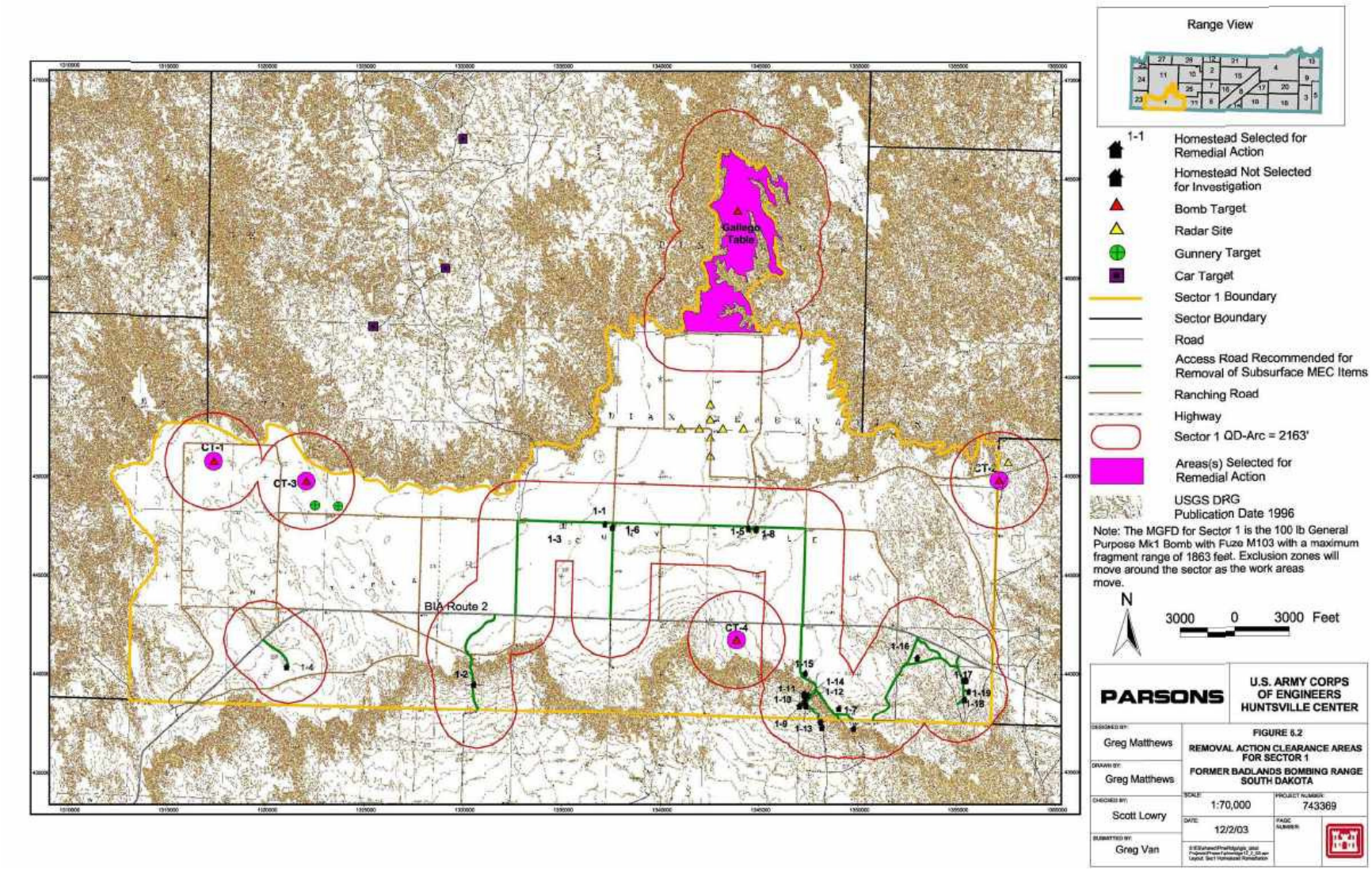

Figure 9. Removal action clearance areas for Sector 1; Former Badlands Bombing Range, South Dakota (Parsons 2004).

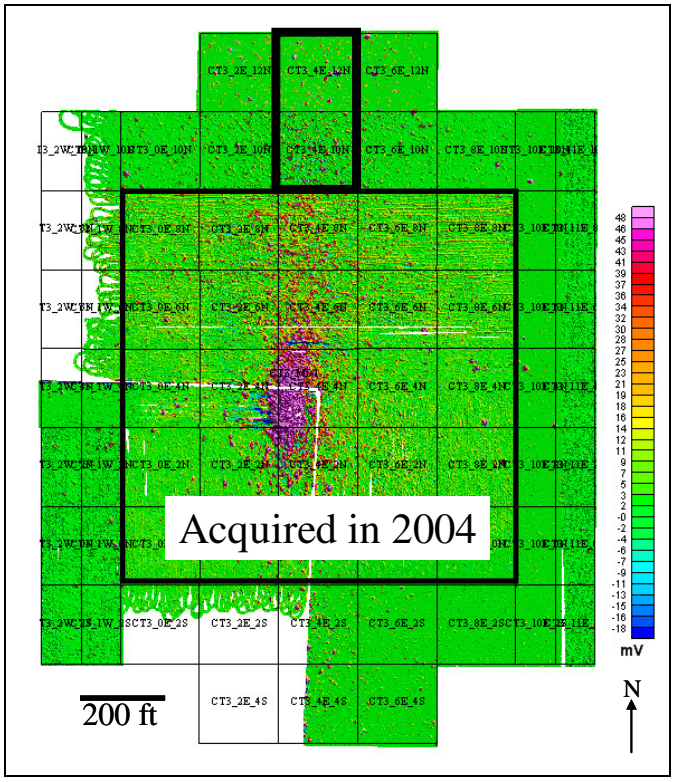

Figure 10. Electromagnetic data acquired at the CT-3A area by Parsons.

Figure 11. Panoramic view of the landscape near CT-3A, BBR.

3.5 Pre-Demonstration Testing and Analysis

Prior to mobilization of the AETC hardware, Parsons acquired EM61 MkII array data over the study area. Parsons processed the data and selected targets.

3.6 Testing and Evaluation Plan

3.6.1 Demonstration Set-up and Start-up

The equipment were packed and shipped to the site via commercial freight during June 2004. Leveraged onsite infrastructure included secure storage sheds, electrical power, base station broadcasts for Differential GPS corrections, and an existing calibration grid. A variety of UXO, large fragments, and construction debris were buried (Figure 12).

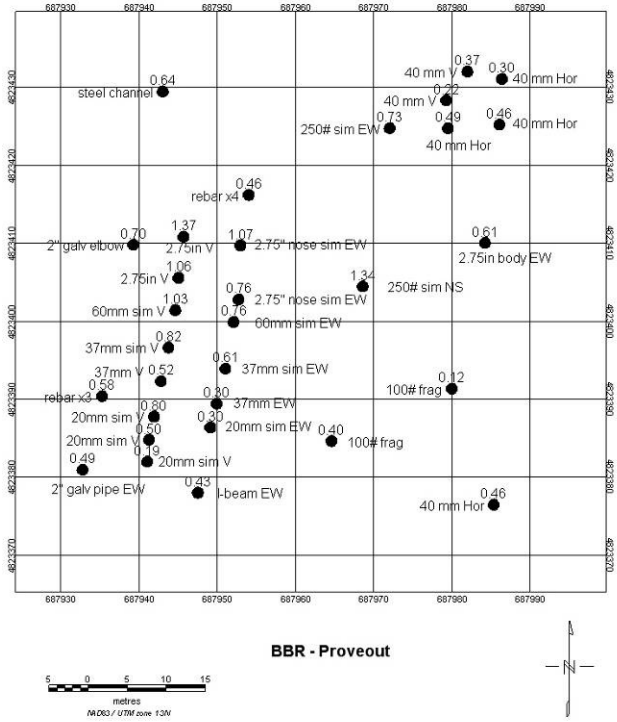

Figure 12. Layout of the BBR geophysical prove out. Burial depth, in meters, is shown above each target symbol.

3.6.2 Period of Operation

Parsons acquired EM data in July 2005. Their data was processed and delivered to AETC late July 2005. The NRL-based magnetometer and EMI systems underwent a shakedown during August 2005. The equipment was packed and shipped via commercial shippers early September. Tom Furuya, AETC Incorporated, and Mark Howard, NAEVA Geophysics mobilized to the site. Magnetic and EMI data were acquired over the calibration area and survey grids during September 12 – 16, 2005. The equipment and field personnel demobilized and left the site September 17th. Preliminary results were presented at the November 2005 and April 2006 In-progress Reviews. A detailed review was presented the ESTCP Office in June 2006.

3.6.3 Area characterized or Remediated

The survey area and prove out grid covered 1.11 hectares (2.75 acres). False-color data images for the geophysical prove out and survey grids are shown in Figure 13 through Figure 15 respectively.

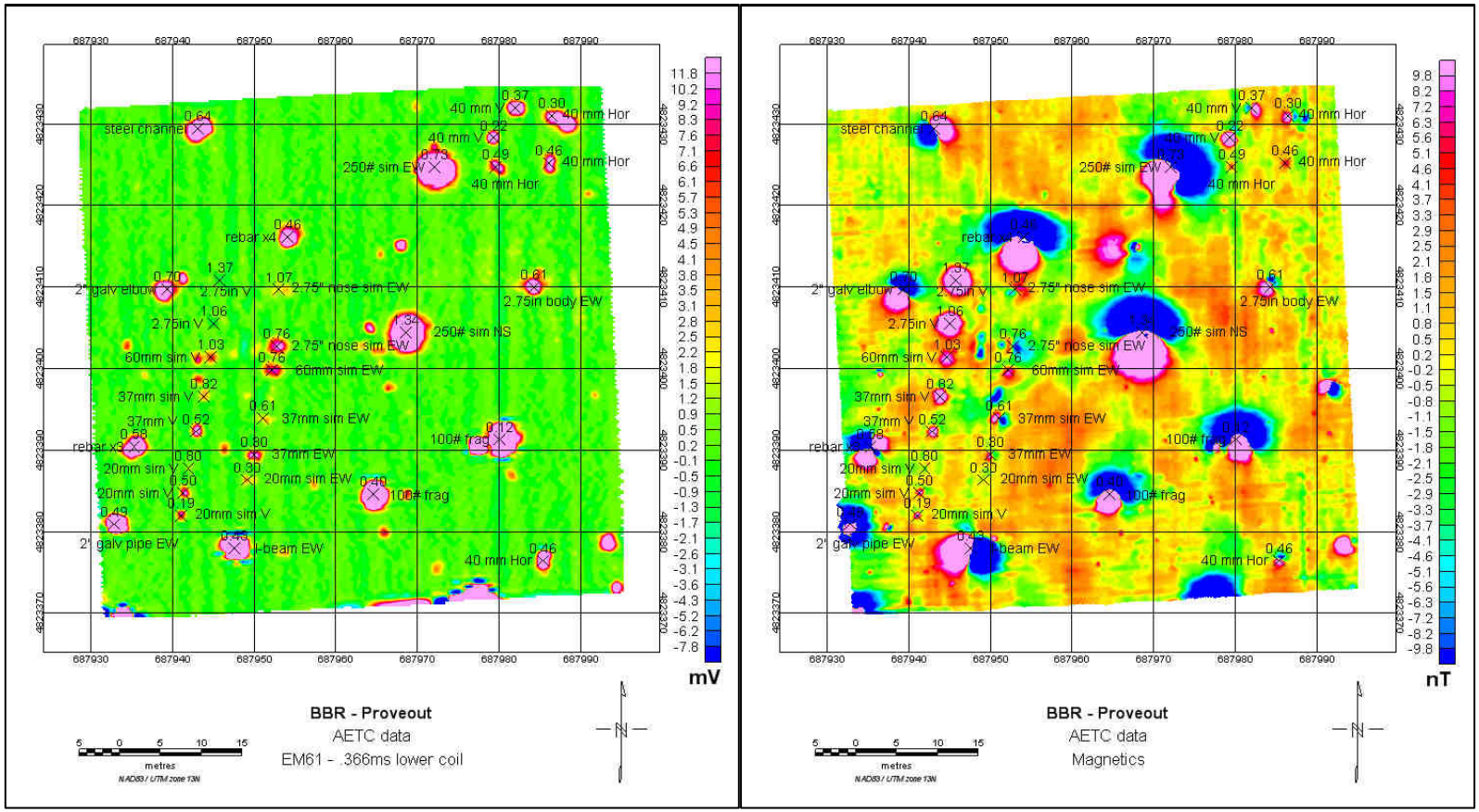

Figure 13. Geophysical data acquired at the BBR prove out grid. The left map shows electromagnetic data and the right displays magnetic signatures.

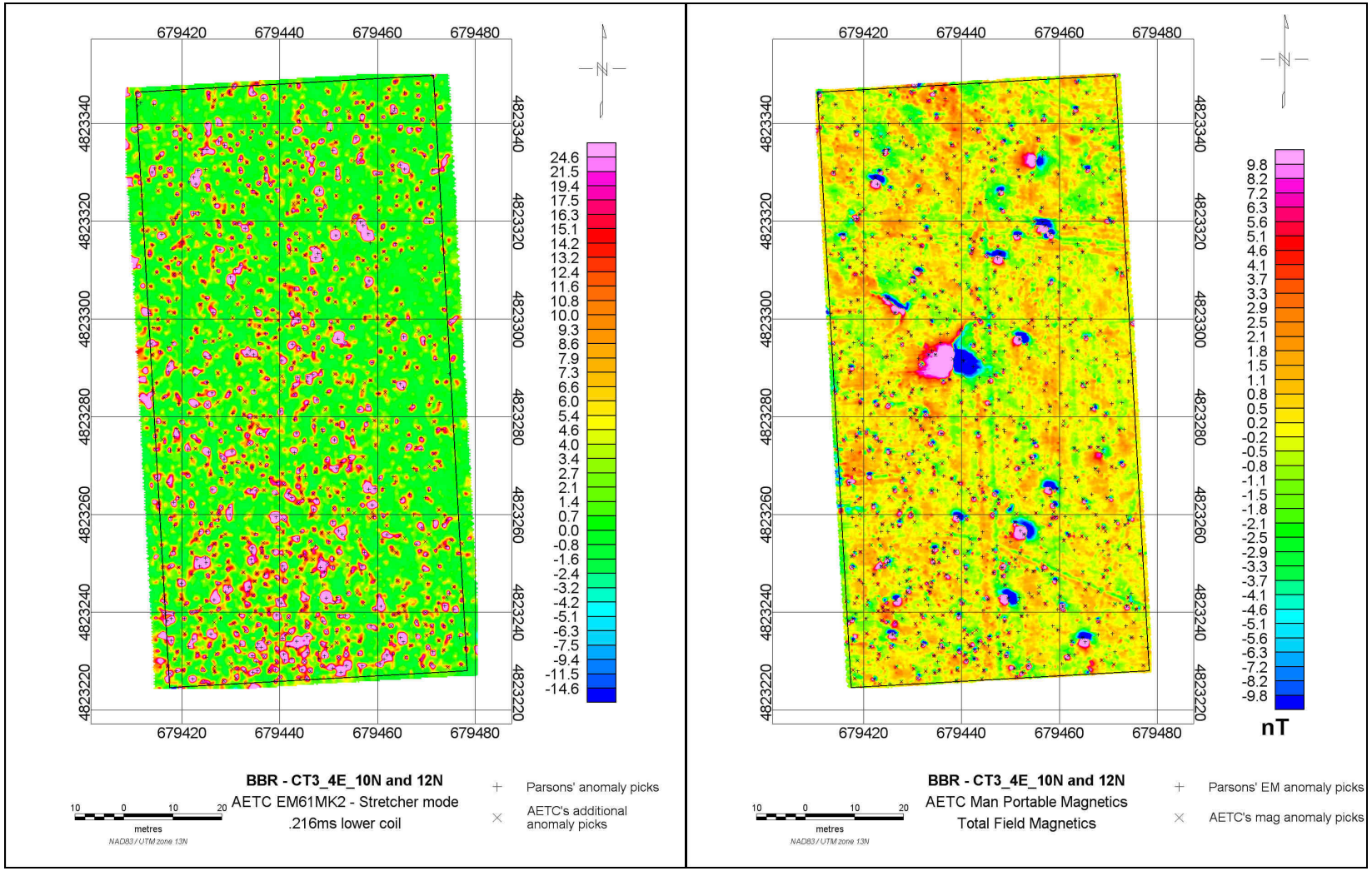

Figure 14. Electromagnetic (left) and magnetic (right) data acquired over two of Parsons 61mx61m (200ft x 200ft) grids.

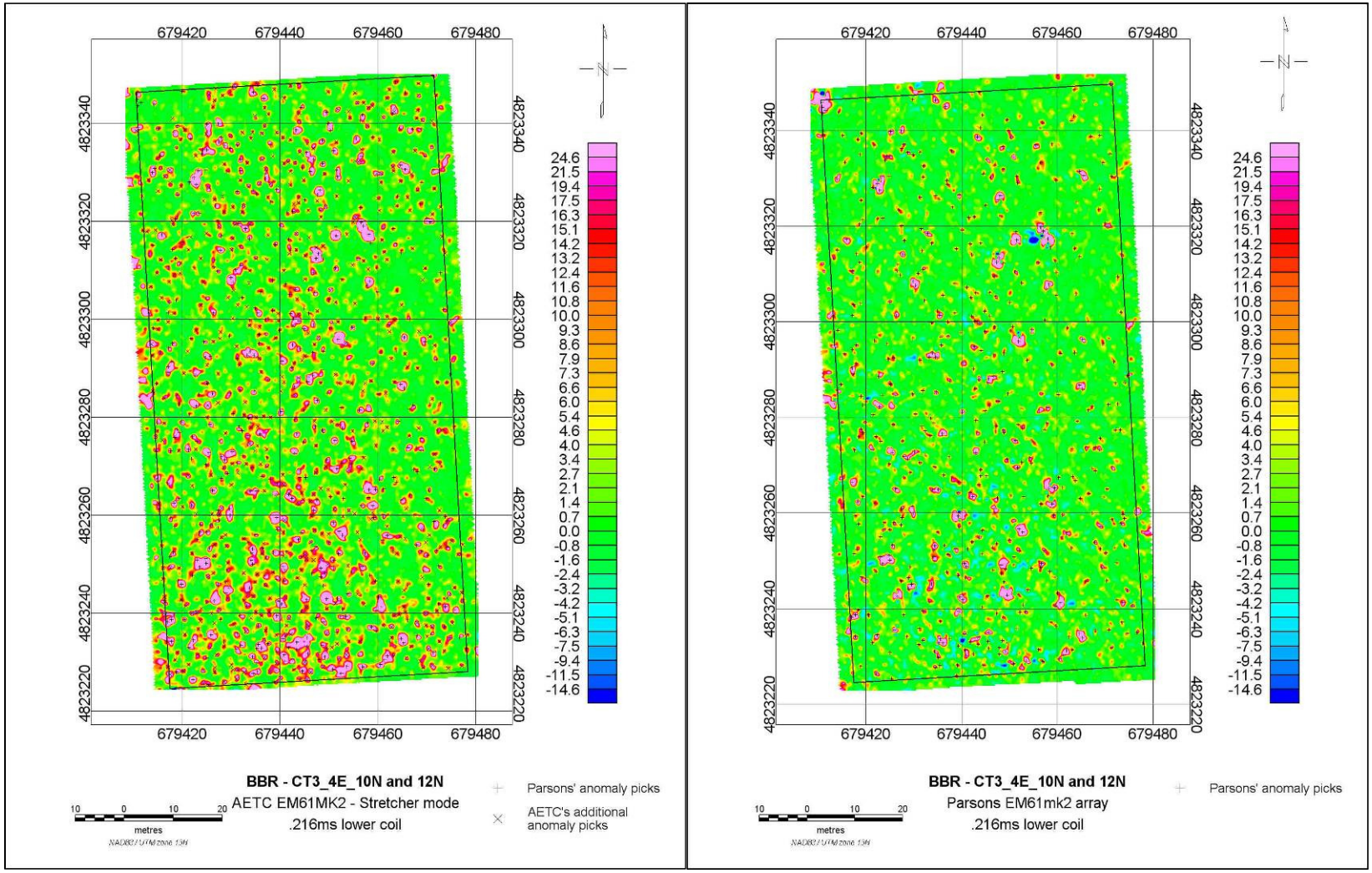

Figure 15. Comparison of EM61 MkII data acquired by the man-portable litter configuration (left) and Parsons' three-coil array (right).

4. Performance Assessment

4.1 Performance Criteria

Table 2. Criteria for this Demonstration

Performance Criterion	Description	Primary or Secondary
Location Accuracy	The nominal radial distance error	Primary
Depth Accuracy	Nominal absolute depth error	Primary
False Positive Rejection Ratio	Fraction of false alarms rejected without loosing a TOI	Primary
Ease of Use	Data analysts' experienced with Oasis montaj should be able to utilize the software without manuals and without hands-on training.	Secondary
Robustness	Analysis not artificially limited by bugs or system design flaws	Secondary
Analysis Time	Times required making a decision for each anomaly and prepare required documentation supporting the decision. .	Secondary

4.2 Performance Confirmation Methods

The 500-plus anomalies identified by Parsons were excavated as part of their removal action (Table 3). This ground truth information, in addition to digital photographs, served as the basis for evaluating the discrimination and classification criterions.

Table 3. Spreadsheet used by Parsons to report Excavation Information

Original Geophysical Survey							Reacquisition		Dig Results							
Grid	AnomalyID	Northing	Easting	Ch 3	Total Ch	units	Response	Offset	DigResults	Nomenclature	Quantity	Completeness	Composition	Depth	Weight	Length
CT3_4E_10N	CT3_4E_10N_001	449536.00	1320080.00	34	195	Mv	38	6	Munitions Debris	RKT, 2.25", Prac, SCAR	1	Warhead	Aluminum	5	2	3
CT3_4E_10N	CT3_4E_10N_002	449537.50	1320083.00	14	127	Mv	19	12	Munitions Debris	RKT, 2.25" Component	1	Scrap Pieces	Ferrous Metal	2	1	5
CT3_4E_10N	CT3_4E_10N_003	449540.75	1320085.00	8	60	Mv	10	6	Munitions Debris	RKT, 2.75" Component	1	Scrap Pieces	Mixed Metals	3	1	5
CT3_4E_10N	CT3_4E_10N_004	449537.00	1320091.63	6	22	Mv	11	0	Munitions Debris	RKT, 2.75" Component	1	Scrap Pieces	Aluminum	2	1	4
CT3_4E_10N	CT3_4E_10N_005	449522.75	1320096.75	18	143	Mv	21	6	Munitions Debris	RKT, 2.75" Component	1	Scrap Pieces	Mixed Metals	3	0.3	5
CT3_4E_10N	CT3_4E_10N_005	449522.75	1320096.75	18	143	Mv	21	6	Munitions Debris	.50 cal Debris	1	Warhead	Mixed Metals	3	0.3	5
CT3_4E_10N	CT3_4E_10N_006	449517.75	1320093.50	6	31	Mv	12	12	Munitions Debris	.50 cal Debris	1	Warhead	Ferrous Metal	4	0.7	3
CT3_4E_10N	CT3_4E_10N_006	449517.75	1320093.50	6	31	Mv	12	12	Munitions Debris	RKT, 2.75" Component	1	Scrap Pieces	Ferrous Metal	4	0.7	3

4.3 Data Analysis, Interpretation, and Evaluation

4.3.1 Geophysical Prove Out (GPO)

The performance of the litter-carried and towed-array EMI surveys of the GPO is summarized in Figure 16. The results are presented as plots of the dipole fit error as a function of signal to noise ratio. Here, dipole fit error is defined as $\varepsilon = \sqrt{1 - r^2}$ x 100, where r^2 is the squared correlation

coefficient between the best model fit and measured anomaly data, and SNR is defined as $100x\ peak\ anomaly\ signal/\mathrm{var}iance(noise)$. The mean dipole fit error for the litter-carried fit results is 22.7 (standard deviation of 20.2) and for the towed array fit results is 34.9 (standard deviation of 23.6).

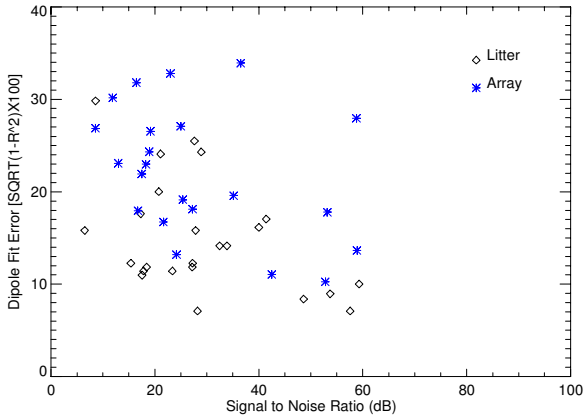

Figure 16. Scatter plot of the SNR versus dipole fit error for Litter-mode EMI data acquired over the geophysical prove out.

Size estimates from the dipole fits are compared with measured UXO diameters for each of the survey modes in Figure 17. The Non-UXO items emplaced within the GPO included rebar, angle iron, cylinders, and pipes. For non-UXO items, we plot estimated size versus width. The statistics are summarized in Table 4. Although there is a bit of scatter for the both dynamic survey modes, the litter mode produced more accurate estimates than the towed array. The cued interrogation produced the most accurate estimates. As expected, we see the accuracy of the size estimates improve as the fit error decreases. Example data for the litter-carried survey data are shown in Figure 18. See Appendix A for additional plots showing fit results for a variety of fit errors.

Depth estimates from the dipole fits area compared with actual target depths for each of the survey modes in Figure 19. At this threshold of fit error (~32%), we observe a fair amount scatter for all survey modes. Because the GPO was put in a number of years ago as part of the ongoing Corps of Engineers cleanup activities, we do not know the accuracy of the ground truth information. The statistics are summarized in Table 4.

Target shape classification based on dipole fits relies on the relationship of eigenvalues of the magnetic polarizabity tensor (here, referred to as betas). We normally order the betas from largest to smallest. Only fits with all three βs > 0 are physically realistic. Spherical targets should have all three betas equal, cylinders $\beta_1 > \beta_2 = \beta_3$, discs $\beta_1 = \beta_2 > \beta_3$ and irregularly shaped objects $\beta_1 > \beta_2 > \beta_3$. Figure 20 shows scatter plots of the beta ratios β_1/β_2 and β_2/β_3 for each of the survey modes. For symmetric objects, we expect that $\beta_2 \approx \beta_3$. This expected pattern is observed for the cued data but not for the two dynamic surveys.

Table 4. Error Statistics for Size and Depth Estimates; GPO; Fit Errors <32%

	Survey Mode	% Mean Error (UXO)	% Mean Error (Non-UXO)
Size Estimate	Array	73	50
	Litter	40	45
	Cued	10	13
Depth Estimate	Array	113	42
	Litter	28	95
	Cued	39	32

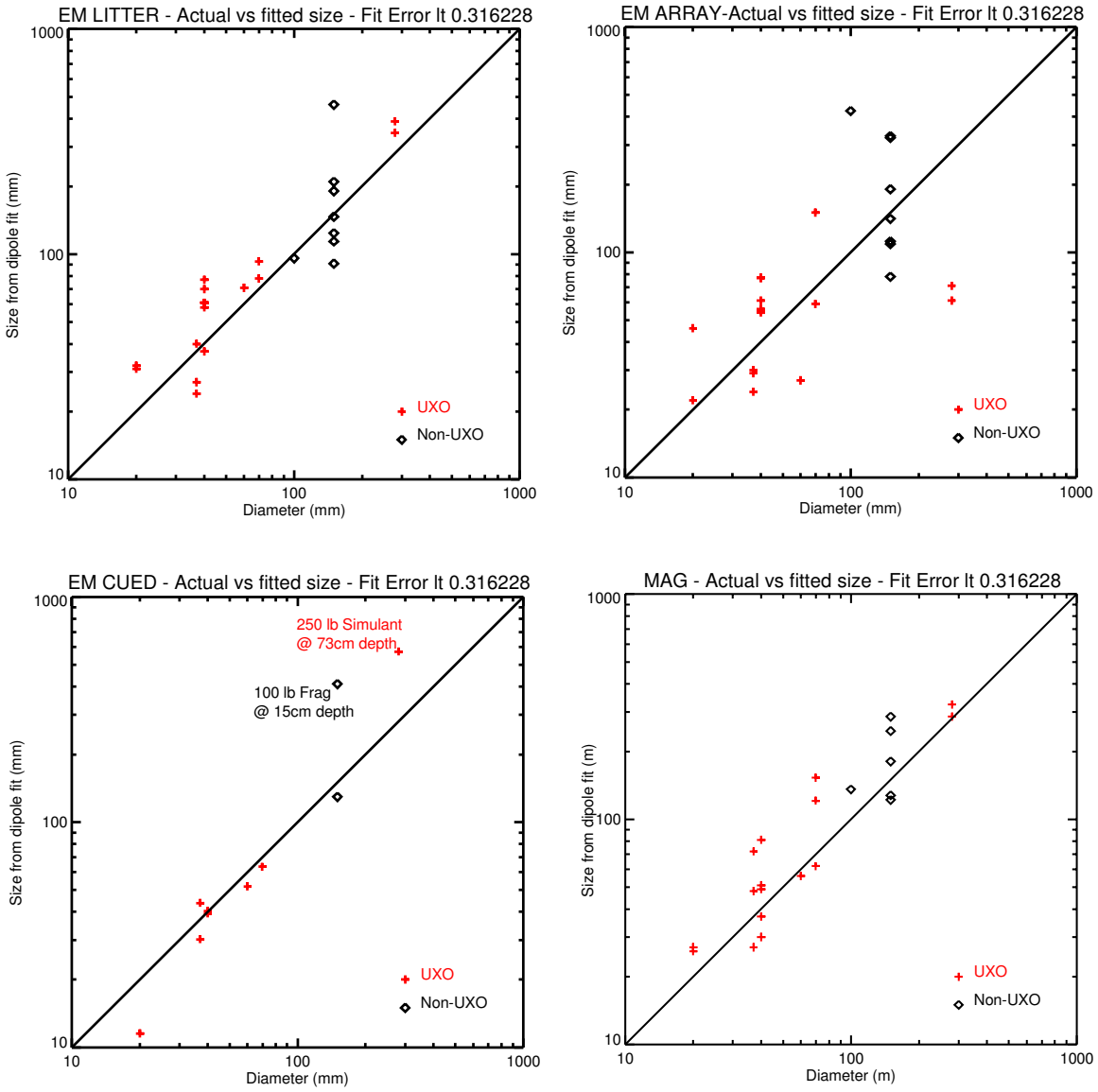

Figure 17. Scatter plot of the diameter versus estimated size for targets in the GPO for each of the survey modes. Targets with fit errors less than ~32% are included in these plots.

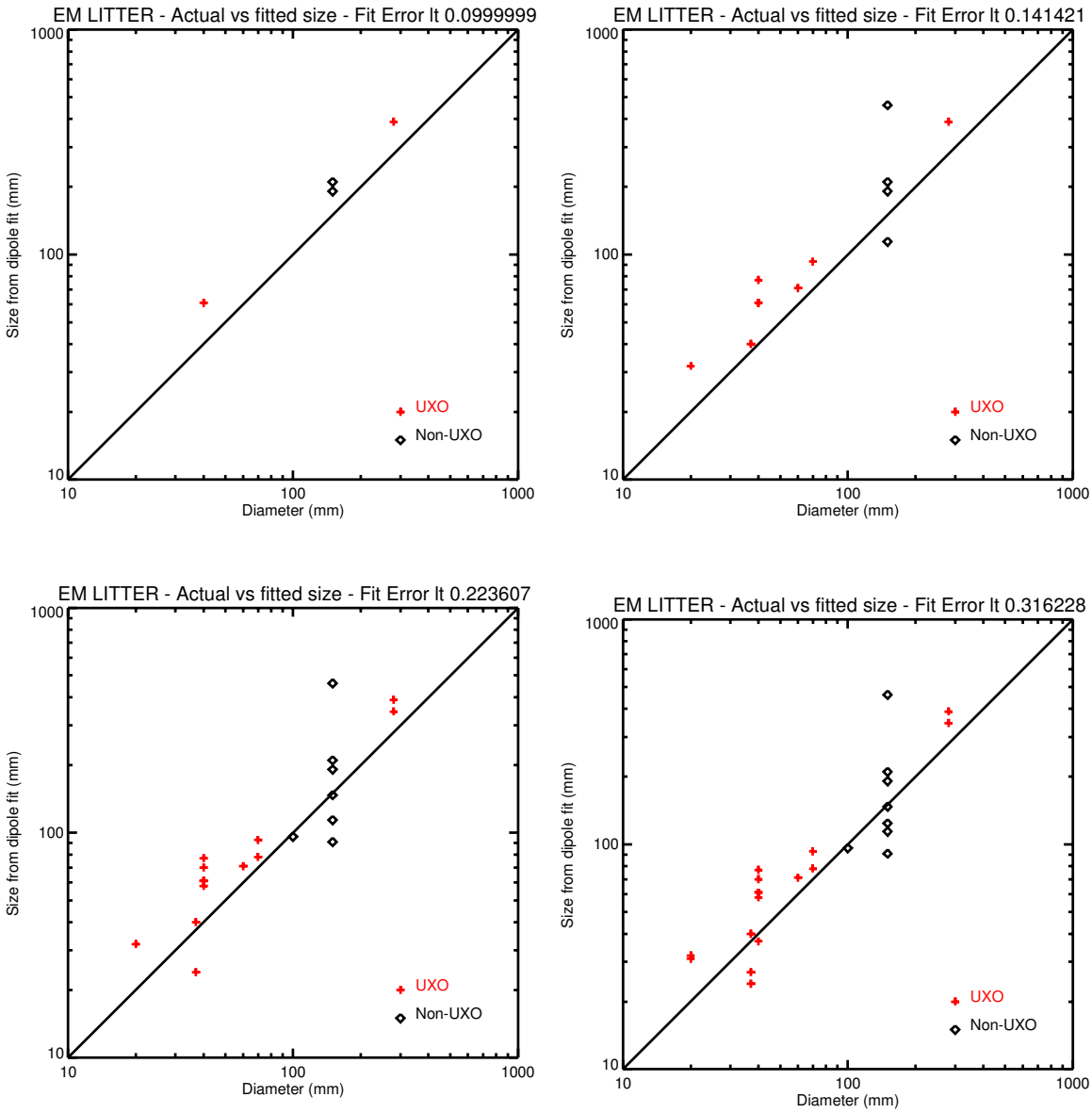

Figure 18. Scatter plot of the diameter versus estimated size for different dipole fit error thresholds.

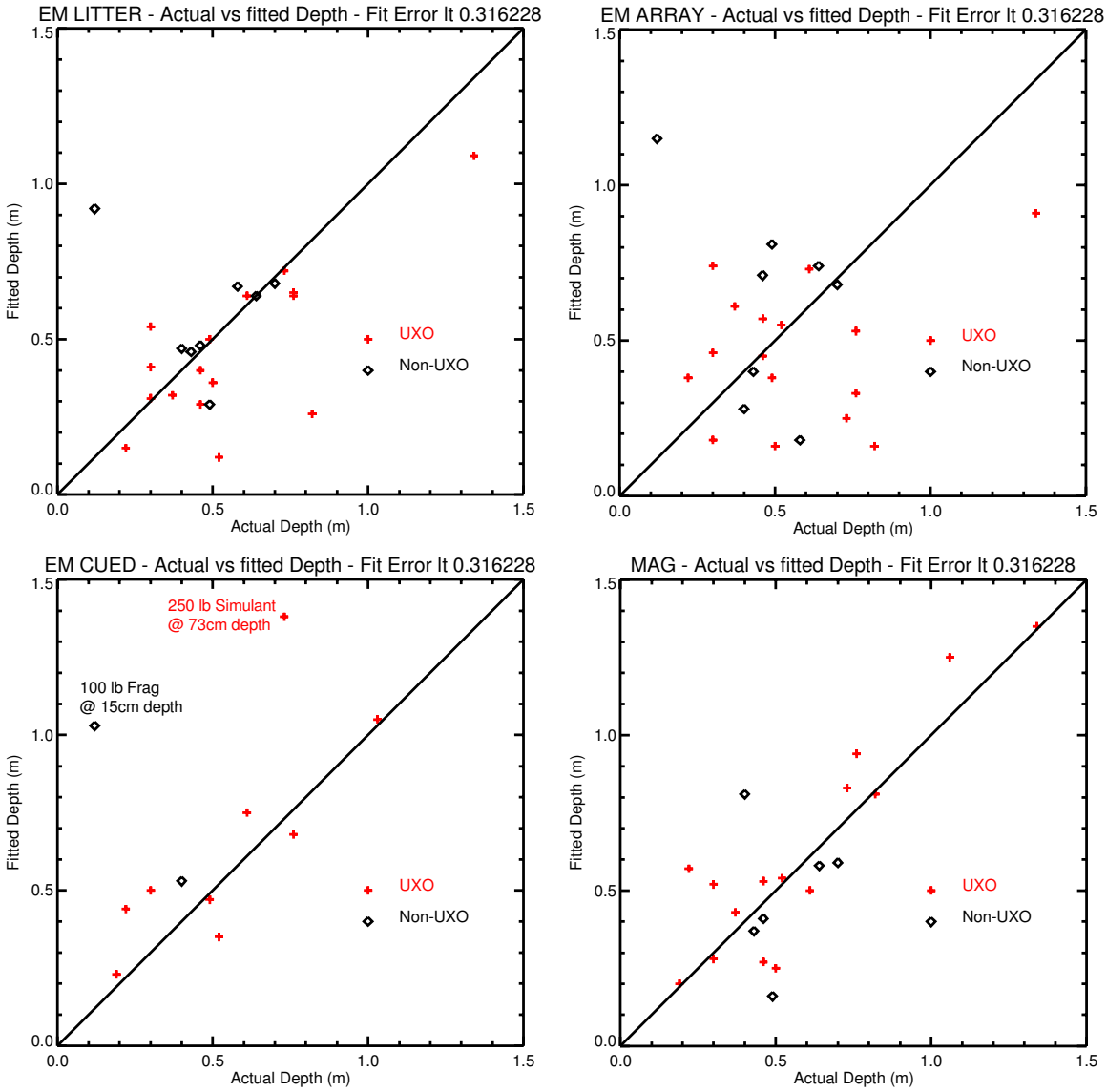

Figure 19. Depth estimates from the dipole fits compared with actual target depth for each of the the survey modes. See Appendix A for additional plots for different fit errors.

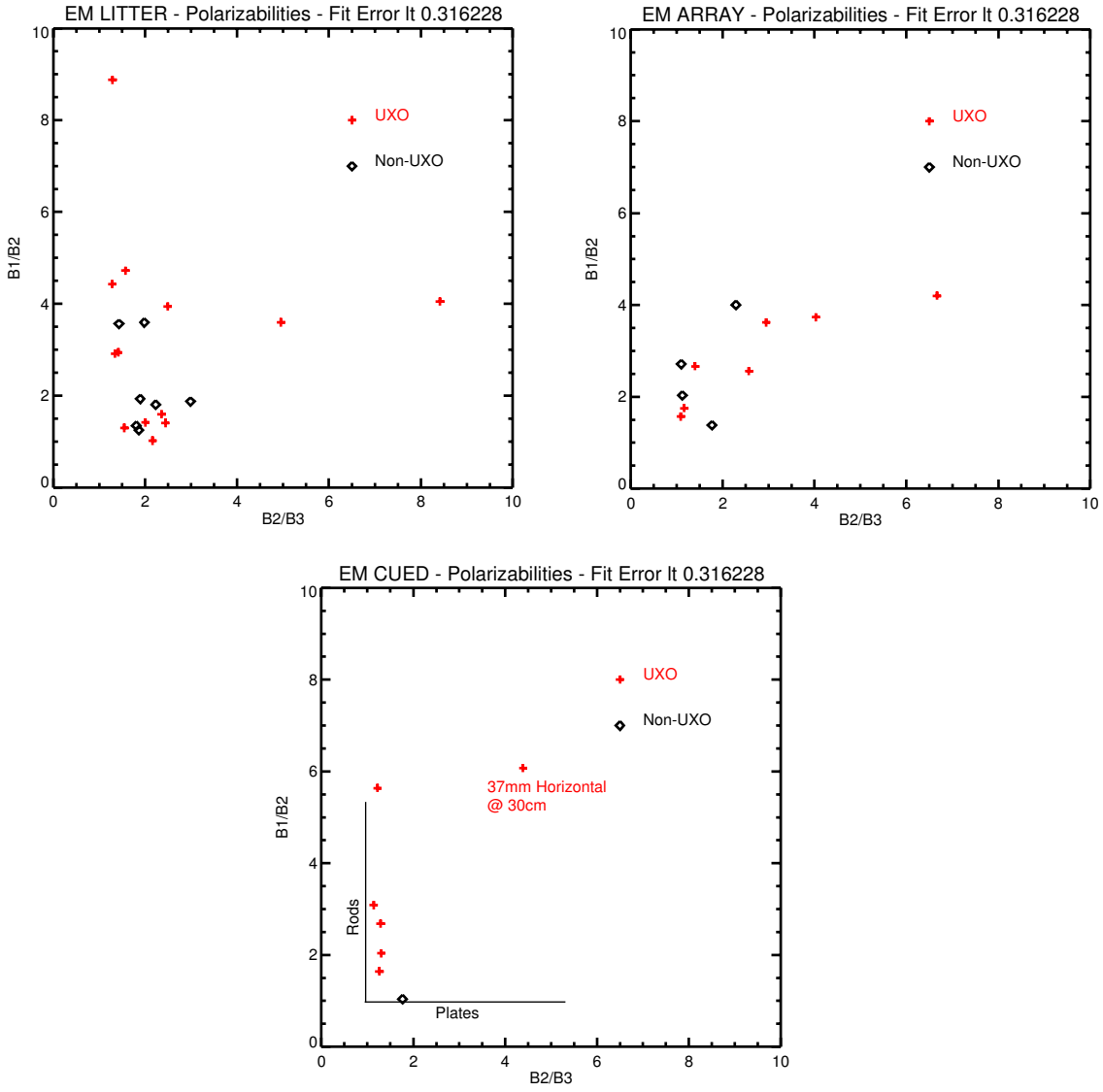

Figure 20. Polarizability plots for GPO targets that have with fit errors less than ~32% for different survey modes. See Appendix A for additional plots for different fit errors.

4.3.2 CT-3A Survey Area

Excavation Results from CT-3

473 excavated anomalies were analyzed as part of this demonstration. Eleven TOI items were unearthed; including, four 20mm projectiles, six 2.25" aluminum warheads, and one 2.75inch MK1 ferrous rocket warhead (Figure 21). The vast majority of the remaining objects were 2.75inch-related munitions debris and 50-cal munitions debris (Table 5). Photographs of commonly-recovered munitions debris are shown in Figure 22.

Table 5. Dig Results from CT-3A Grids

TOI	20mm	4
	2.25inch aluminum warheads	6
	2.75inch ferrous rocket warhead	1
Debris	2.75inch munitions debris	334
	50-cal munitions debris	80
	2.25inch munitions debris	16
	M38 bomb components	6
	Non-descript trash, other, or no-contact	26
	TOTAL	473

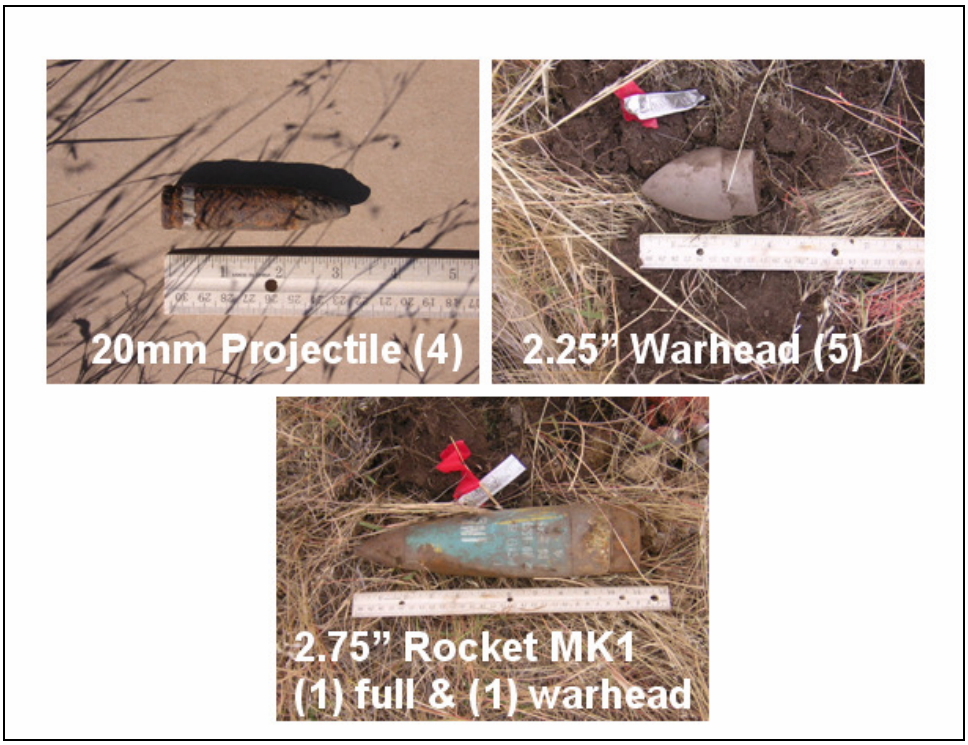

Figure 21. Three types of MEC were recovered within the CT-3A survey area. The include four 20mm projectiles, six 2.25inch warheads, and one ferrous 2.75in Mk1 rocket warhead.

Figure 22. Photographs of non-UXO objects recovered from the CT-3A bombing site.

Comparative Performance of Survey Modes

The performance of the two dynamic EMI surveys is graphically presented in Figure 23. As before, the results are presented as plots of the dipole fit error as a function of the SNR. The mean fit error is 33.9 (standard deviation of 27.3) for the litter-carried data and 30.0 (standard deviation of 17.5) for the towed array data.

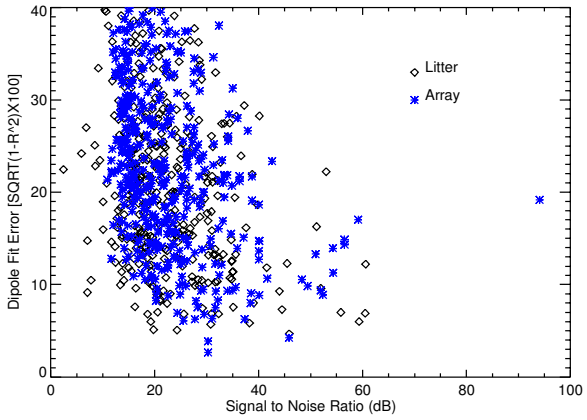

Figure 23. Dipole fit error versus target SNR for Litter and Array survey modes; CT-3A survey area.

For baseline purposes, cued data were acquired at the marked locations in Figure 24. When these locations were selected using Parsons' towed-array EMI data, we did not know a prior the nature of the source. Efforts were made to select isolated targets that possess a range of amplitudes and spatial footprints. EMI litter-carried and towed-array data collected over a number of the cued targets is presented in Appendices C and D.

Performance of the cued interrogations, as measured by the dipole fit error versus SNR, is considerably better than either of the two dynamic surveys. Figure 25 shows results for each of the survey modes. Including the outliers, the average dipole fit error for cued data is 5.1%. Figure 26 directly compares fit errors for the cued versus dynamic datasets. With one exception (anomaly #10066), the cued fit errors are substantially smaller than the corresponding dynamic surveys. Anomaly #10066 is characterized by a 2m by 1m irregular, low amplitude, non-symmetrical EMI signature. When this anomaly was excavated, it was discovered that the source was 20 to 30 inch-size munitions debris fragments.

Fit statistics for the cued targets within the CT-3A survey area are shown for all survey modes in Table 6.

Table 6. Comparison of select fit parameters for cued targets.

ID	Recovered Depth (m)	Fit Error CUED	Fit Depth (m) CUED	∑(Beta's) CUED	Fit Error ARRAY	Fit Depth (m) ARRAY	∑(Beta's) ARRAY	Fit Error LITTER	Fit Depth (m) LITTER	∑(Beta's) LITTER
10007	0.13	2%	0.09	1.04	4%	0.10	1.65	22%	0.39	12.613
10031	0.46	3%	0.29	0.72	19%	0.31	0.71	19%	0.25	0.863
10066	0.51	19%	0.71	-3.58	12%	0.02	0.47	35%	0.8	10.698
10069	0.05	1%	0.08	0.27	23%	0.38	1.71	11%	0.34	1.633
10078	0.08	1%	0.05	0.54	49%	0.10	0.88	43%	0.08	1.199
10079	0.05	7%	0.09	0.07	12%	0.13	0.15	25%	0.43	0.673
10080	0.08	2%	0.03	0.06	15%	0.13	0.27	32%	0.35	0.74
10108	0.05	4%	0.04	0.05	11%	0.08	0.07	32%	0.36	0.209
10113	0.05	3%	0.00	0.11	14%	0.00	0.14	19%	0.03	0.498
10120	0.05	3%	0.02	0.25	21%	-0.02	0.40	13%	0.28	2.174
10122	0.05	2%	0.06	0.17	68%	0.17	0.43	7%	0.22	0.623
10124	0.05	1%	0.04	0.17	27%	0.37	2.10	29%	0.3	1.495
10134	0.05	2%	0.04	0.20	27%	0.35	1.09	36%	0.03	0.355
10157	0.05	5%	0.07	0.05	23%	0.39	0.47	33%	0.51	0.866
10184	0.05	3%	0.11	0.09	13%	0.13	0.26	26%	0.44	1.334
10229	0.05	11%	0.05	0.27	43%	0.72	1.30	41%	0.56	1.504
10235	0.05	3%	0.08	0.05	35%	0.40	0.72	27%	0.34	0.461
10238	0.08	2%	0.18	0.43	12%	0.12	0.23	12%	-0.02	0.25
10290	0.08	16%	0.12	0.25	31%	-0.03	0.08	30%	0.33	3.668
10293	0.05	3%	0.03	0.38	9%	0.22	2.52	6%	0.2	1.847
10294	0.05	11%	0.00	0.04	23%	0.36	0.30	14%	0.51	0.97
AVERAGE	0.10	5%	0.10	0.08	23%	0.21	0.76	24%	0.32	2.13
Std Deviation	0.13	5%	0.15	0.88	15%	0.19	0.71	11%	0.20	3.28

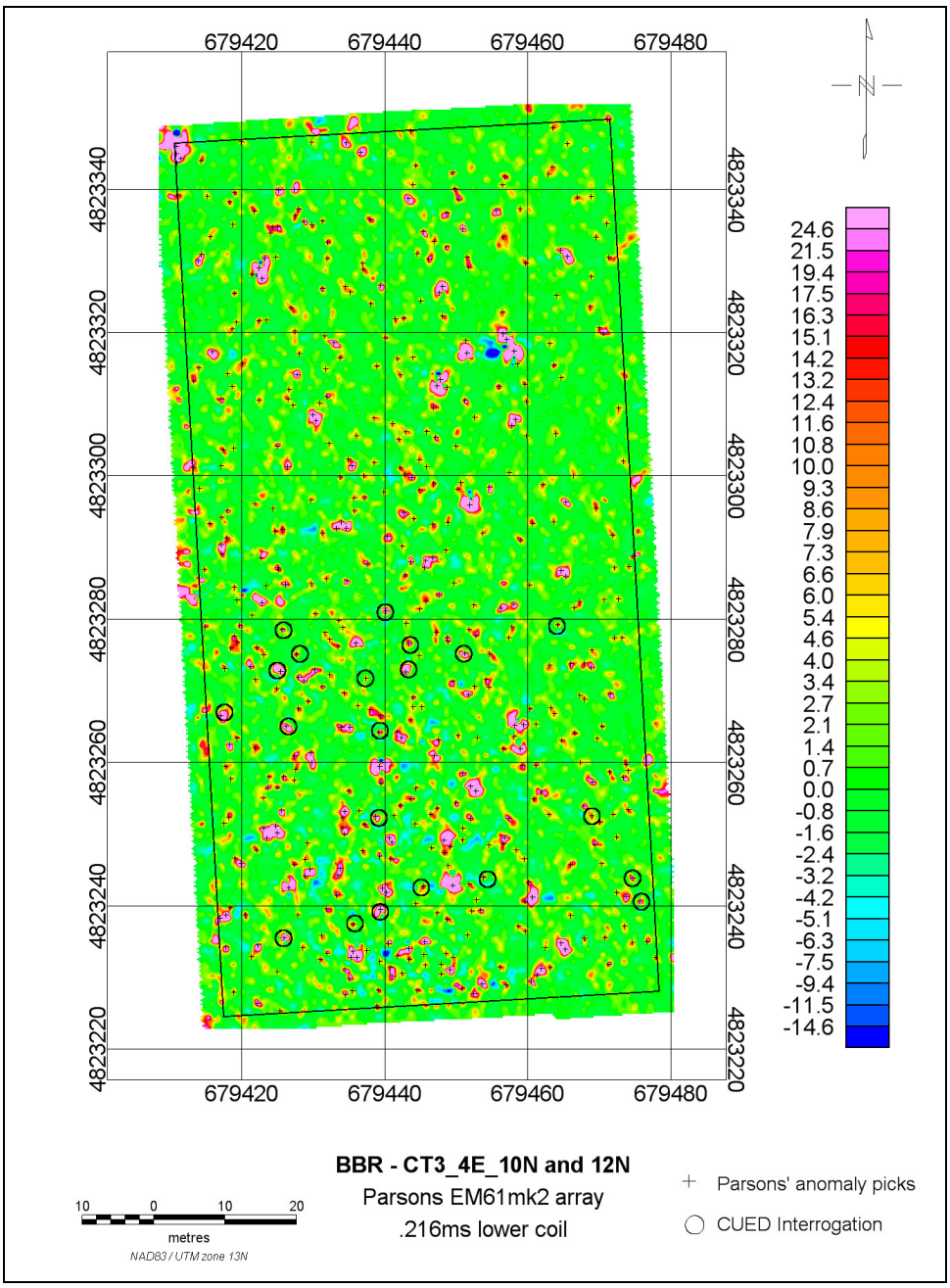

Figure 24. False color map of EM61 towed-array data showing the locations of targets selected for cued interrogations.

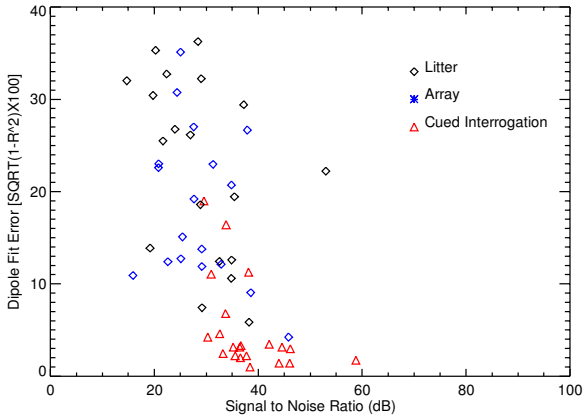

Figure 25. Scatter plot of dipole fit error versus SNR for Litter, towed-Array, and Cued interrogations for common targets in the CT-3A survey area.

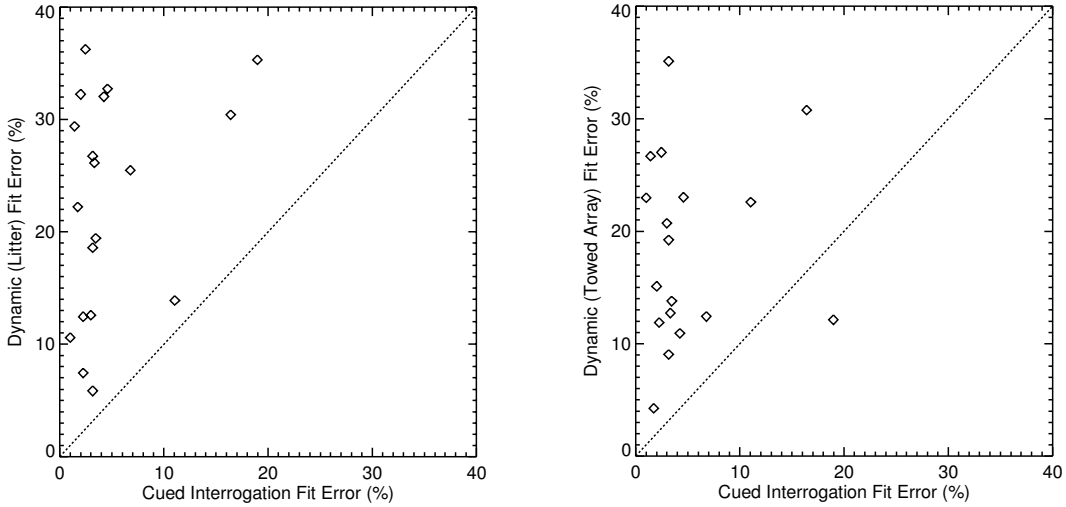

Figure 26. Scatter plots of inverted fit results for cued versus dynamic deployments - common, native targets within the CT-3A survey area. Left – cued versus litter mode. Right – cued versus towed array.

Parameter Estimates from the CT-3A Grids

Figure 27 presents scatter plots of the inverted model parameters for the litter-carried EMI data. Black dots identify parameter values for individual anomalies. Recovered TOI objects are identified using colors and symbols.

The estimated burial depths are not accurate for a majority of the small shallow objects. Figure 28 presents scatter plots of the burial depth as recorded during excavation versus the estimated depth for a variety of fit errors and all EMI survey modes. We note that (i) very few targets possess fit errors less than roughly 10% for the dynamic surveys (shown in red and blue symbols), and (ii) the results are very poor for targets buried less than 20cm below ground level. The litter-carried and towed-array systems performed similarly. On average, estimated depths are within a 5-10cm for fit errors less than 10%, but the RMS error is ~20cm for both survey modes, which amounts to approximately 1/3 of the target/coil separation (40cm standoff + 10cm burial). For these data, the fit depth error is not a strong function of fit quality. The mean and RMS depth error for all of the survey data are plotted as functions of dipole fit error in Figure 29 and Figure 30. For each plotted fit error value, the mean and RMS error are calculated over the band ±0.003, which typically includes 10-15 samples.

There is evidence that the data density and observed signal strength may not be adequate to support reliable inversion for many of the targets, even if the fit quality is high. In such case the dipole model can reproduce the data, but there is not enough data to constrain the fit to the correct target parameters. Figure 31 presents a scatter plot showing the number of points within individual anomaly footprints that are greater than 20mV versus dipole fit error. As shown in this figure, the vast majority of anomalies possess fewer than 20 measurements with values greater than 20mV. Figure 32 presents a similar plot comparing the number of points within the anomaly with values greater than 20mV with the depth error. As before, depth errors decrease as the number of high amplitude measurements increase.

Estimated size is plotted against peak signal and fit depth in Figure 33. Results for both EMI surveys and the magnetic survey are shown. Black symbols are used to show the fitted features for all anomalies found in the CT-3A survey area. TOI items are superimposed using color symbols. Red identifies the recovered 2.25 inch aluminum warheads and 20mm projectiles, and blue marks the ferrous 2.75inch MK1 rocket warhead.

With regards to location accuracy, the mean location error for recovered 20mm projectiles, 2.25inch warheads, and 2.75inch warheads was 20.7cm with a standard deviation of 7.6cm. Including the clutter, the average location error was 26.3cm with a standard deviation of 16.8cm.

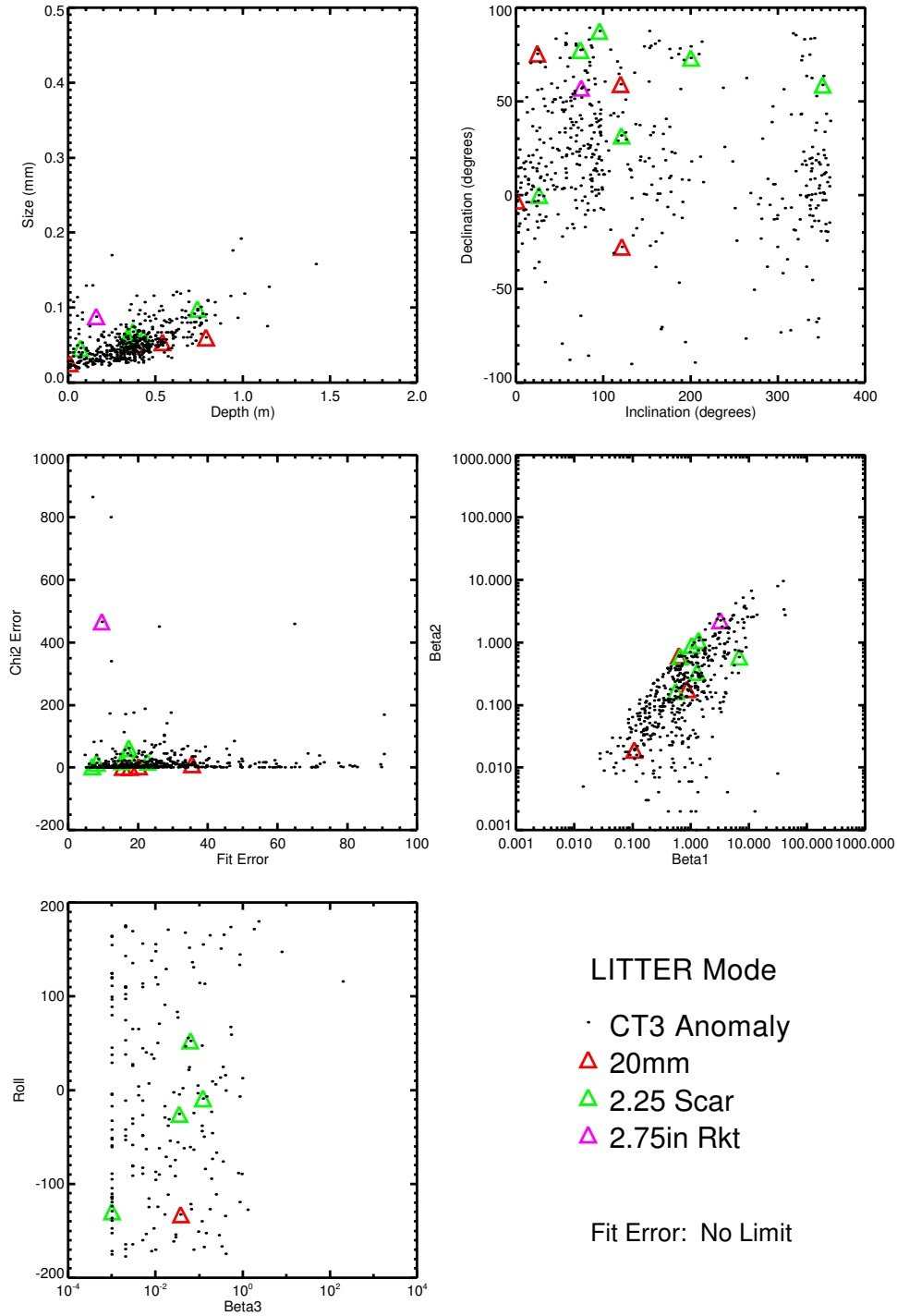

Figure 27. Feature space plots for data acquired in the CT-3A survey area (black dots). The recovered MEC items are overlain and color coded for reference. Appendix B presents results for a variety of fit errors.

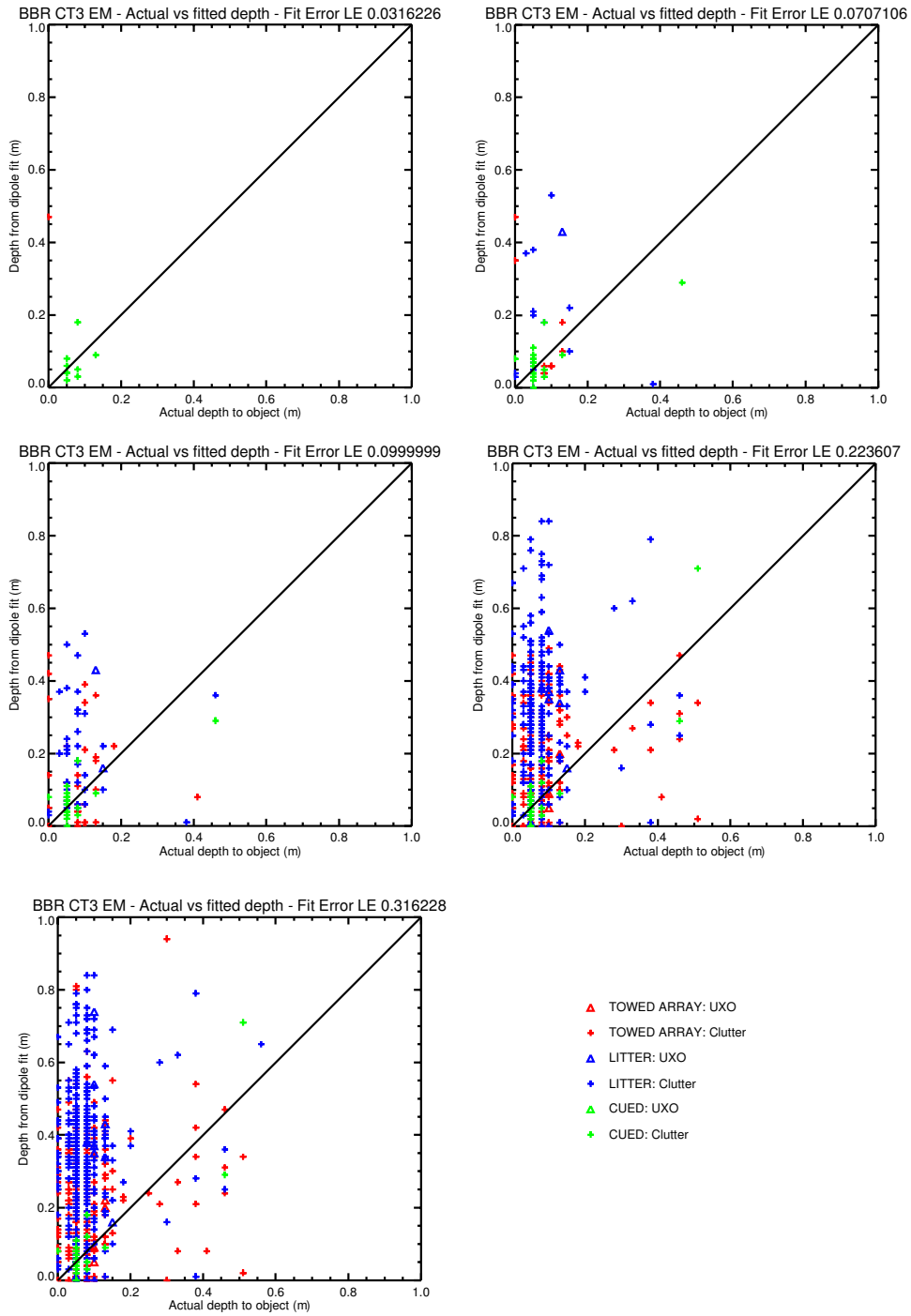

Figure 28. Reported versus estimated depth for CT-3A targets as a function of survey modes and fit errors.

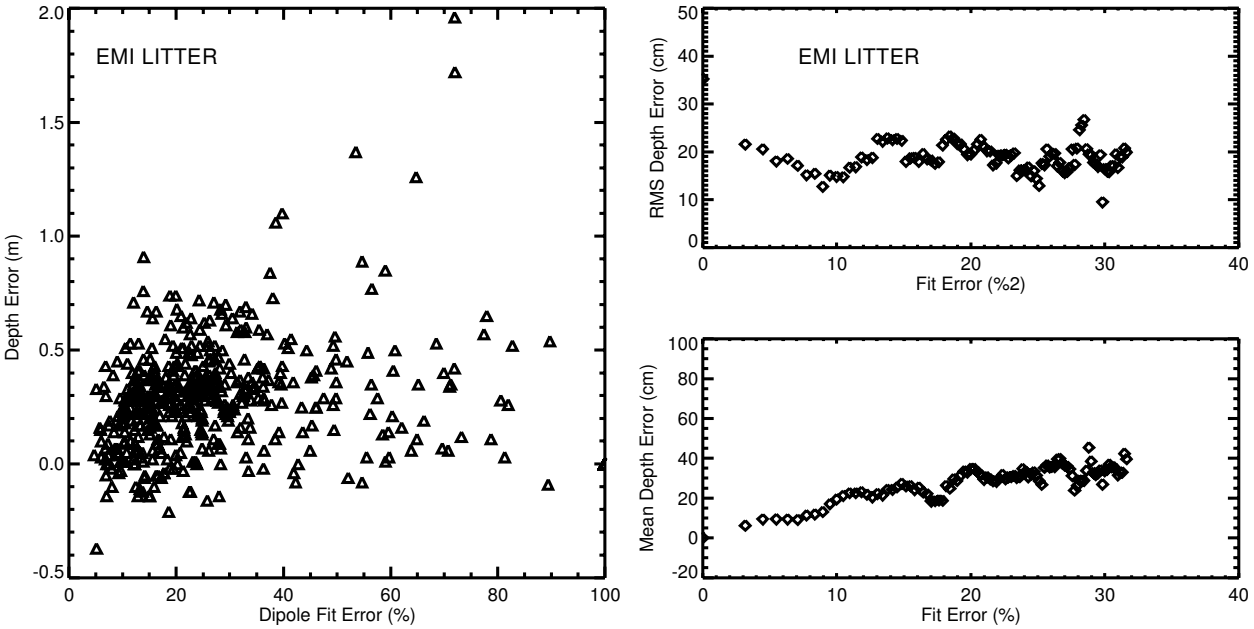

Figure 29. Left – scatter plot of dipole fit error versus depth error for the litter-carried EMI system. Right – RMS and mean depth errors binned over discrete fit errors.

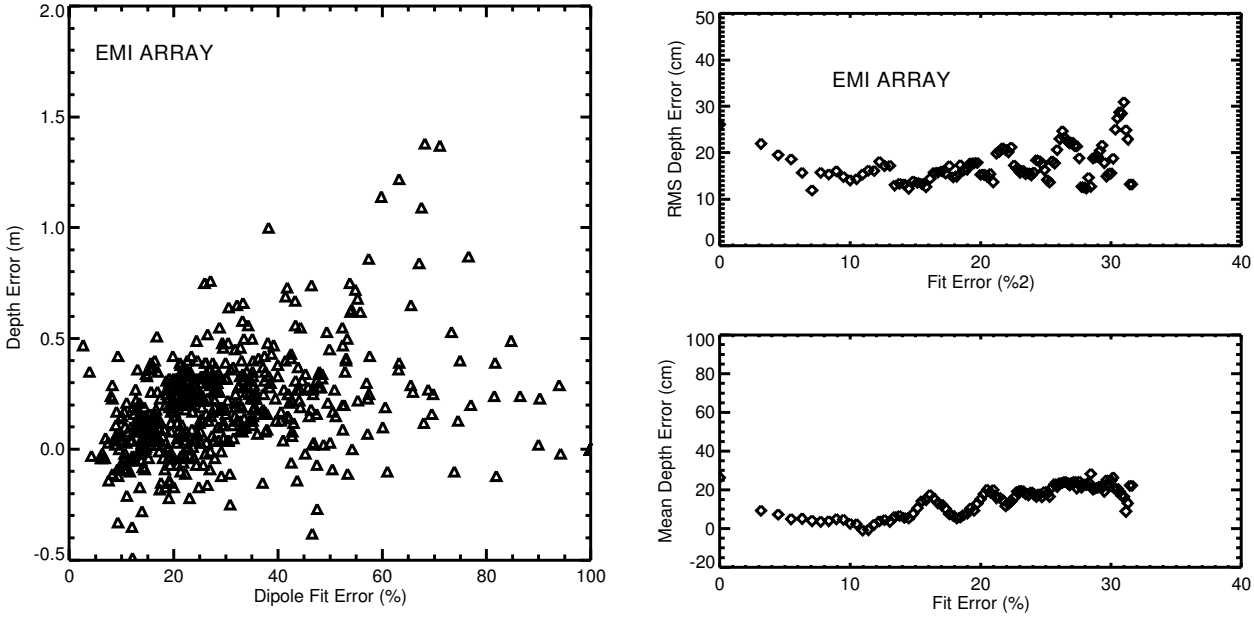

Figure 30. Left – scatter plot of dipole fit error versus depth error for the towed Array EMI system. Right – RMS and mean depth errors binned over discrete fit errors.

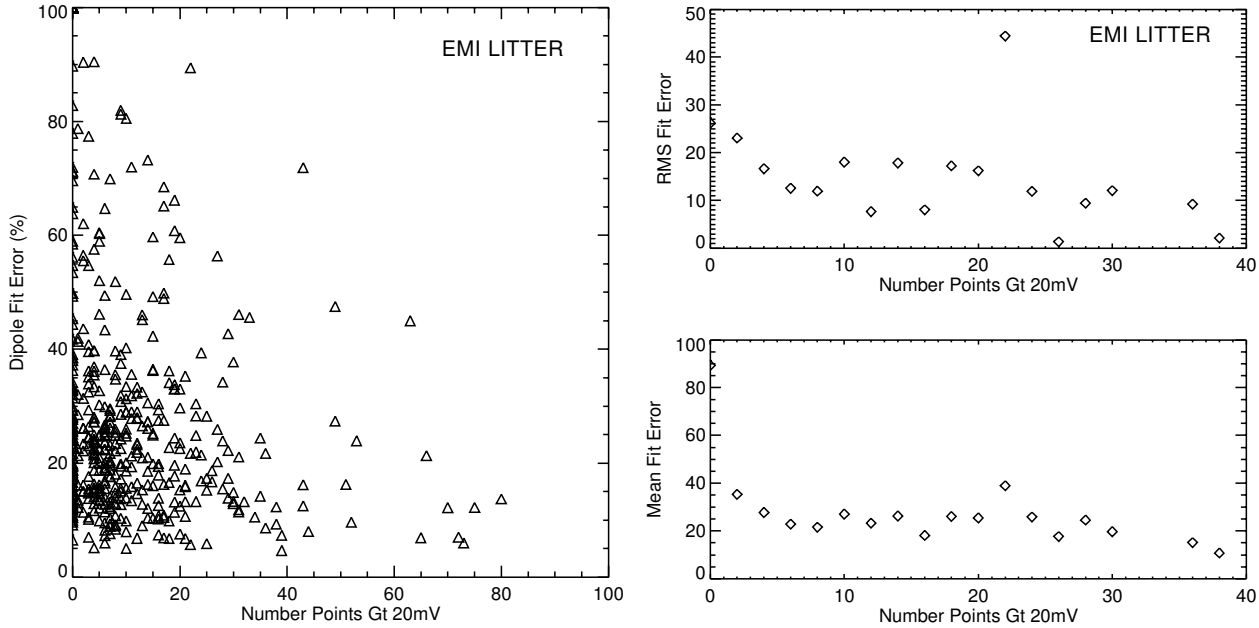

Figure 31. Left – scatter plot showing the number of points within individual anomaly footprints that are greater than 20mV versus dipole error for the litter-carried EMI system. Right – RMS and mean depth errors binned over discrete fit errors.

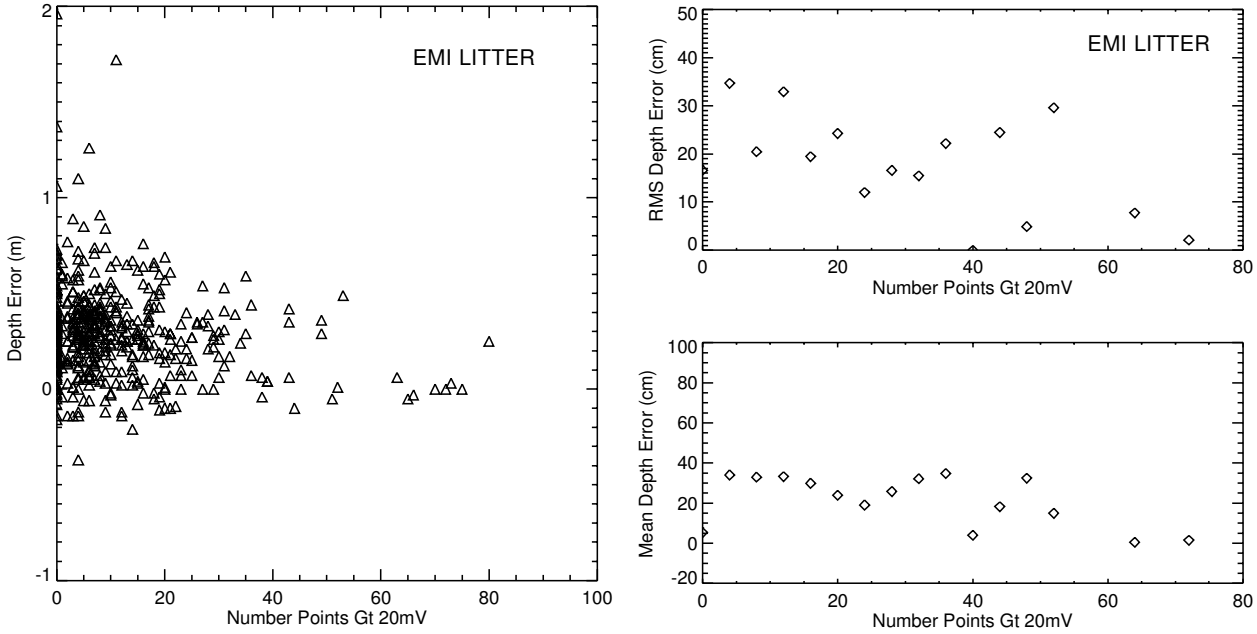

Figure 32. Left – scatter plot showing the number of points within individual anomaly footprints that are greater than 20mV versus depth error for the litter-carried EMI system. Right – RMS and mean depth errors binned over discrete fit errors.

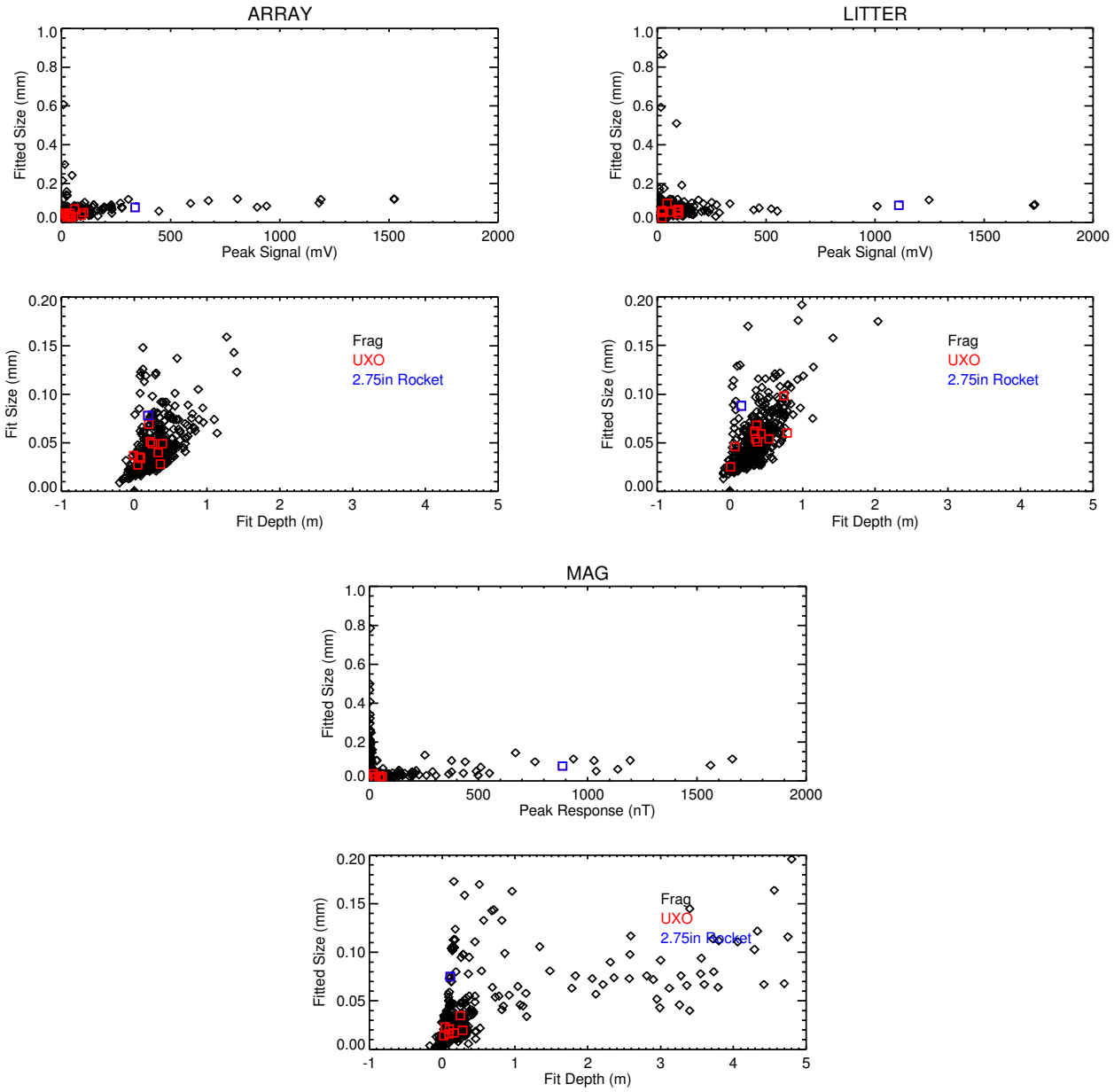

Figure 33. Plots showing the peak signal and fitted depth versus fitted size for the towed Array EMI system (top left), litter-carried EMI system (top right), and magnetic sensors (bottom). TOI items are superimposed using color symbols. Red identifies all the recovered TOIs (2.25 inch aluminum warheads and 20mm projectiles), and blue marks the ferrous 2.75inch MK1 rocket warhead.

As a whole, data acquired in a grid during the cued interrogations was better characterized by dipole models than the standard towed-array or litter-carried EMI surveys (Figure 34). As a result,

the residual dipole fit errors are significantly smaller. We attribute the performance improvements to the fact that (i) the coil is slightly closer to the ground in the cued interrogations, and (ii) the relative spatial positions are precise (errors measured in millimeters).

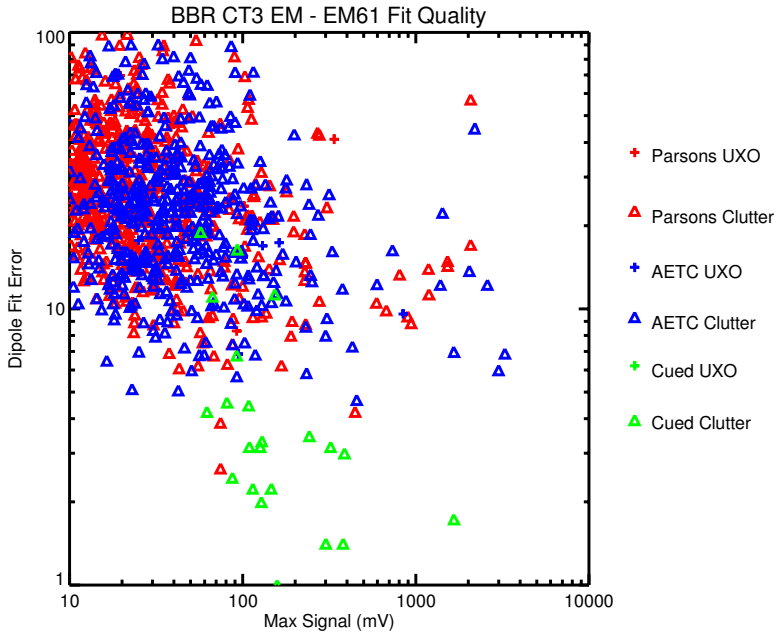

Figure 34. Scatter plot showing the maximum signal (in mV) versus the dipole fit error for all target analyzed within the CT-3A survey area.

Receiver Operating Characteristic (ROC) Curves

For these data, target classification is problematical for three reasons. First, the GPO data available for training is severely limited. The objects buried in the geophysical prove out do not adequately represent objects that were recovered within the CT-3A survey area. There was, for example, no site-specific clutter or 2.25inch aluminum warheads emplaced in the GPO. The GPO was designed and constructed by the Corps of Engineers to aid in detection surveys, not specifically to aid discrimination investigations. Second, the fitted features of the buried UXO and simulants within the GPO do not cluster or indicate axial symmetry (Figure 35). This is not surprising, however, given the dipole fit errors of over 20% (Figure 16). Third, the number of recovered TOIs within the CT-3A survey area is severely limited. The TOIs, defined in Parsons' Demonstration Plan as items larger than 40mm projectiles, include six 2.25inch aluminum warheads, and one 2.75inch ferrous rocket warhead.

Performance results for these TOIs are presented using receiver operating characteristic (ROC) curves in Figure 36 through Figure 38. We selected features that are intrinsic to the target; namely, the magnetic polarizabilities and their ratios (Table 7).

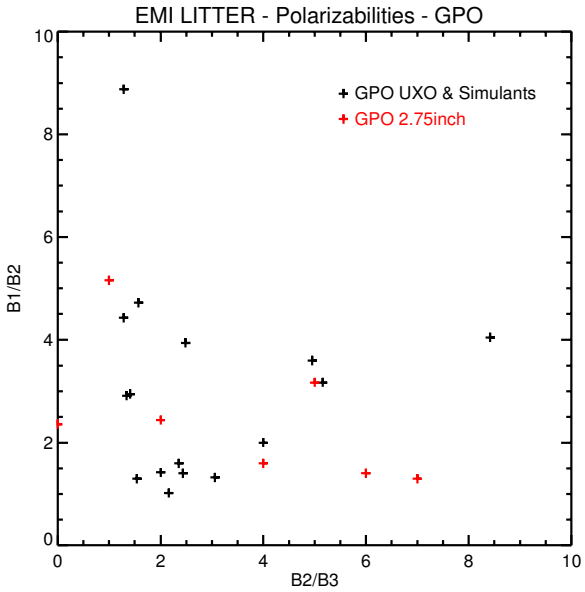

Figure 35. Scatter plot showing polarizability ratios for objects buried in the GPO. There were no examples of 2.25inch aluminum warheads. Fit results for the 2.75inch nose simulants, rockets, and rocket bodies are plotted in red.

Table 7. Selected Model Parameters, or features, used as input to the GLRT classifier

Data Type	Features selected for use by the GLRT classifier
Magnetic data	Moment, Solid Angle, Depth or Solid Angle
EMI data	β1, β2, β3 or β1, β2, β3, β1/β2, β2/β3

Figure 36 shows results for the case in which training and testing was restricted to CT-3-recovered UXO larger than 40mm (as per the site Demonstration Plan). Here, this includes the 2.25inch aluminum warheads, and the 2.75inch rocket. Marginal to poor discrimination capabilities is observed for both survey modalities.

Figure 37 shows results for the case in which the classifier was trained using UXO items from the GPO (green) and the CT-3A area (black and blue), and tested on all CT-3-recovered UXO – including the 20mm rounds. No discrimination capability is observed for both survey modes regardless of training.

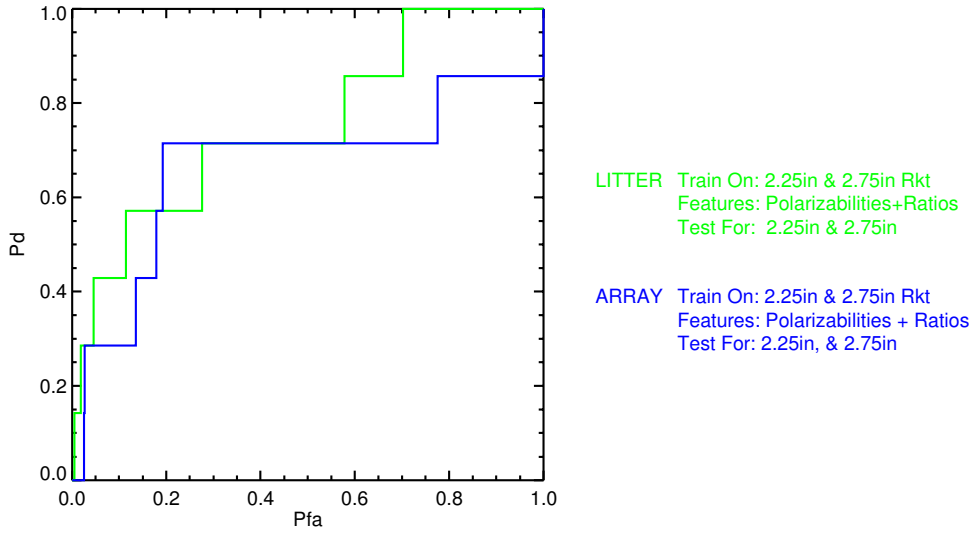

Figure 36 . Receiver Operating Characteristic (ROC) curve for EMI data acquired in the CT-3A area and classified according to the color-coded legend.

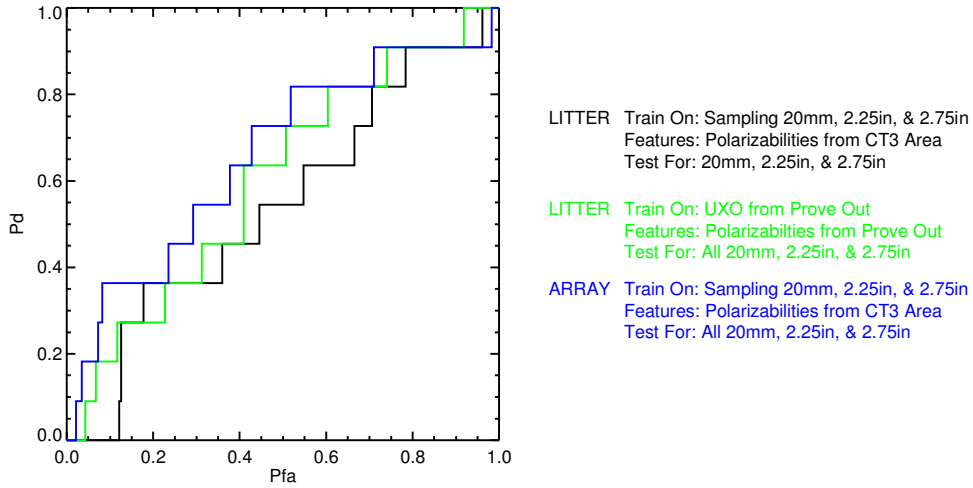

Figure 37. Receiver Operating Characteristic (ROC) curve for EMI data acquired in the CT-3A area and classified according to the color-coded legend. As shown here, no discrimination capability is realized if the objective is to discriminate all 20mm, 2.25inch warheads, and 2.75inch rockets and warheads from the munitions debris that is present.

Figure 38 shows results for three different discrimination objectives. The black curve was generated by training and testing for 20mm, 2.25inch, and 2.75inch TOI. The red curve was generated training and testing for 2.25 and 2.75inch TOI only. The green curve shows performance results if the objective is to only discriminate the 2.75in rocket from the munitions debris. As seen in this figure, it is possible to differentiate the ferrous 2.75inch rocket warhead from the multitude of munitions debris, but not the smaller 2.25inch aluminum warhead. This

result is not unexpected given the large measured response of the 2.75in rocket relative to that generated by the munitions debris (Figure 33).

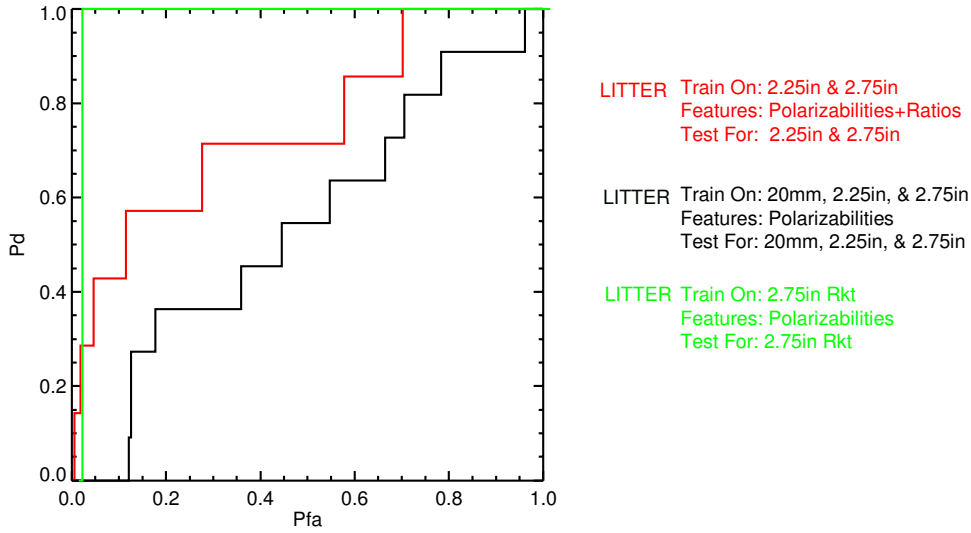

Figure 38. Receiver Operating Characteristic (ROC) curve for EMI data acquired in the CT-3A area and classified according to the color-coded legend.

Because the number of TOIs is small, the ROC curves shown in Figure 36 through Figure 38 allow the GLRT classifier to train and test on the entire population. Because of this, the performance results may not be indicative of future performance. Figure 39 and Figure 40 present performance results using a simpler, alternate metric based on the fitted size. For EMI, the fitted size is defined as the cubed root of the sum of the polarizability response coefficients. For magnetic data, it is scaled magnetic moment.

Figure 39 is for the case where the TOIs only includes ferrous 2.75inch rocket warheads and prioritized according to the fitted size. In Figure 40, the TOIs include the 2.75inch and 2.25 SCAR warheads. For comparison purposes, results based on the peak measured signal strength (instead of the fitted size) is shown using dashed lines.

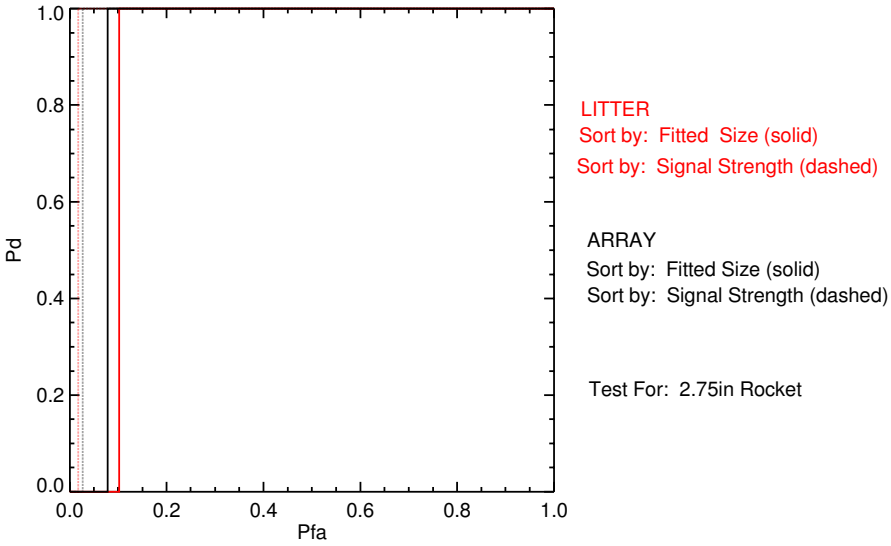

Figure 39. Receiver Operating Characteristic (ROC) curve for litter-carried and towed-array EMI data based on fitted size; TOI: 2.75inch rocket only.

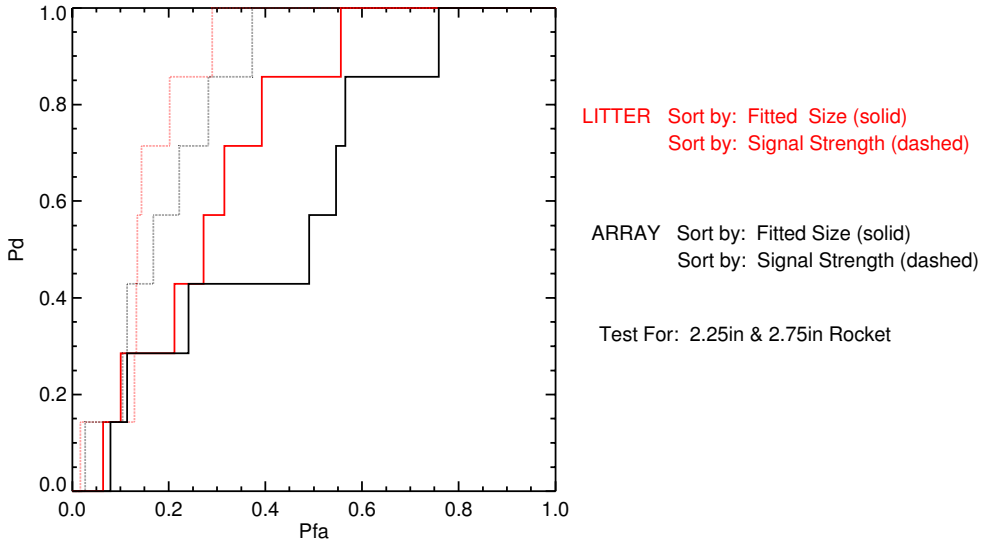

Figure 40. Receiver Operating Characteristic (ROC) curve for litter-carried and towed-array EMI data based on fitted size; TOI: 2.25inch & 2.75inch rocket warheads.

Figure 41 shows discrimination performance results for the magnetic sensor based on fitted size and observed magnitude (analytic signal). For magnetometry data, we do no consider the 2.25inch aluminum warheads or 20mm projectiles to be legitimate discrimination targets at this site for two reasons. First, because the 2.25inch warheads are aluminum, they should not produce an invertible magnetic signature. Second, because the site is littered with small munitions debris, we cannot confidently say that the low amplitude responses, ranging from 4-10nT, observed in the vicinity of the 20mm projectiles are caused by the subject item. By way of example, there are invertible

magnetic signatures within 0.25m of five of the six 2.25inch aluminum warheads. Because of these factors, we are limited to looking for a single item, the ferrous 2.75inch rocket warhead, within a sea of small munitions debris.

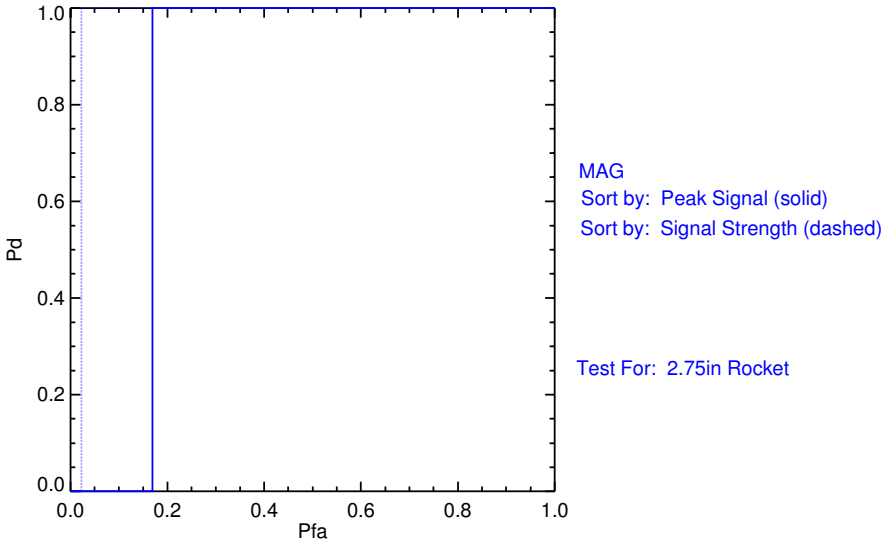

Figure 41. Receiver Operating Characteristic (ROC) curve for Mag data acquired in the CT-3A area and prioritized according to the fitted magnetic moment.

Table 8 expresses the results in a slightly different manner. Here, we show the percentage of targets that possess fitted sizes and signal strengths that are 50% or 80% that of the subject TOI. The results shown below include all fitted anomalies – we have not segmented based on the quality of the fit. As a result, the fitted size performance results are degraded relative to signal strength by inaccurate inversion results due to overlapping signatures and spatial registration errors.

Table 8. Percent of false positives that possess fitted sizes below specific thresholds

TOI Definition	Survey Mode	½ Fit Size	½ Signal Strength	0.8*Fit Size	0.8*Signal Strength
2.75inch Rocket Only	LITTER	39%	97%	80%	97%
	ARRAY	55%	85%	84%	96%
	MAG	68%	96%	79%	97%
2.25inch & 2.75inch warheads	LITTER	3%	39%	26%	62%
	ARRAY	1%	29%	7%	52%

4.3.3 Qualitative Metrics

UX-Analyze characterizes and classifies individual anomalies. Steps taken within the characterization phase include identifying anomalies, selecting the spatial footprint of the anomaly, and reviewing the results. The most labor intensive portion of the characterization phase is identifying the spatial extent of each anomaly and editing individual samples that are inconsistent. UX-Analyze provides graphical presentations and appropriate tools to assist the analyst. Once completed, individual anomalies are inverted manually or in batch mode. The output of the characterization phase is a list of model parameters for each anomaly which is then submitted to the classifier. Steps taken during the classification phase include creating or updating a library for training purposes, selecting and calling the classifier.

UX-Analyze adheres to the look and feel of Oasis montaj and, as such, is quickly mastered by experienced Oasis montaj users. It is easy to use and includes an on-line help menu. Researchers at Weston, Parsons, and the Naval Research Laboratory have used UX-Analyze during recent months in their projects without incident. During the course of this demonstration, Oasis montaj underwent a number of major upgrades that affected the performance and robustness of UX-Analyze. A large number of technical stumbling blocks were created when Oasis montaj package migrated from version 5 to version 6. UX-Analyze was integrated into the official build of Oasis montaj in Version 6.2, which allows it to be licensed, installed, and managed using Geosoft's on-line licensing system. Fixes to a normalization issue within the GLRT classification routines were completed in December 2006. Fixes to a figure of merit calculation were completed in March 2007. All known coding inconsistencies and bugs have been corrected as of this report. The current Oasis montaj release is 6.4, and we do not experience systematic difficulties while characterizing and classifying these magnetic and EMI data.

4.3.4 Discussion

The objective of the Corps of Engineers ordnance and explosive (OE) removal action is to remove all items ranging between a 40mm projectile and a 500lb bomb at depths of less than 11-diameters of the object, to a clearance depth of four feet. We analyzed data from part of the bombing target with the hope of identifying particular TOIs that could be discriminated from the plethora of munitions debris that is present at this locale. Excavation results produced no intact UXO within the study area. Recovered TOIs within the two, CT-3-bombing grids studied here included four 20mm projectiles, six 2.25inch aluminum SCAR warheads, and one ferrous 2.75inch rocket warhead.

Discriminating the 20mm projectiles and 2.25inch aluminum warheads from the plethora of munitions debris responses based on their inverted source parameters proved challenging. Even though the litter-based EMI sensor was carried along transects spaced 0.5m apart, the majority of signatures were observed on only a single profile. As a result of the limited spatial views of the target (e.g., we did not illuminate the targets from all angles due to the anomalies small footprint)

and the low amplitudes, the EMI inversion results do not, as a rule, provide accurate size, shape, and depth estimates even when the dipole fit error is small.

As measured by the dynamic survey platforms, the anomalies were predominantly spatially limited and could not be well represented by a dipole model. The majority have dipole fit errors much greater than 10% (Figure 34) and does not, therefore, support discrimination decisions based on inverted source parameters. Previous experience suggests that the major factors limiting field performance are positioning errors, background noise, overlapping signatures, and data density. Systematic or random noise in the sensor readings caused by these factors linearly affects the inverted magnetic polarizabilities and degrades discrimination performance. Figure 42 shows the relationship between errors in target parameter estimates (βs) and the dipole fit error based on Monte-Carlo simulations (Bell, 2005). In order to get target parameters with sufficient accuracy (< 30-50%) to support target classification, we need dipole fit errors of 5% or less.

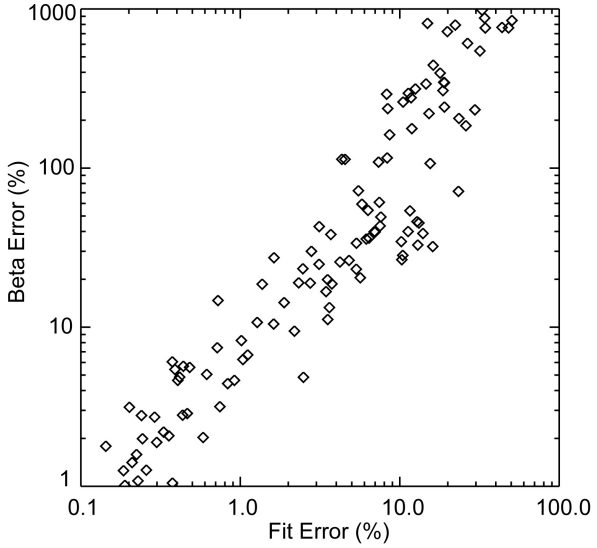

Figure 42. Beta error versus dipole fit error from Monte Carlo simulations.

In stark comparison to the litter-carried and towed-array EMI data, the gridded EMI data acquired in a cued fashion was well represented by a dipole model. For targets within the CT-3A bombing target, the mean dipole fit error was 5% compared to ≥23% for the dynamic surveys. Furtheremore, with the exception of one horizontal 37mm buried at 30cm, the inverted shape parameters for symmetric targets in the GPO appear symmetric.

A significant number of the munitions debris can be screened by setting appropriate thresholds if the stakeholders and regulators set specific TOIs for the site. If the TOI is restricted to 2.75inch ferrous warheads and larger items, for example, these data indicate that as many as 97% of the excavate munitions debris could have been safely left in the ground. Alternatively, if the TOIs include 2.25inch and larger objects, 30% to 60% of the munitions debris can remain depending

on whether the amplitude threshold is set to 50% or 80% of that observed for the subject 2.25inch aluminum warheads.

In addition to analyzing individual anomalies that were selected by Parsons using their towed array EMI data for ground truthing, we looked for additional, comparable targets in the litter-carried data that might be evident due to the more conservative transect spacing. The towed array data was acquired along transect spaced one meter apart, and the litter carried data was acquired along transect spacing that were nominally 0.5m apart. We identified over 340 additional targets in the litter-carried EMI data set. The extra anomalies are characteristically small, having peak responses of 20mV or less, which is similar to that observed for the 20mm projectiles and small munitions debris, and were typically located between the towed-arrays transects. Although these additional targets were not unearthed as part of the Corps of Engineers removal action, it is clear by the number of extra anomalies and by the high number of single-transect anomalies (in the towed-array data) that small items are preferentially detected along survey lines compared to between the transects.

Although largely complimentary, the magnetic survey detected a few, noteworthy potential source targets that were not readily observed in the EMI data sets. First, two 2.75inch rockets in the GPO (Figure 13) possess easily identifiable magnetic dipoles but no EMI response. Second, two large anomalies are observed within the CT-3A survey grids (Figure 43). The source of these later anomalies is not known, but the coordinates and fit information has been passed on to the Omaha Corps of Engineers.

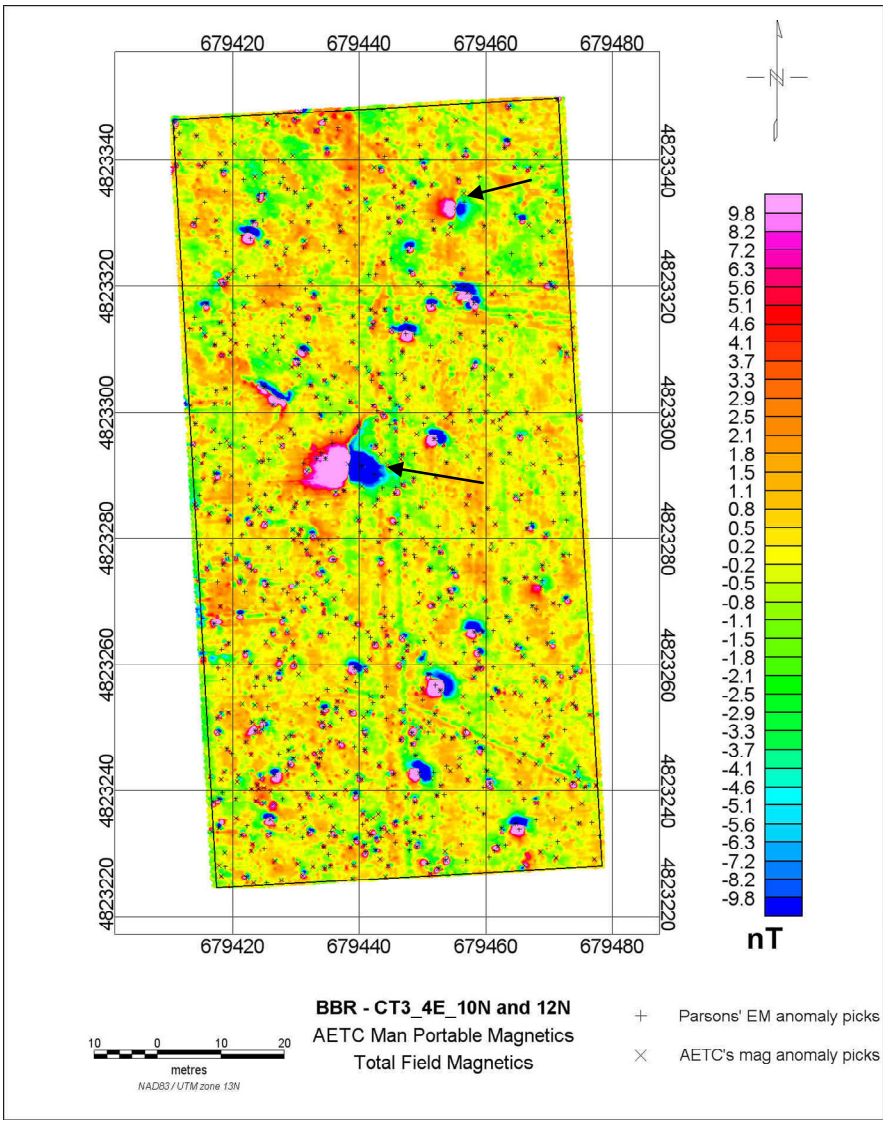

Figure 43. Black arrows identify two large magnetic anomalies that do not have corresponding EMI signatures.

5. Cost Assessment

5.1 Cost Reporting

This demonstration focuses on characterizing and classifying anomalies observed in magnetic and electromagnetic data. It encompasses, therefore, only a subset of costs that are typically associated with acquisition demonstrations. The relevant cost categories for data analysis are shown in Table 9.

Table 9. Cost categories and details

Cost Category	Details	Sub Category	Time (hours)	Costs* ($)
Pre-processing	Re-leveling & digital filtering prior to inversion	EM61 Towed Array	8	800
		EM61 Litter	40	4000
		EM61 Cued	4	400
		Mag	16	1600
Anomaly extraction	Culling anomaly signatures from site database	EM61 Towed Array	16	1600
		EM61 Litter	24	2400
		EM61 Cued	0	0
		Mag	16	1600
Data characterization and classification	Inverting anomaly data for model parameters & performing feature-based classification	EM61 Towed Array	16	1600
		EM61 Litter	16	1600
		EM61 Cued	4	400
		Mag	16	1600
Documentation	Preparing Dig Sheets using UX-Analyze functions	All data types	~100 per minute	--
Reporting	Technical Report	--	350	35,000
		TOTAL		52,600

*assumes an fully-loaded labor rate of $100 per hour

6. Implementation Issues

6.1 End-Users Issues

The primary end-users of this data analysis technology will likely be high-end geophysical service providers, technically orientated DoD oversight personnel, and government-sponsored researchers. In order to be successfully transitioned to the production community, this technology must not only be accepted by the Environmental Protection Agency and the Corps of Engineers, it must initiate a change in the requested deliverables regarding data analysis for UXO concerns.

Currently, the Corps of Engineers Data Item Description (DID) OE-005-05.01, which details the required information for each anomaly, does not ask for estimates of the targets' features (viz., such as target depth, apparent size, orientation, etc.) It only requests the amplitude of the anomaly and a prioritized ranking. This program explored the methods and logic involved with creating a prioritized dig list.

7. References

Section 349 (Public Law 105-85), Partnerships for Investment in Innovative Environmental Technologies.

Barrow,, B., and Nelson, H., 1998, *Collection and Analysis of Multi-sensor Ordnance Signatures with MTADS*, J. Environ. Engineering Geophysics, **3**, p. 71.

ESTCP Cost and Performance Report 199526, *Multi-sensor Towed Array Detection System*, http://www.estcp.org/documents/techdocs/199526.pdf.

Parsons, 2004, Final Removal Action Work Plan for the Former Badlands Bombing Range, U.S. Army Engineering Support Center, Huntsville and USACE-Omaha District, Contract No. DACA87-00-D-0038.

Senate Report 106-50, National Defense Authorization Act for Fiscal Year 2000, May 17, 1999. Research and Development to Support UXO Clearance, Active Range UXO Clearance, and Explosive Ordnance Disposal, pages 291–293.

Department of Defense, Unexploded Ordnance Response: Technology and Cost, Report to Congress, March 2001

G. Robitaille, J. Adams, C. O'Donnell, and P. Burr, 1999, *Jefferson Proving Ground Technology Demonstration Program Summary*, SFIM-AEC-ET-TR-99030, http://aec.army.mil/usaec/technology/jpgsummary.pdf.

Thomas Bell, "Geo-location Requirements for UXO Discrimination," SERDP/ESTCP Geolocation Workshop, Annapolis, June 2005.

8. Points of Contact

ESTCP

Anne Andrews	ESTCP 901 North Stuart Street Suite 303 Arlington, VA 22203	Tel: 703-696-3826 Fax: 703-696-2114 Anne.Andrews@osd.mil	Program Manager UXO Thrust Area
Katherine Kaye	HydroGeologic, Inc. 1155 Herndon Parkway Suite 900 Herndon, VA 20170	Tel: 410-884-4447 Fax: 703-478-0526 jef@hgl.com	Program Assistant UXO Thrust Area

SAIC (formerly AETC Incorporated)

Dean Keiswetter	SAIC 120 Quade Drive Cary, NC 27513	Tel: 919-653-0215x103 Fax: 919-653-0219 keiswetterd@saic.com	PI
Tom Bell	SAIC 1225 Jefferson Davis Highway Suite 800 Arlington, VA 22202	Tel: 703-413-0500x254 Fax: 703-413-0512 bellth@saic.com	Co-PI
Tom Furuya	SAIC 120 Quade Drive Cary, NC 27513	Tel: 919-653-0215x104 Fax: 919-653-0219 tfuruyat@saic.com	Data Analyst

Parsons

Greg Van	Parsons 1700 Broadway, Suite 900 Denver, CO 80290	Tel: 303-764-1927 Fax: 410-278-1589 Greg.Van@parsons.com

US Army Corps of Engineers Omaha District

Richard Grabowski	US Army Corps of Engineers Attn: CENWO-ED-GG (Grabowski) 106 South 15th Street Omaha, NE 68102-1618	Tel: 402-221-7784 Fax: 410-278-1589 Richard.J.Grabowski@usace.army.mil

Appendix A - Parameter Estimates from the Prove Out

Size

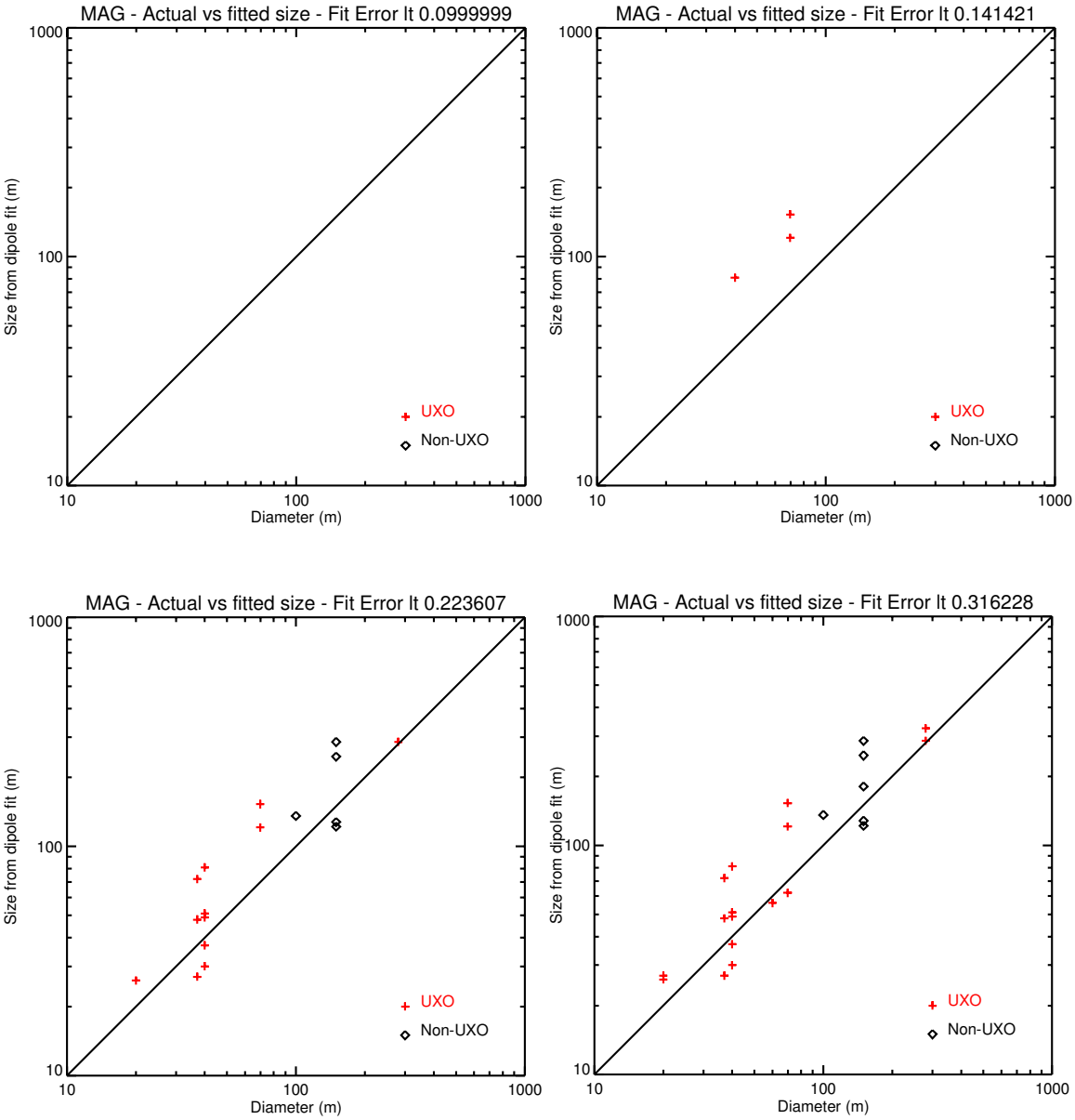
MAG - Actual vs fitted size - Fit Error lt 0.0999999
MAG - Actual vs fitted size - Fit Error lt 0.141421
MAG - Actual vs fitted size - Fit Error lt 0.223607
MAG - Actual vs fitted size - Fit Error lt 0.316228
Size from dipole fit (m)
Diameter (m)
10
100
1000
UXO
Non-UXO

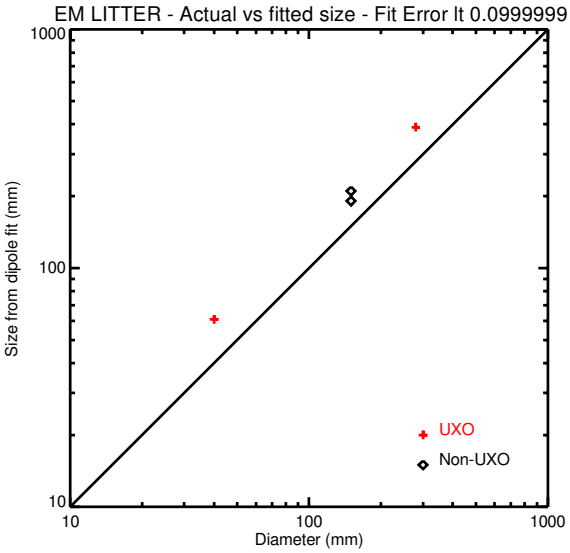
EM LITTER - Actual vs fitted size - Fit Error lt 0.0999999
Size from dipole fit (mm)
Diameter (mm)
1000
100
10
10
100
1000
UXO
Non-UXO

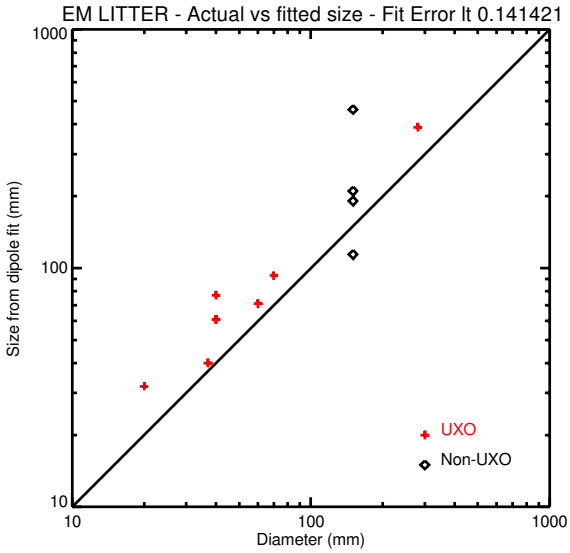
EM LITTER - Actual vs fitted size - Fit Error lt 0.141421
Size from dipole fit (mm)
Diameter (mm)
1000
100
10
10
100
1000
UXO
Non-UXO

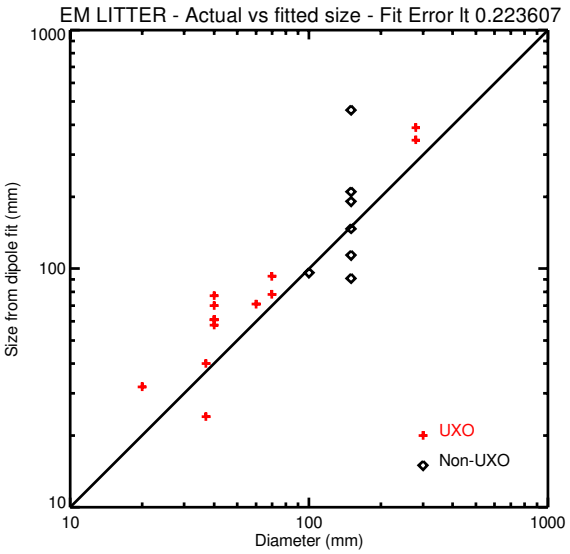
EM LITTER - Actual vs fitted size - Fit Error lt 0.223607
Size from dipole fit (mm)
Diameter (mm)
1000
100
10
10
100
1000
UXO
Non-UXO

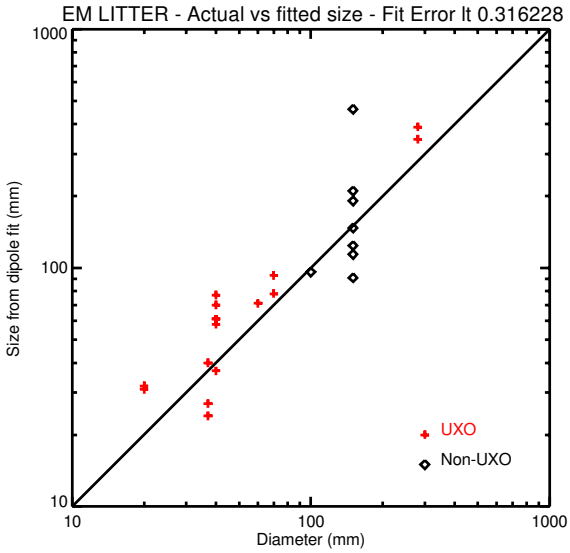
EM LITTER - Actual vs fitted size - Fit Error lt 0.316228
Size from dipole fit (mm)
Diameter (mm)
1000
100
10
10
100
1000
UXO
Non-UXO

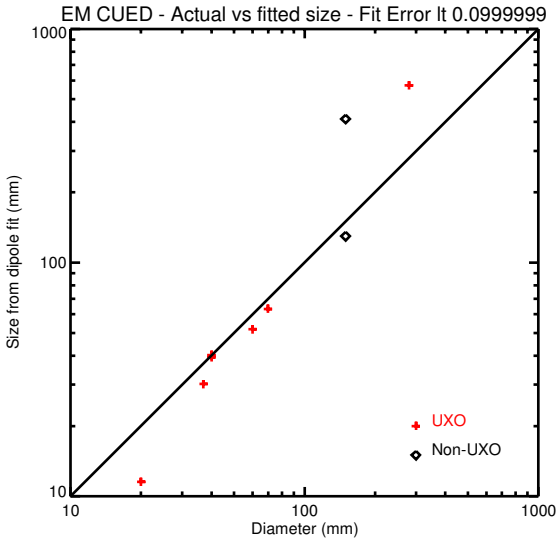
EM CUED - Actual vs fitted size - Fit Error lt 0.0999999
Size from dipole fit (mm)
Diameter (mm)
1000
100
10
10
100
1000
UXO
Non-UXO

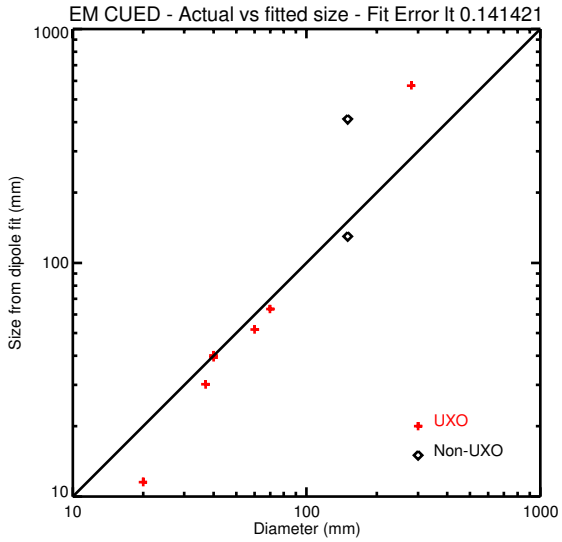
EM CUED - Actual vs fitted size - Fit Error lt 0.141421
Size from dipole fit (mm)
Diameter (mm)
1000
100
10
10
100
1000
UXO
Non-UXO

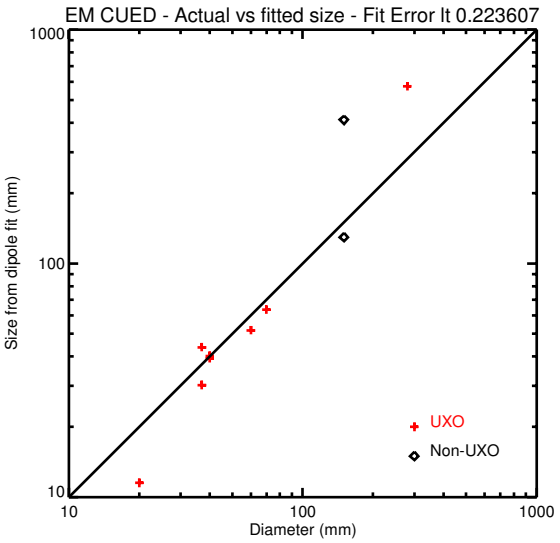
EM CUED - Actual vs fitted size - Fit Error lt 0.223607
Size from dipole fit (mm)
Diameter (mm)
1000
100
10
10
100
1000
UXO
Non-UXO

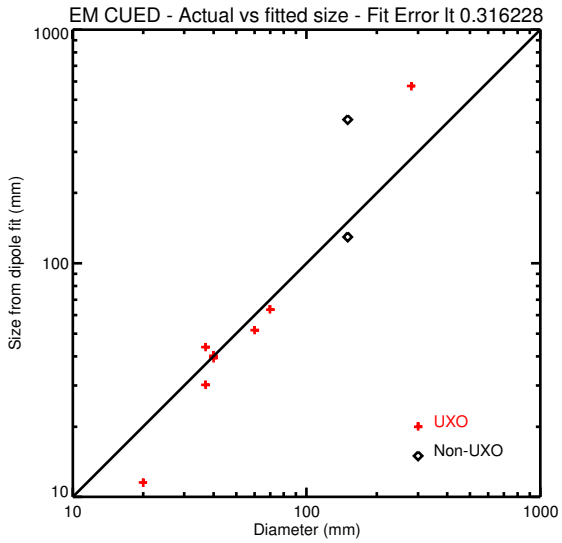
EM CUED - Actual vs fitted size - Fit Error lt 0.316228
Size from dipole fit (mm)
Diameter (mm)
1000
100
10
10
100
1000
UXO
Non-UXO

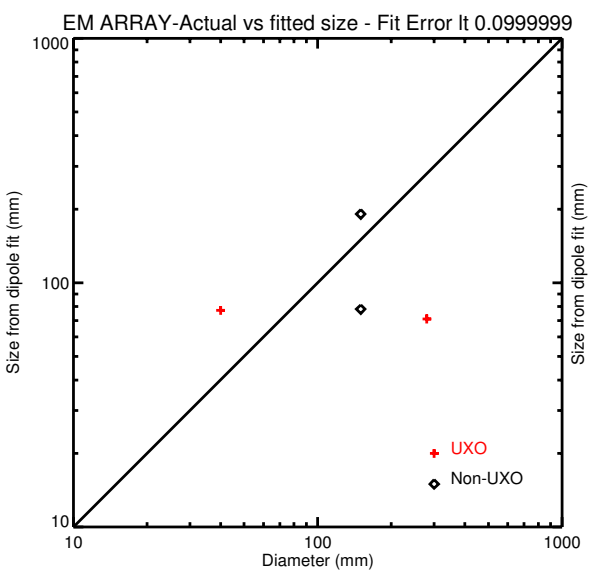
EM ARRAY-Actual vs fitted size - Fit Error lt 0.0999999
Size from dipole fit (mm)
Diameter (mm)
1000
100
10
10
100
1000
UXO
Non-UXO

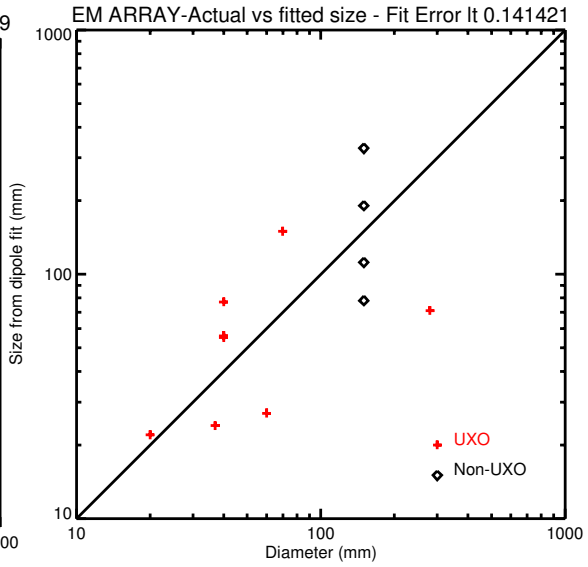
EM ARRAY-Actual vs fitted size - Fit Error lt 0.141421
Size from dipole fit (mm)
Diameter (mm)
1000
100
10
10
100
1000
UXO
Non-UXO

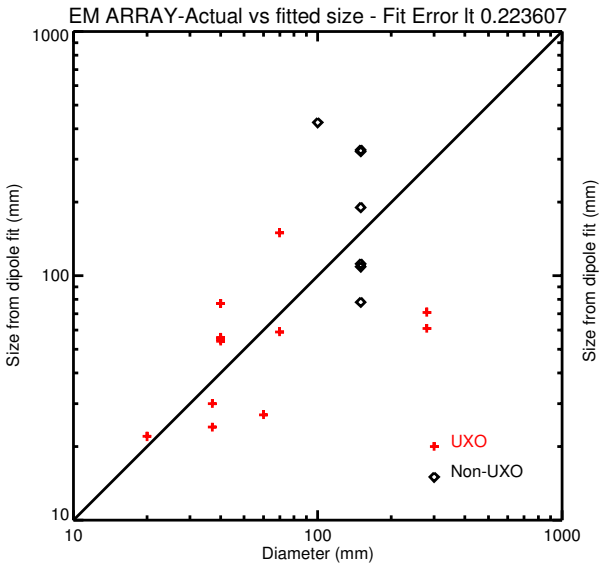
EM ARRAY-Actual vs fitted size - Fit Error lt 0.223607
Size from dipole fit (mm)
Diameter (mm)
1000
100
10
10
100
1000
UXO
Non-UXO

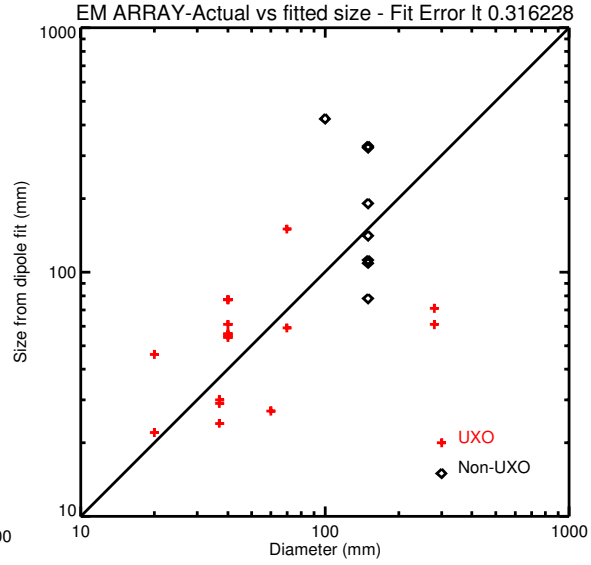
EM ARRAY-Actual vs fitted size - Fit Error lt 0.316228
Size from dipole fit (mm)
Diameter (mm)
1000
100
10
10
100
1000
UXO
Non-UXO

Depth

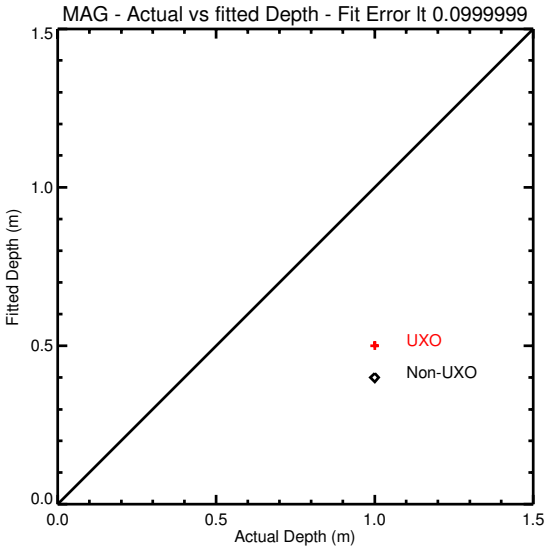
MAG - Actual vs fitted Depth - Fit Error lt 0.0999999
Fitted Depth (m)
Actual Depth (m)
0.0
0.5
1.0
1.5
UXO
Non-UXO

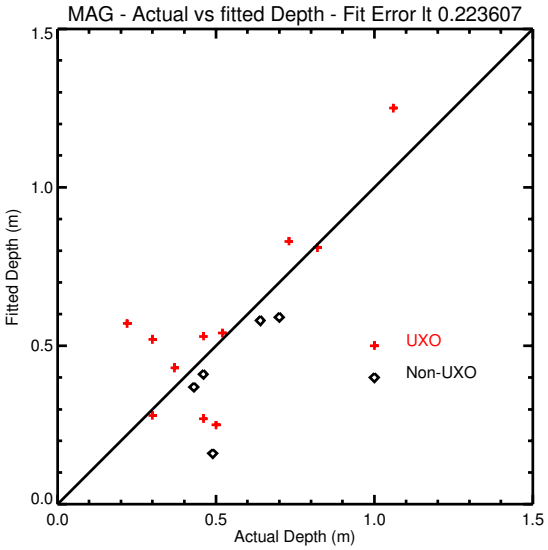
MAG - Actual vs fitted Depth - Fit Error lt 0.223607
Fitted Depth (m)
Actual Depth (m)
0.0
0.5
1.0
1.5
UXO
Non-UXO

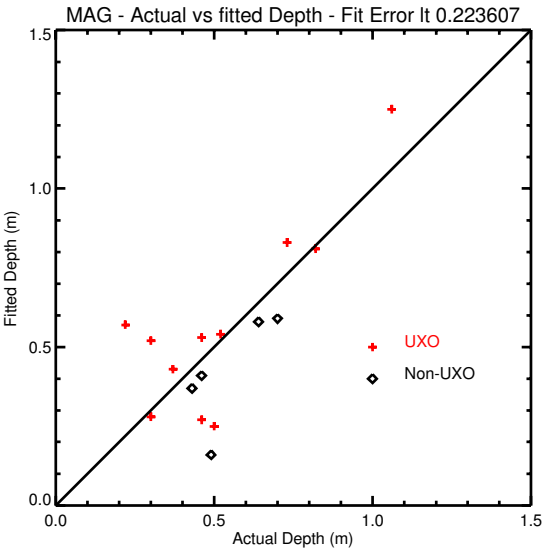
MAG - Actual vs fitted Depth - Fit Error lt 0.223607
Fitted Depth (m)
Actual Depth (m)
0.0
0.5
1.0
1.5
UXO
Non-UXO

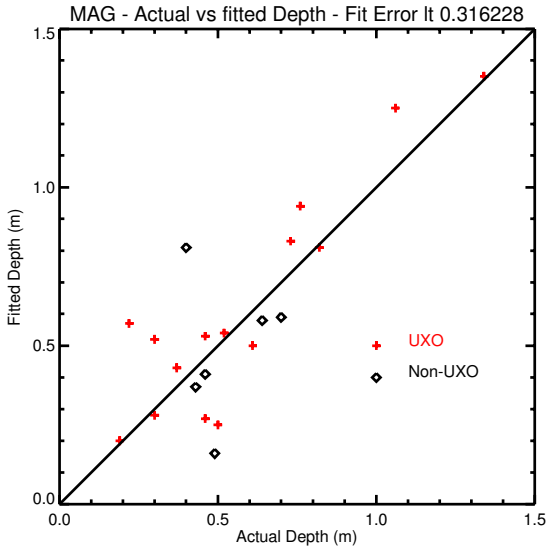
MAG - Actual vs fitted Depth - Fit Error lt 0.316228
Fitted Depth (m)
Actual Depth (m)
0.0
0.5
1.0
1.5
UXO
Non-UXO

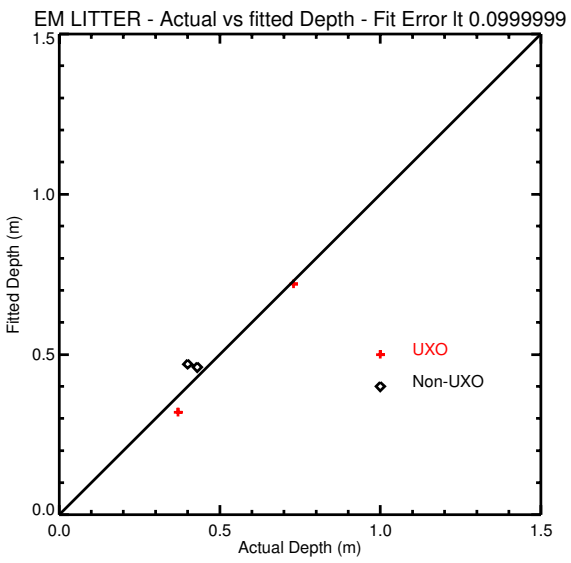
EM LITTER - Actual vs fitted Depth - Fit Error lt 0.0999999
Fitted Depth (m)
Actual Depth (m)
0.0
0.5
1.0
1.5
UXO
Non-UXO

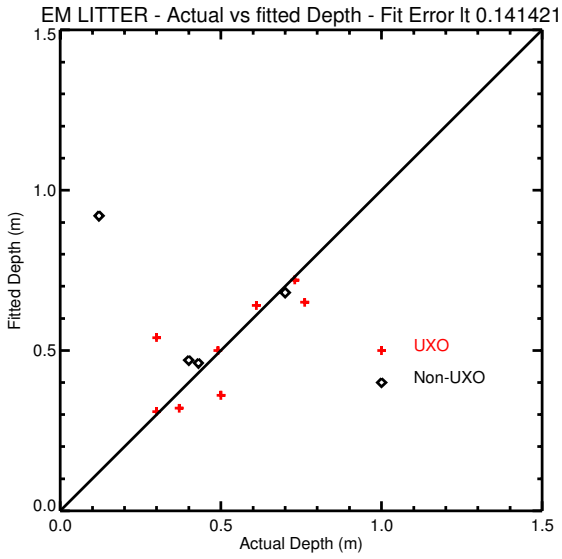
EM LITTER - Actual vs fitted Depth - Fit Error lt 0.141421
Fitted Depth (m)
Actual Depth (m)
0.0
0.5
1.0
1.5
UXO
Non-UXO

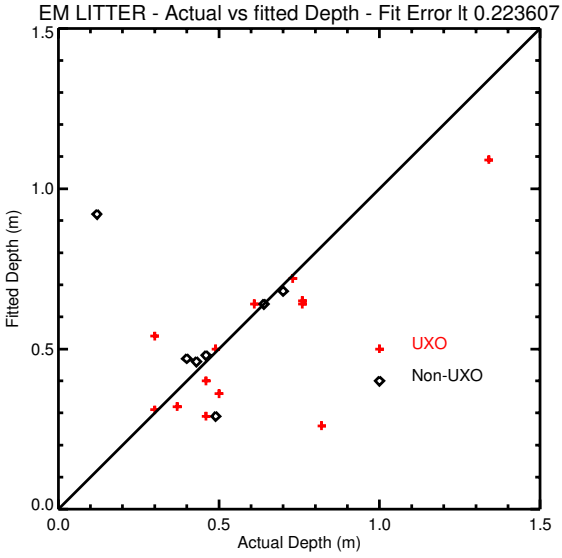
EM LITTER - Actual vs fitted Depth - Fit Error lt 0.223607
Fitted Depth (m)
Actual Depth (m)
0.0
0.5
1.0
1.5
UXO
Non-UXO

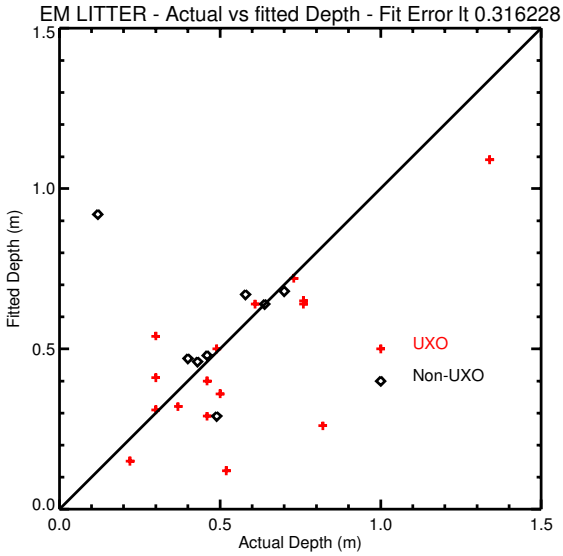
EM LITTER - Actual vs fitted Depth - Fit Error lt 0.316228
Fitted Depth (m)
Actual Depth (m)
0.0
0.5
1.0
1.5
UXO
Non-UXO

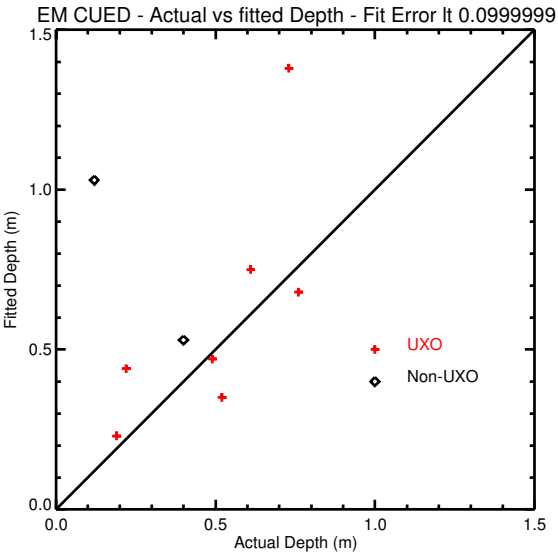
EM CUED - Actual vs fitted Depth - Fit Error lt 0.0999999
Fitted Depth (m)
Actual Depth (m)
0.0
0.5
1.0
1.5
UXO
Non-UXO

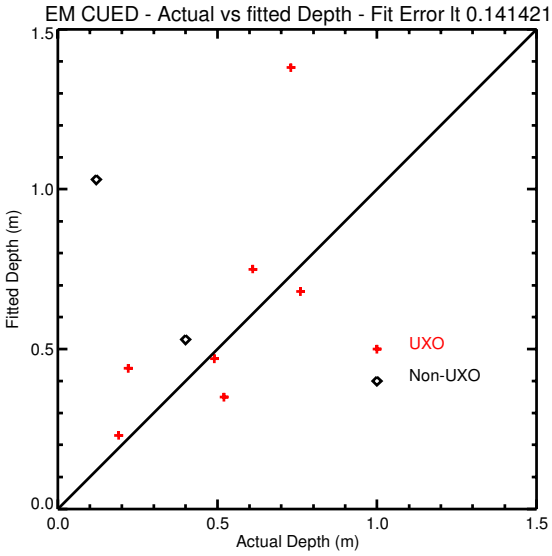
EM CUED - Actual vs fitted Depth - Fit Error lt 0.141421
Fitted Depth (m)
Actual Depth (m)
0.0
0.5
1.0
1.5
UXO
Non-UXO

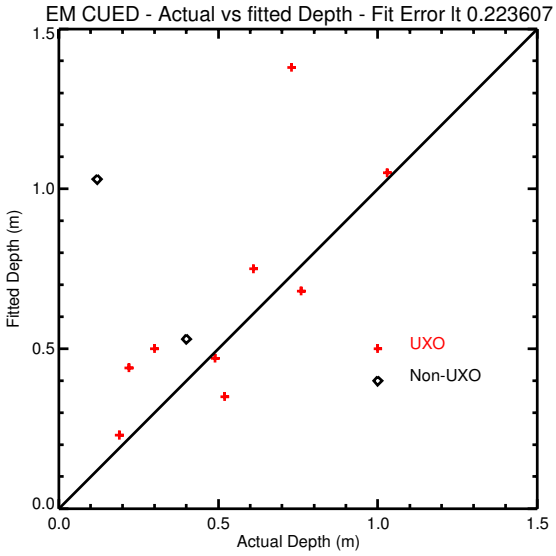
EM CUED - Actual vs fitted Depth - Fit Error lt 0.223607
Fitted Depth (m)
Actual Depth (m)
0.0
0.5
1.0
1.5
UXO
Non-UXO

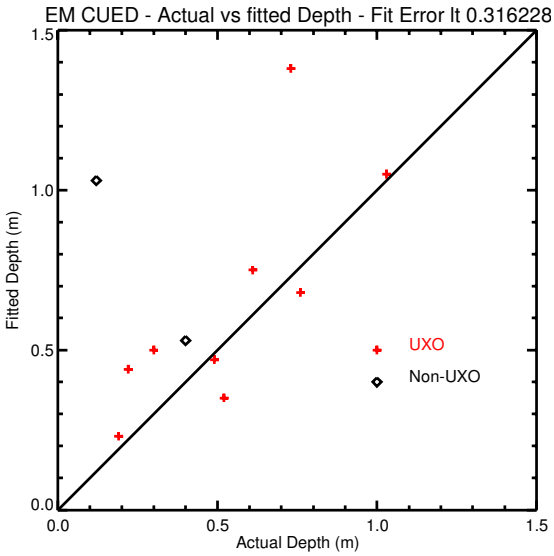
EM CUED - Actual vs fitted Depth - Fit Error lt 0.316228
Fitted Depth (m)
Actual Depth (m)
0.0
0.5
1.0
1.5
UXO
Non-UXO

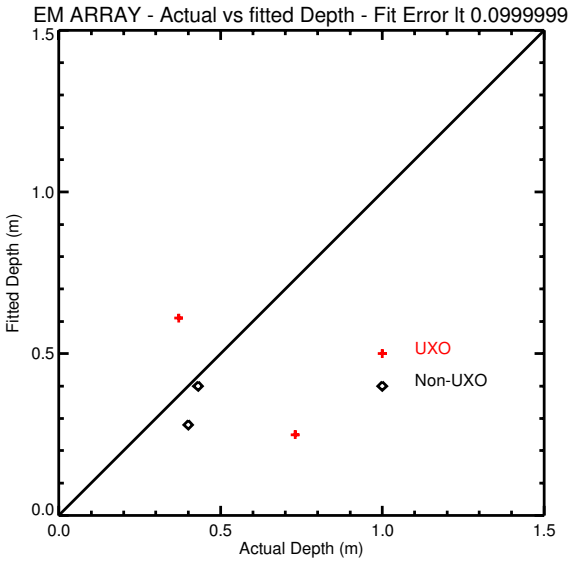
EM ARRAY - Actual vs fitted Depth - Fit Error lt 0.0999999
Fitted Depth (m)
Actual Depth (m)
0.0
0.5
1.0
1.5
UXO
Non-UXO

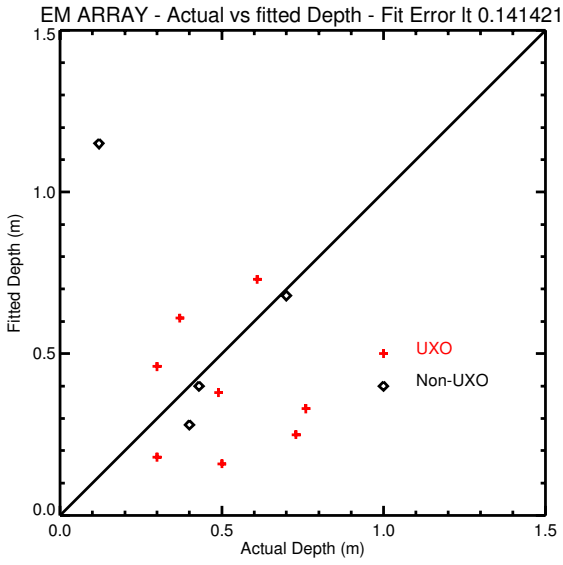
EM ARRAY - Actual vs fitted Depth - Fit Error lt 0.141421
Fitted Depth (m)
Actual Depth (m)
0.0
0.5
1.0
1.5
UXO
Non-UXO

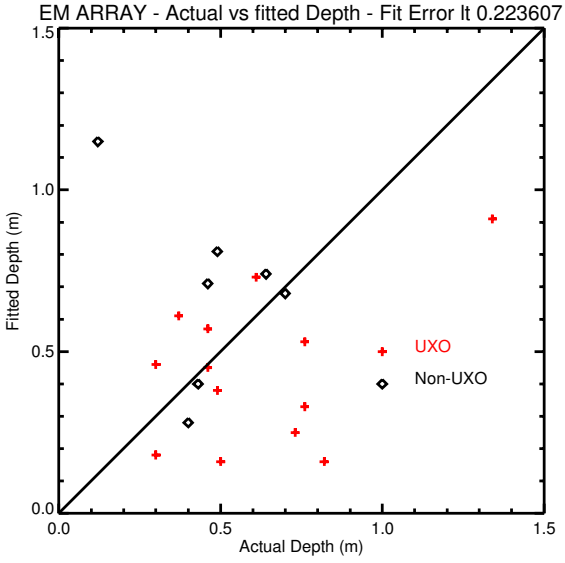
EM ARRAY - Actual vs fitted Depth - Fit Error lt 0.223607
Fitted Depth (m)
Actual Depth (m)
0.0
0.5
1.0
1.5
UXO
Non-UXO

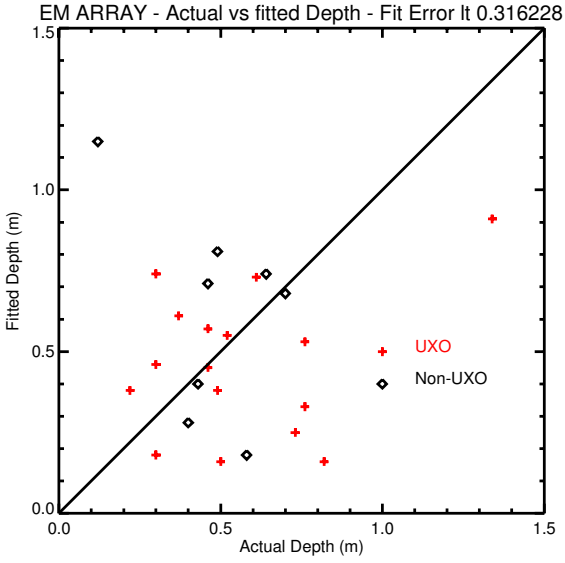
EM ARRAY - Actual vs fitted Depth - Fit Error lt 0.316228
Fitted Depth (m)
Actual Depth (m)
0.0
0.5
1.0
1.5
UXO
Non-UXO

PO Features

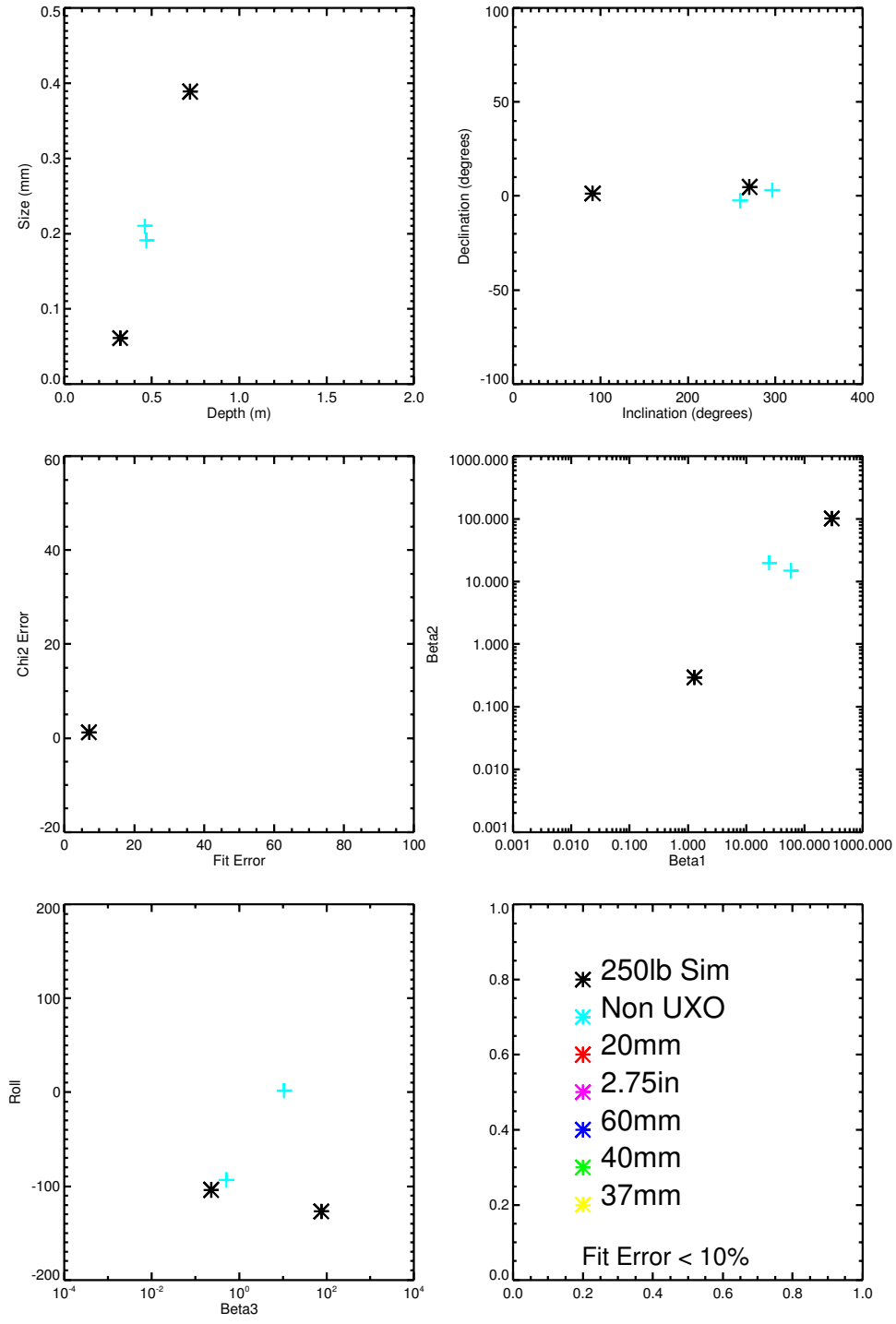
Size (mm)
Depth (m)
Declination (degrees)
Inclination (degrees)
Chi2 Error
Fit Error
Beta2
Beta1
Roll
Beta3
250lb Sim
Non UXO
20mm
2.75in
60mm
40mm
37mm
Fit Error < 10%

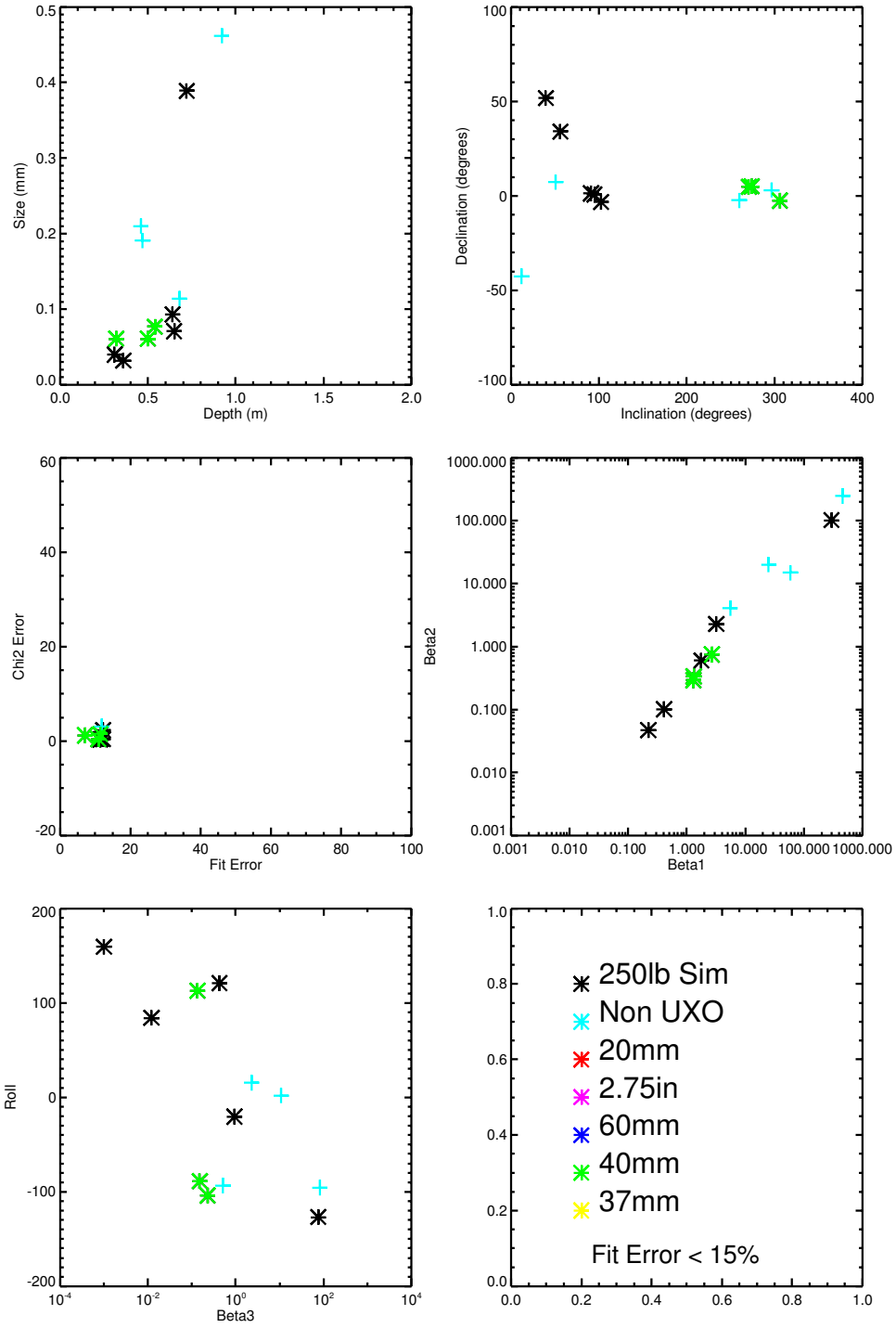
Size (mm)
Depth (m)
Declination (degrees)
Inclination (degrees)
Chi2 Error
Fit Error
Beta2
Beta1
Roll
Beta3
250lb Sim
Non UXO
20mm
2.75in
60mm
40mm
37mm
Fit Error < 15%

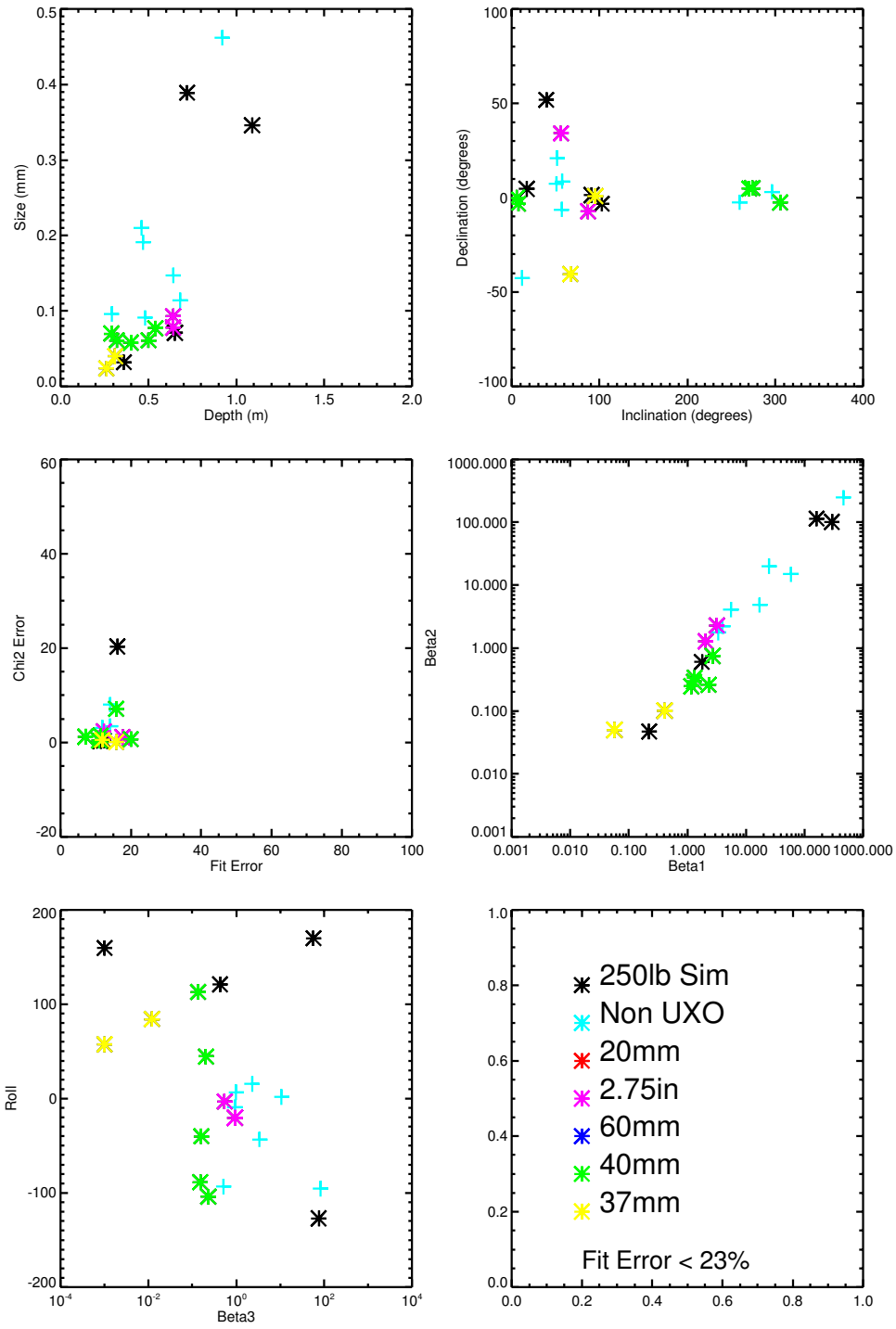
Size (mm)
Depth (m)
Declination (degrees)
Inclination (degrees)
Chi2 Error
Fit Error
Beta2
Beta1
Roll
Beta3
250lb Sim
Non UXO
20mm
2.75in
60mm
40mm
37mm
Fit Error < 23%

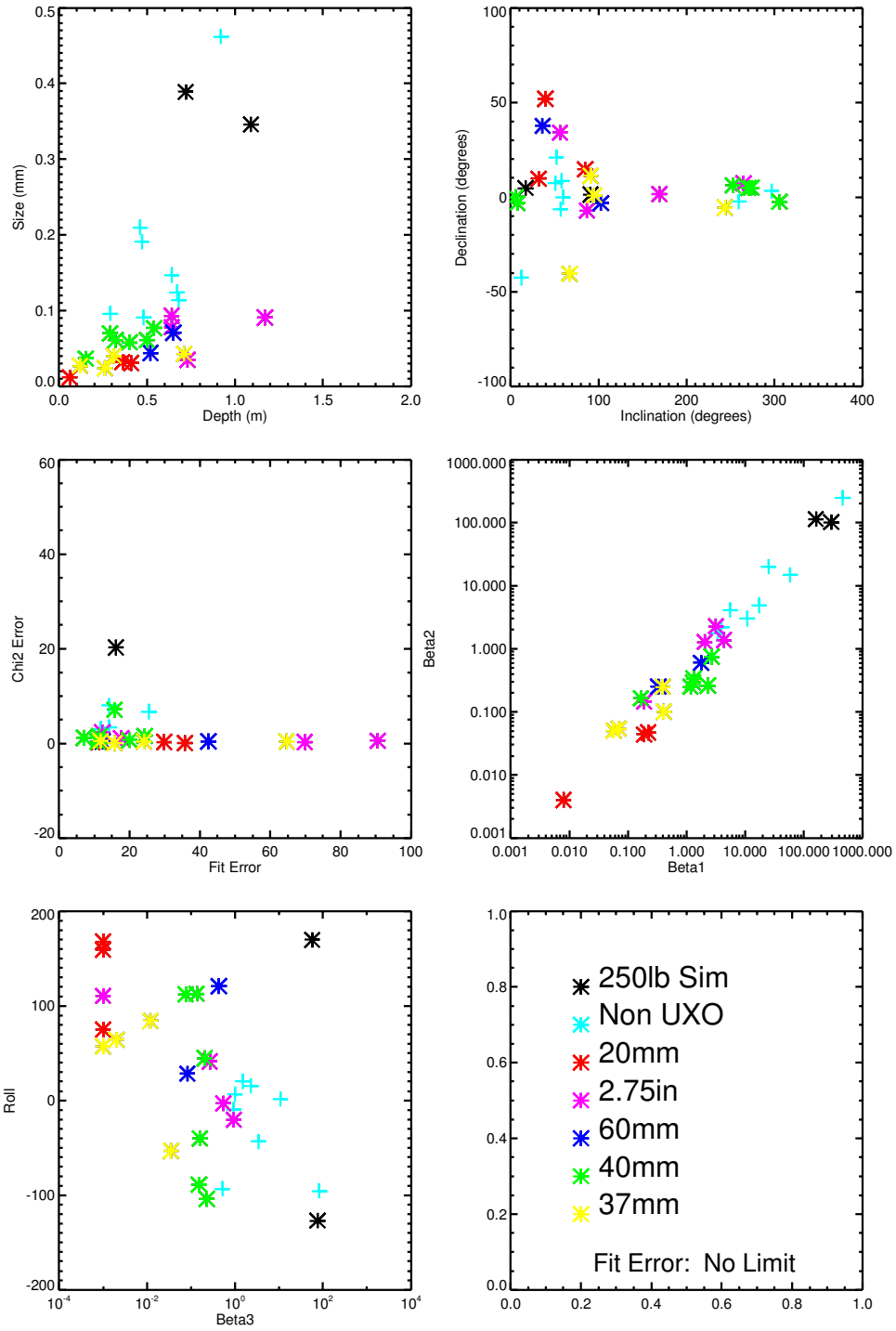
Size (mm)
Depth (m)
Declination (degrees)
Inclination (degrees)
Chi2 Error
Fit Error
Beta2
Beta1
Roll
Beta3
250lb Sim
Non UXO
20mm
2.75in
60mm
40mm
37mm
Fit Error: No Limit

Polarizabilities

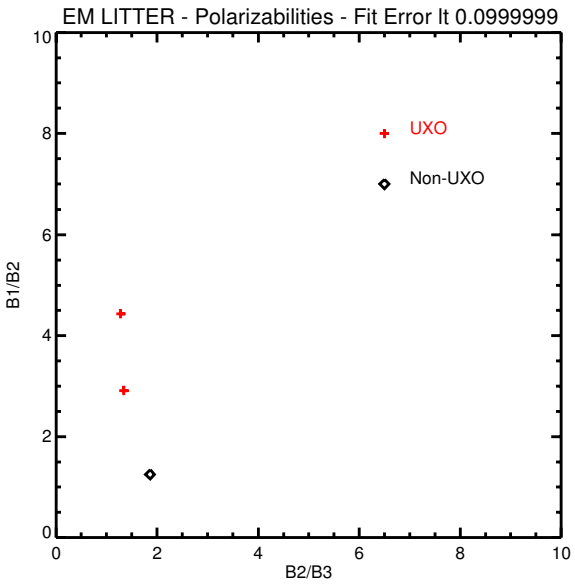

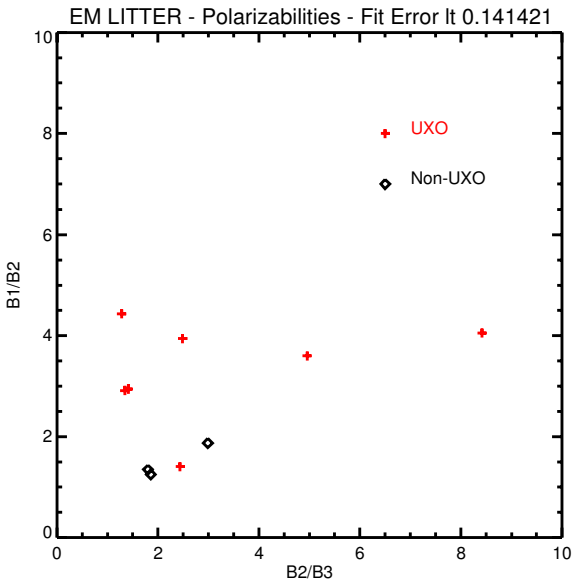

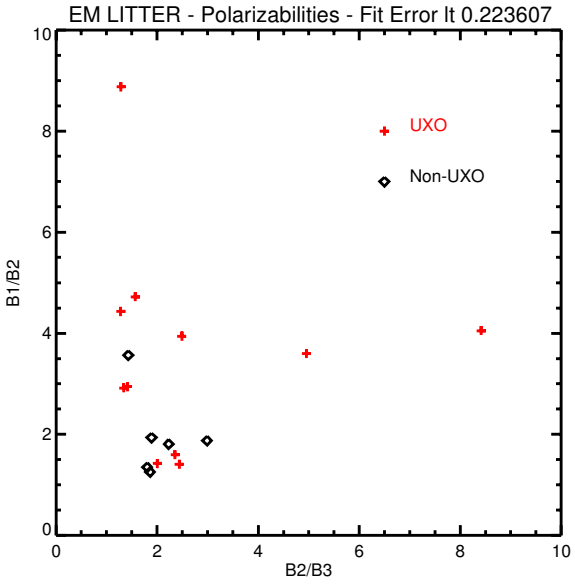

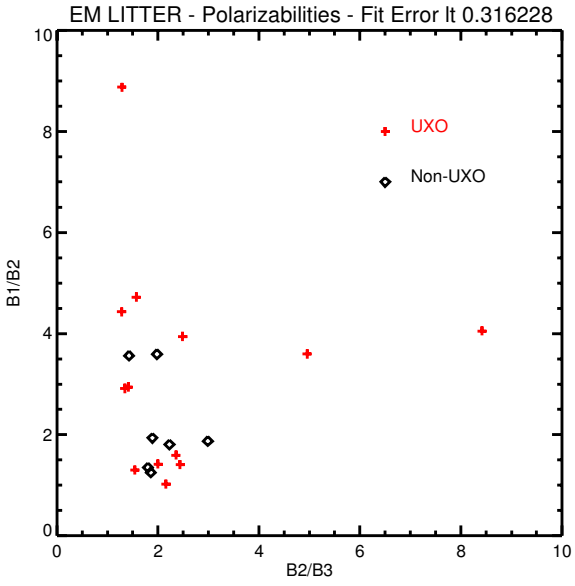

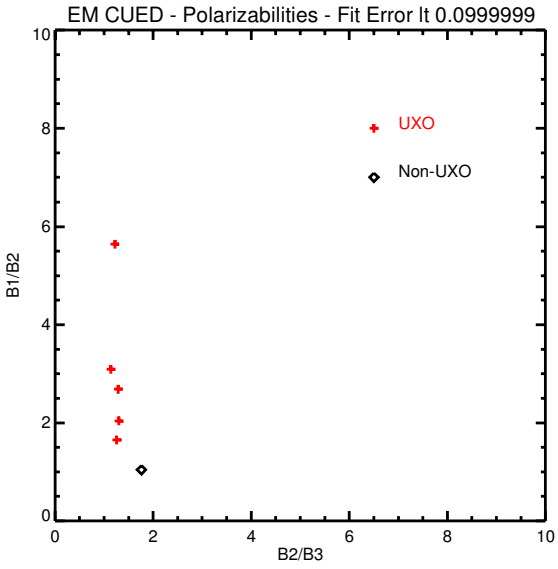
EM CUED - Polarizabilities - Fit Error lt 0.0999999
UXO
Non-UXO
B1/B2
B2/B3
0
2
4
6
8
10

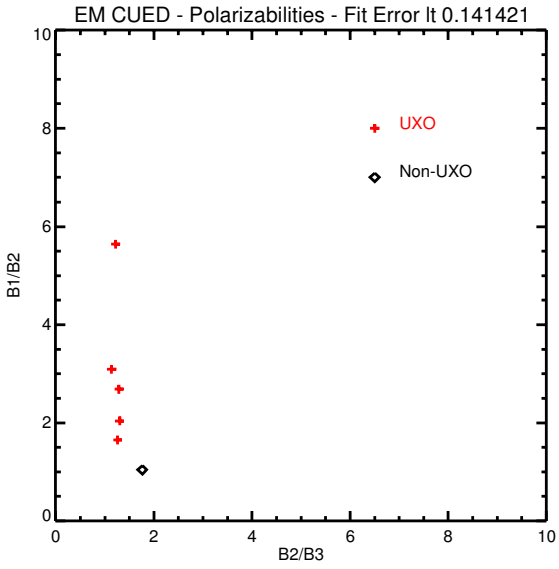
EM CUED - Polarizabilities - Fit Error lt 0.141421
UXO
Non-UXO
B1/B2
B2/B3
0
2
4
6
8
10

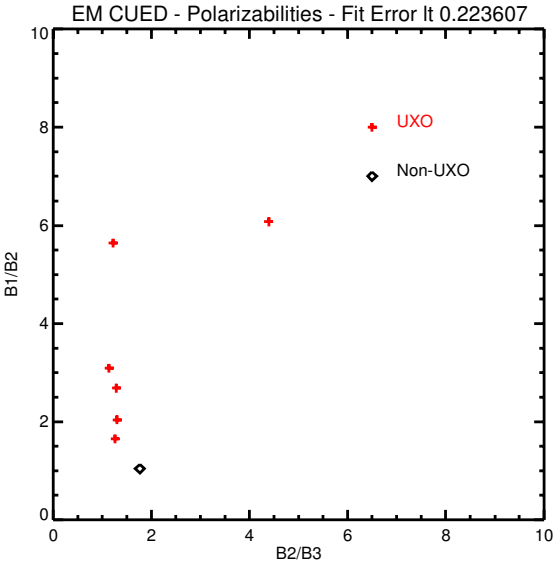
EM CUED - Polarizabilities - Fit Error lt 0.223607
UXO
Non-UXO
B1/B2
B2/B3
0
2
4
6
8
10

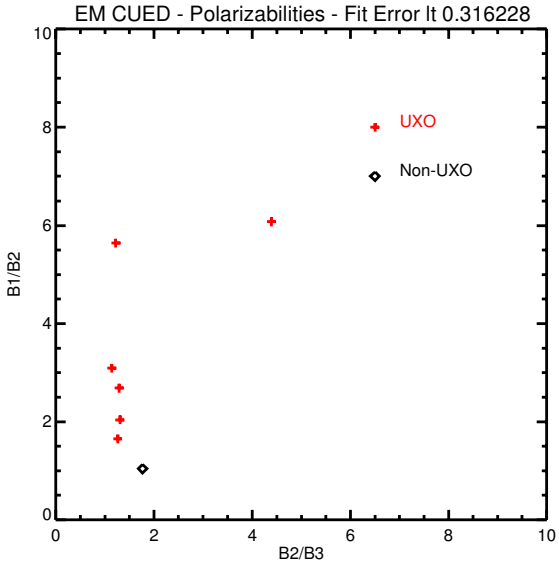
EM CUED - Polarizabilities - Fit Error lt 0.316228
UXO
Non-UXO
B1/B2
B2/B3
0
2
4
6
8
10

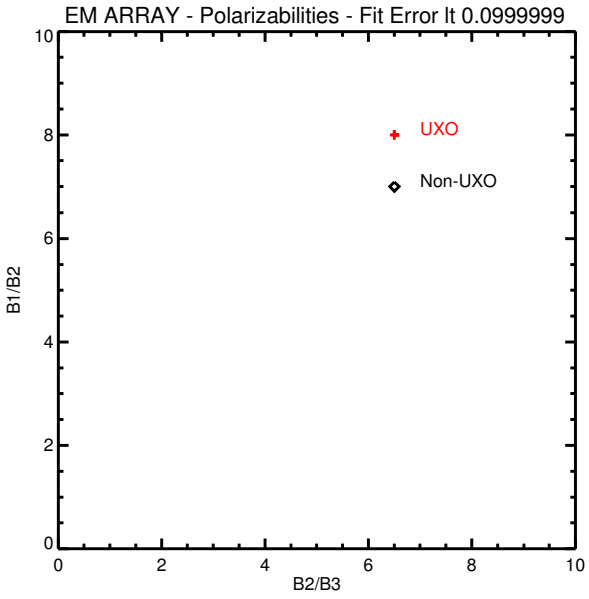
EM ARRAY - Polarizabilities - Fit Error lt 0.0999999
UXO
Non-UXO
B1/B2
B2/B3
0
2
4
6
8
10

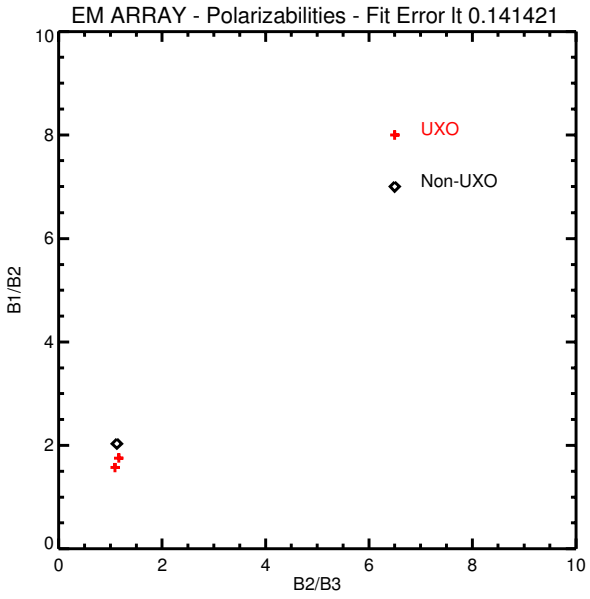
EM ARRAY - Polarizabilities - Fit Error lt 0.141421
UXO
Non-UXO
B1/B2
B2/B3
0
2
4
6
8
10

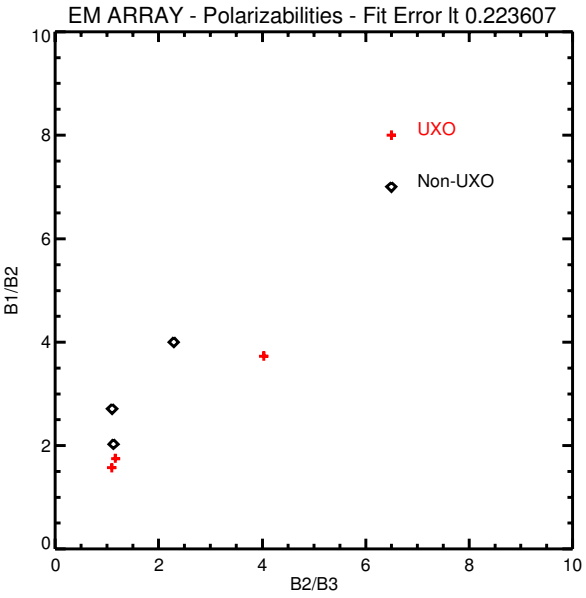
EM ARRAY - Polarizabilities - Fit Error lt 0.223607
UXO
Non-UXO
B1/B2
B2/B3
0
2
4
6
8
10

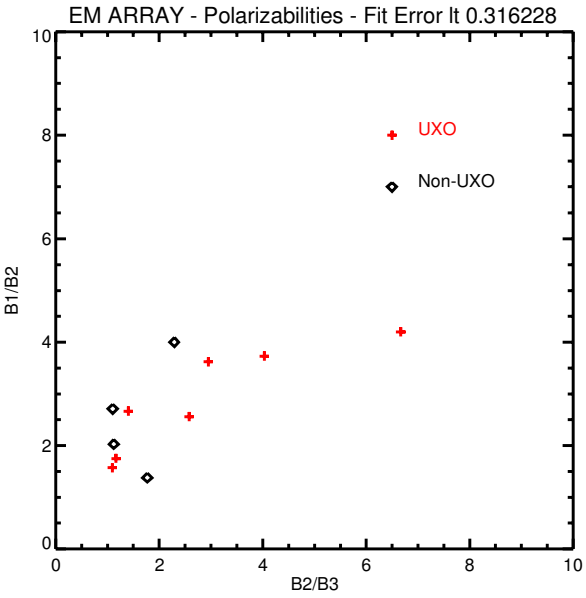
EM ARRAY - Polarizabilities - Fit Error lt 0.316228
UXO
Non-UXO
B1/B2
B2/B3
0
2
4
6
8
10

Appendix B - Parameter Estimates from the CT-3A Survey Area

CT-3A Fitted Feature Distributions

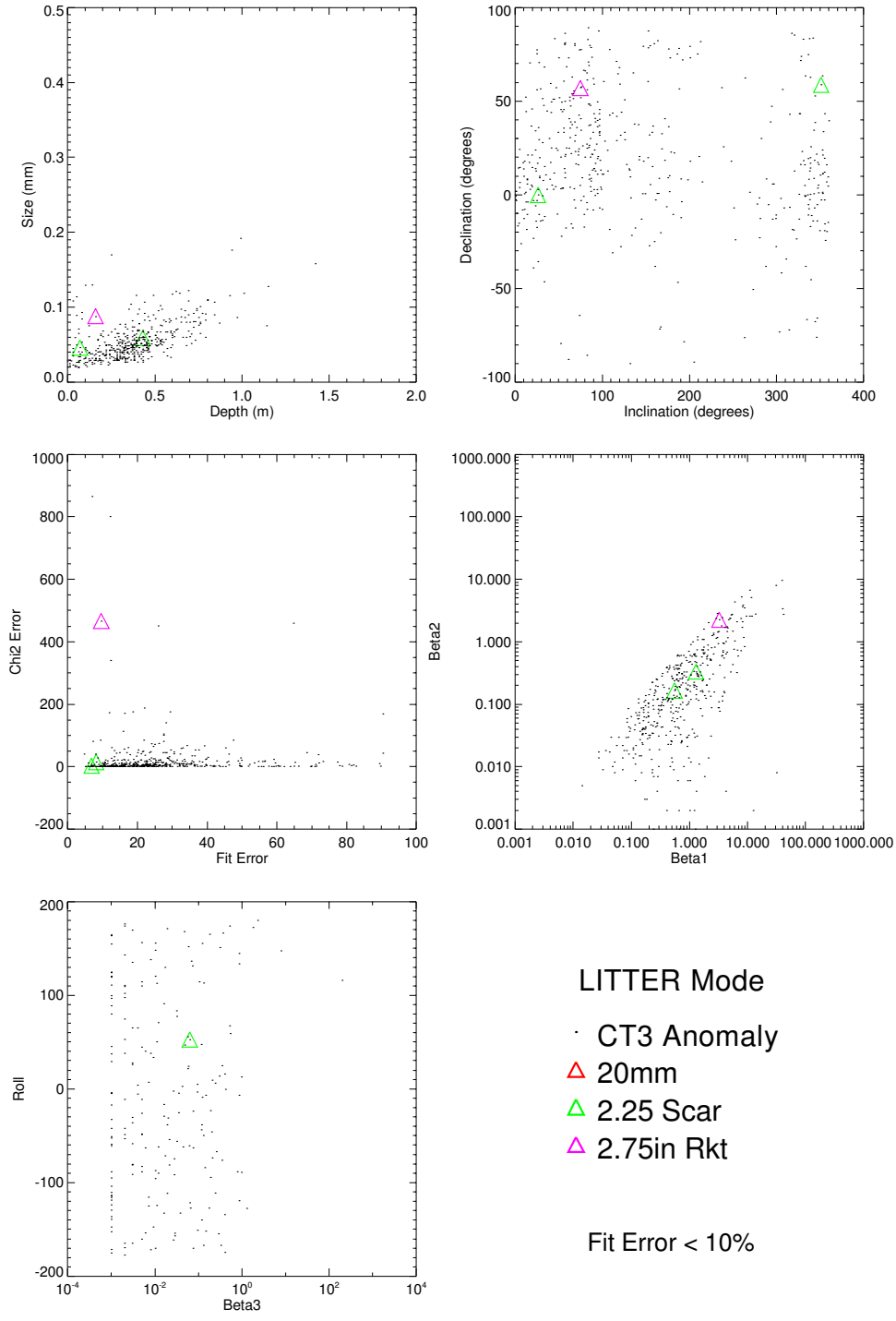

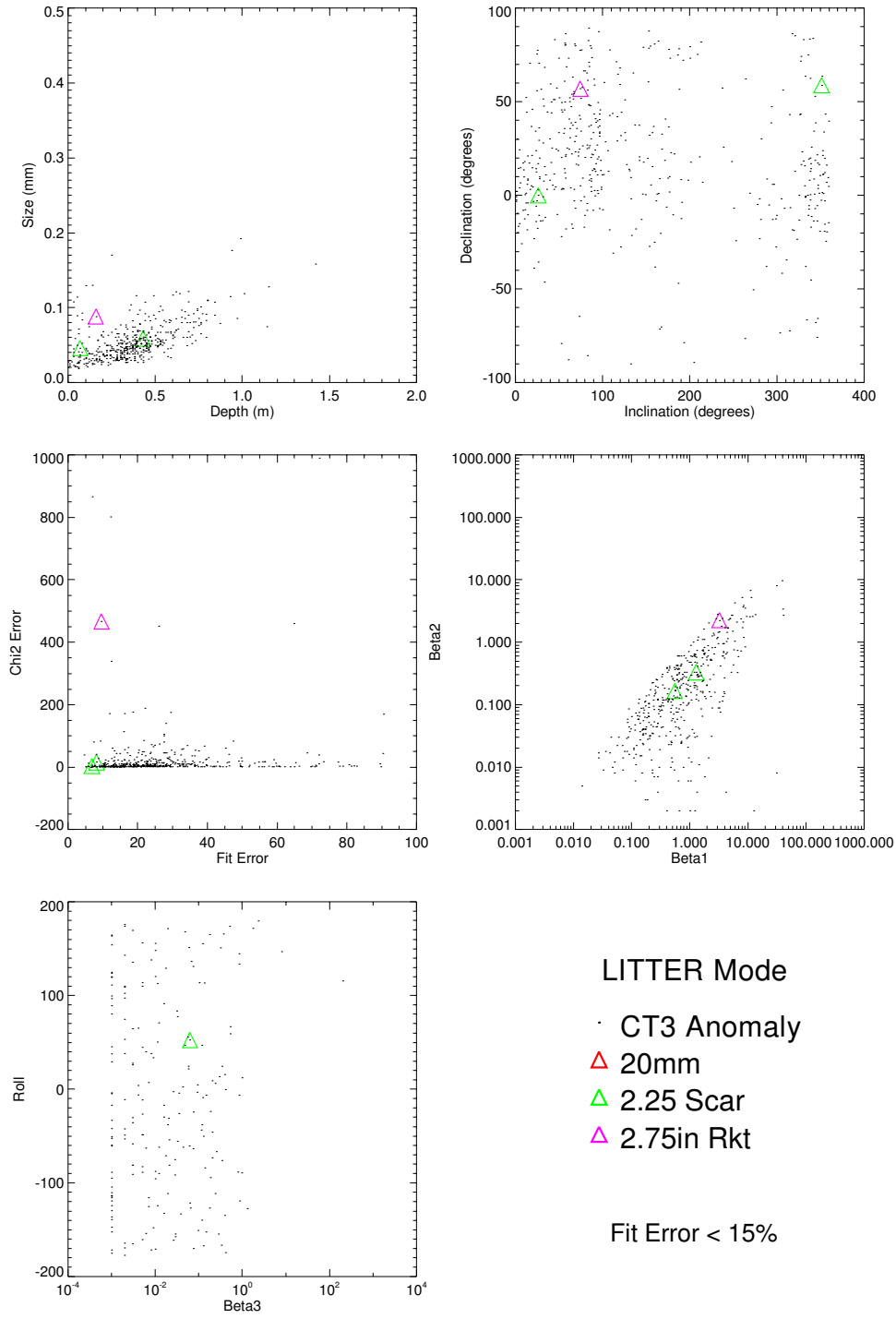
Size (mm)
Depth (m)
Declination (degrees)
Inclination (degrees)
Chi2 Error
Fit Error
Beta2
Beta1
Roll
Beta3
LITTER Mode
CT3 Anomaly
20mm
2.25 Scar
2.75in Rkt
Fit Error < 15%

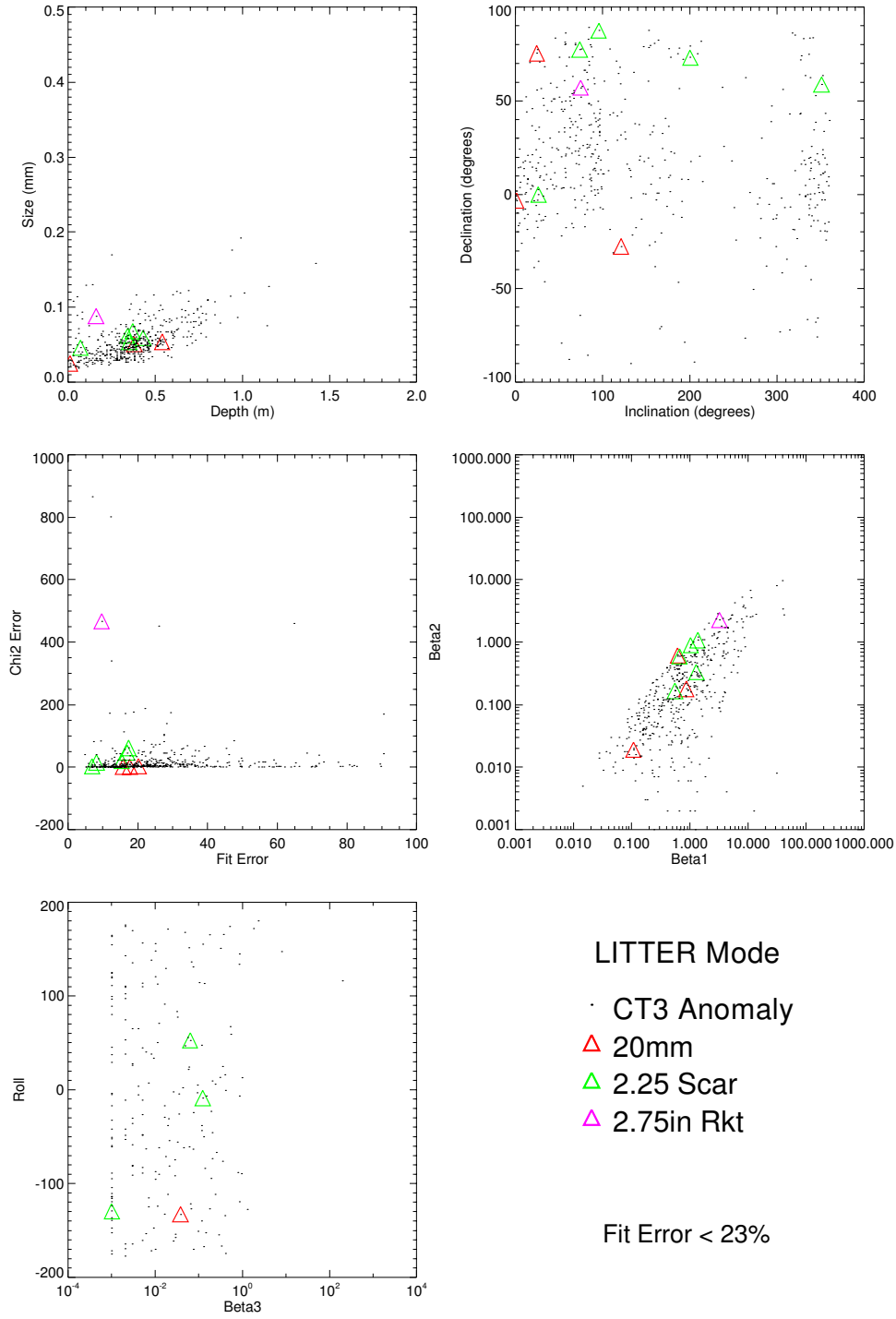
Size (mm)
Depth (m)
Declination (degrees)
Inclination (degrees)
Chi2 Error
Fit Error
Beta2
Beta1
Roll
Beta3
LITTER Mode
CT3 Anomaly
20mm
2.25 Scar
2.75in Rkt
Fit Error < 23%

Appendix C – Litter mode EMI data for Cued Targets

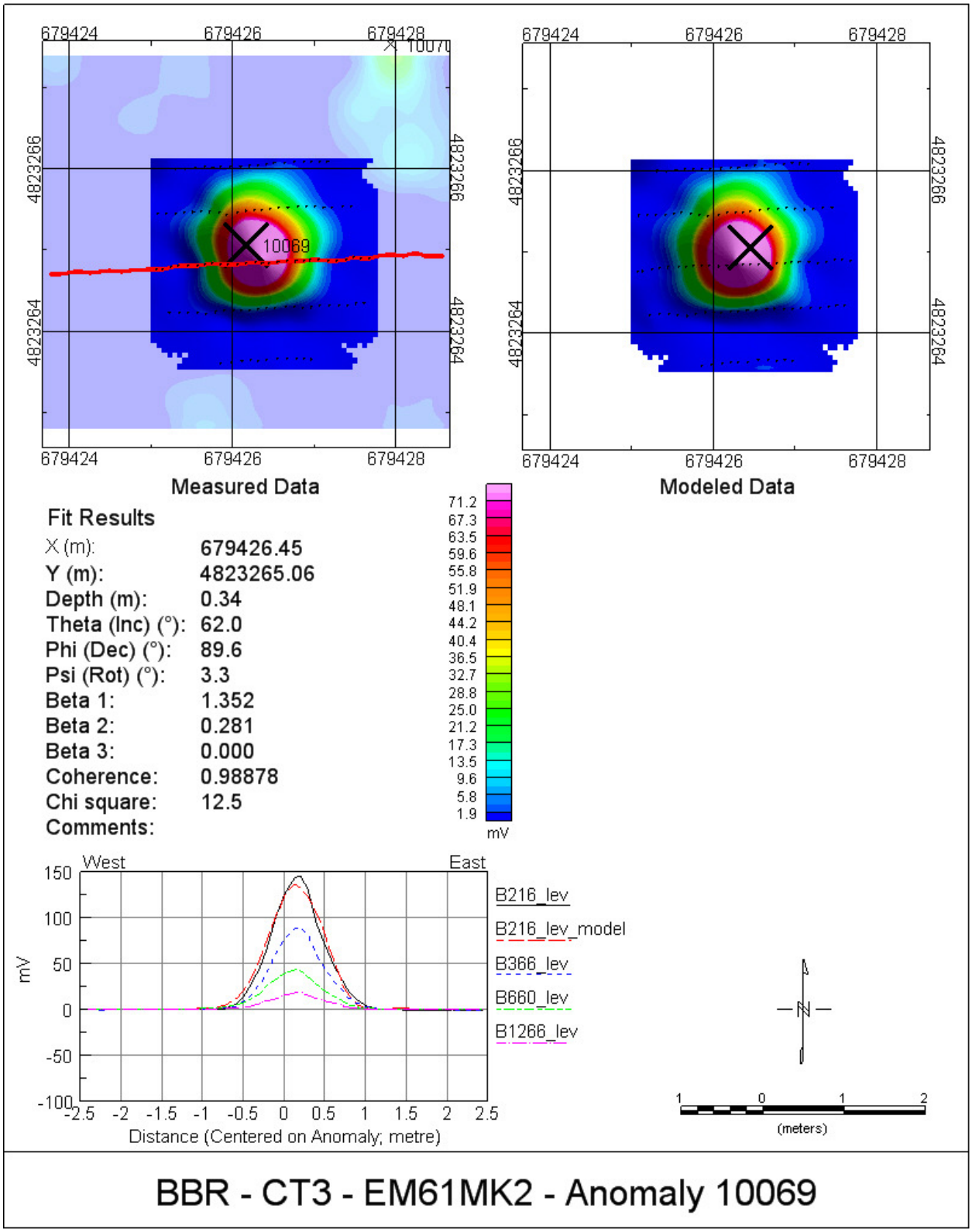

BBR - CT3 - EM61MK2 - Anomaly 10069

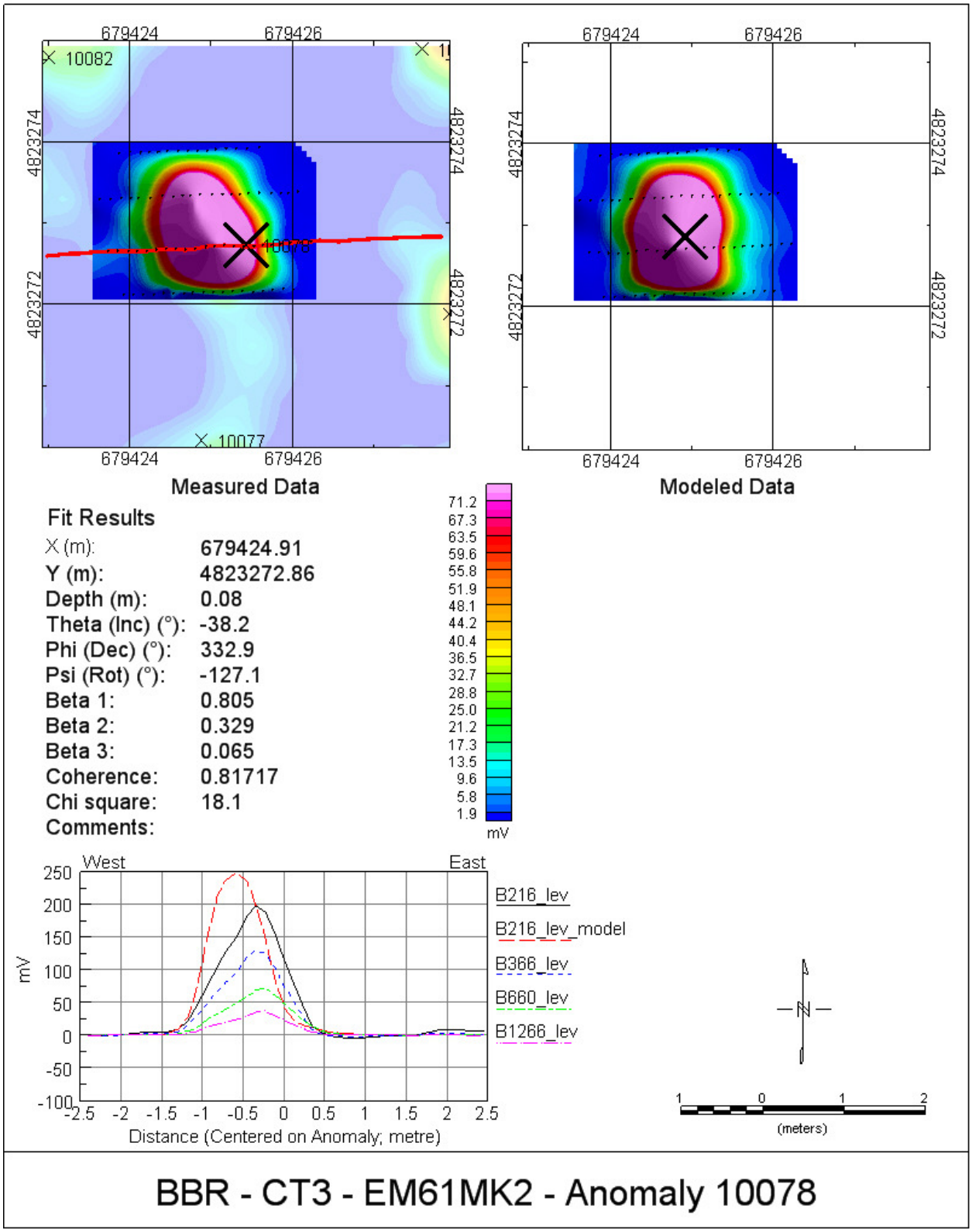

BBR - CT3 - EM61MK2 - Anomaly 10078

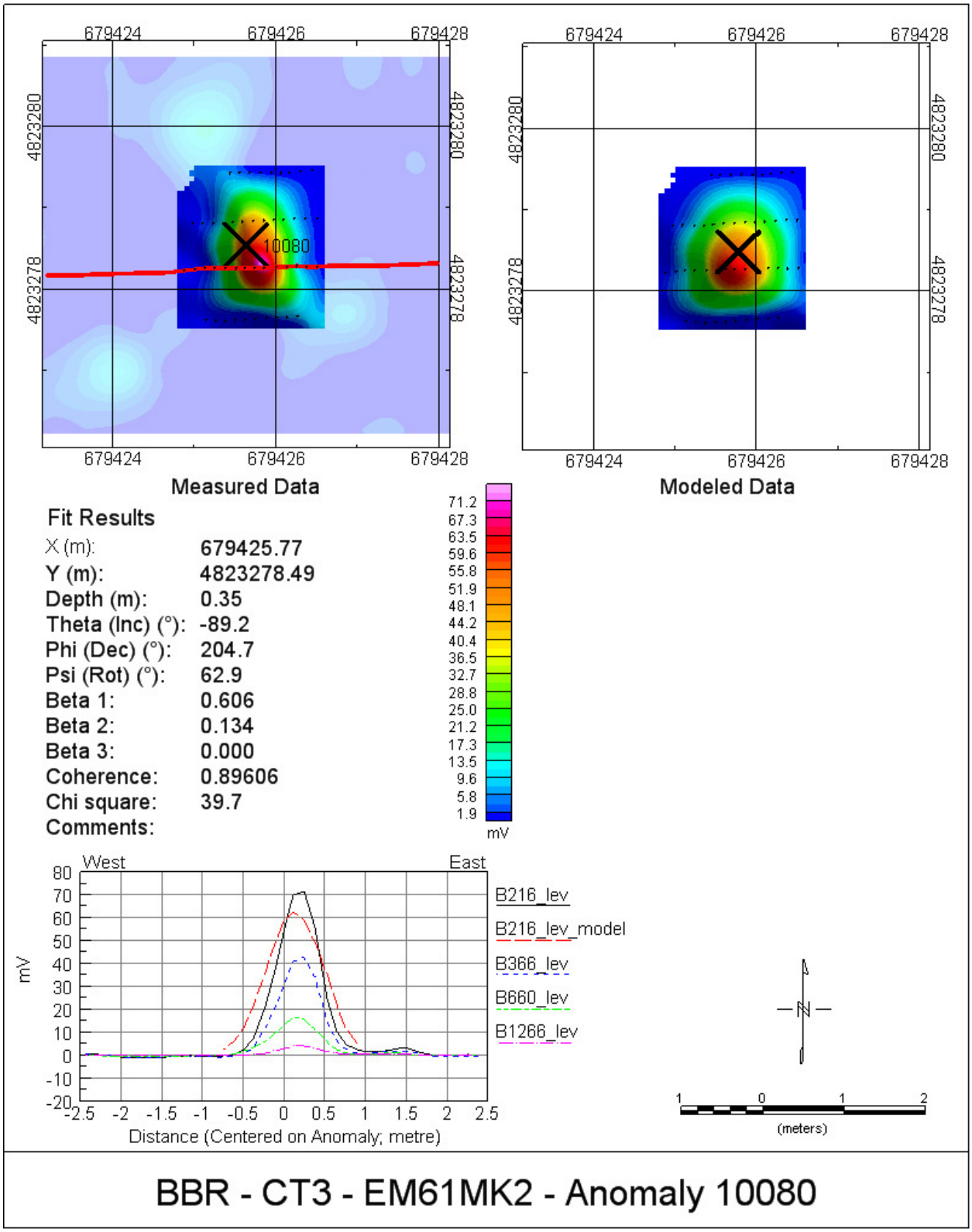

BBR - CT3 - EM61MK2 - Anomaly 10080

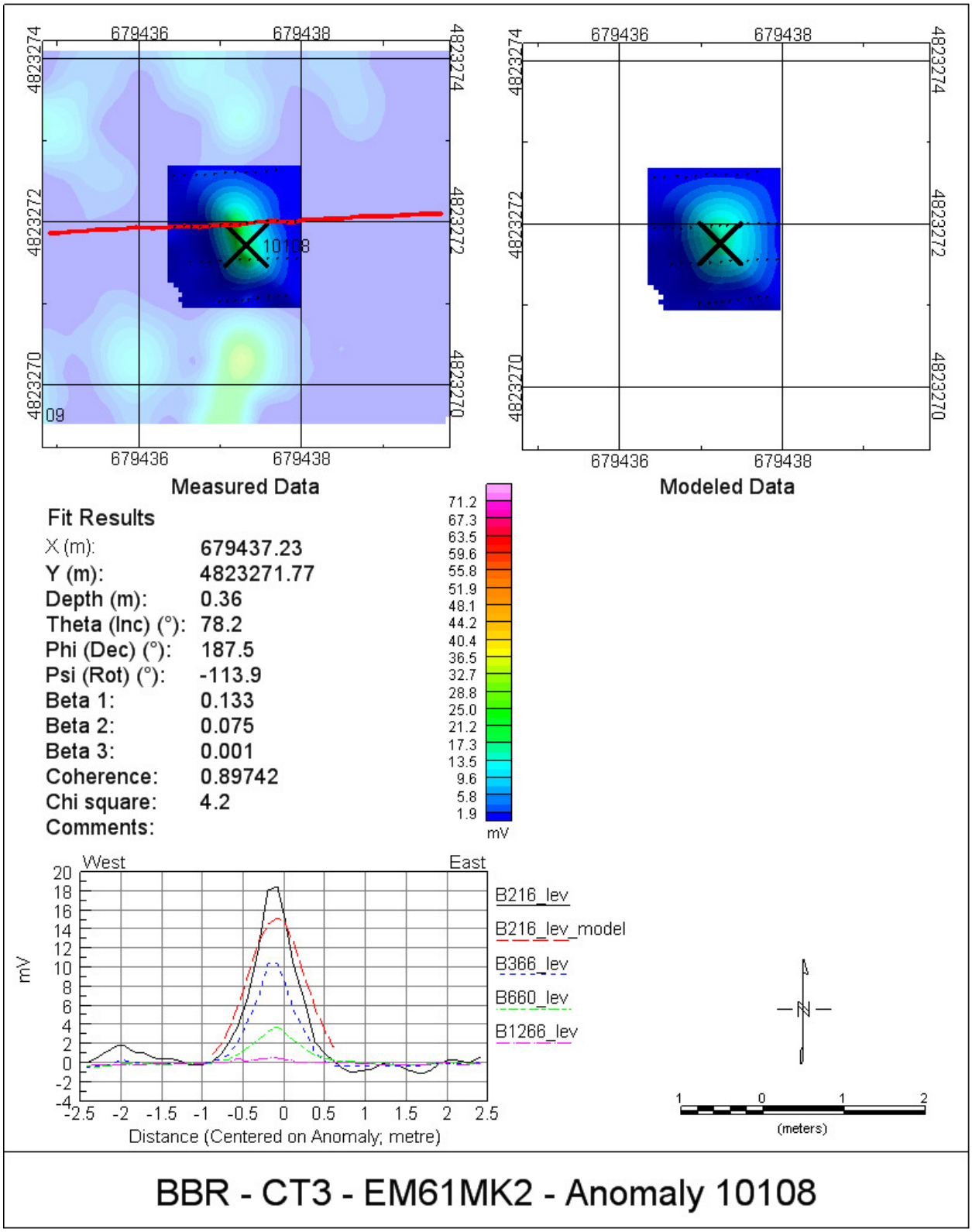

BBR - CT3 - EM61MK2 - Anomaly 10108

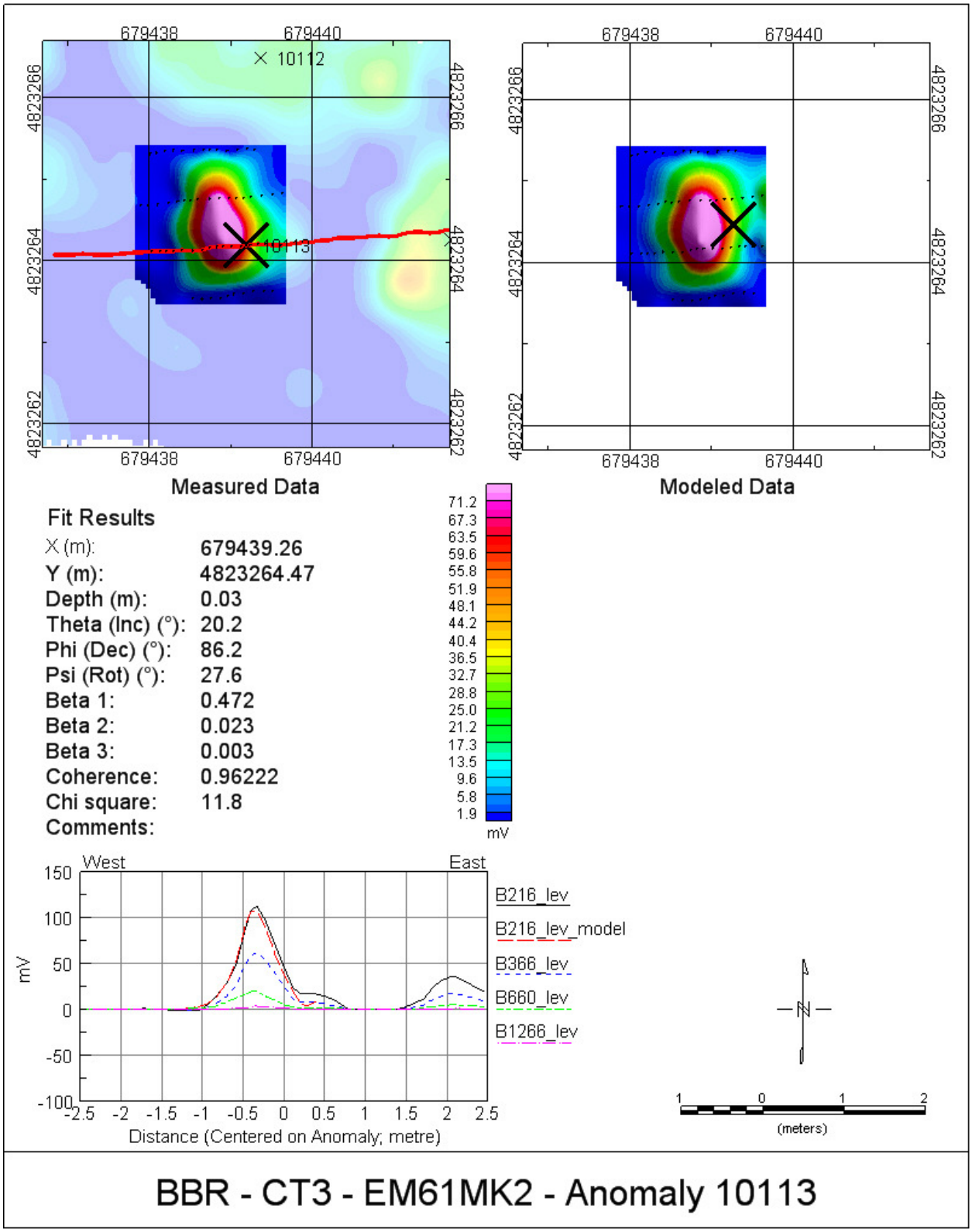

BBR - CT3 - EM61MK2 - Anomaly 10113

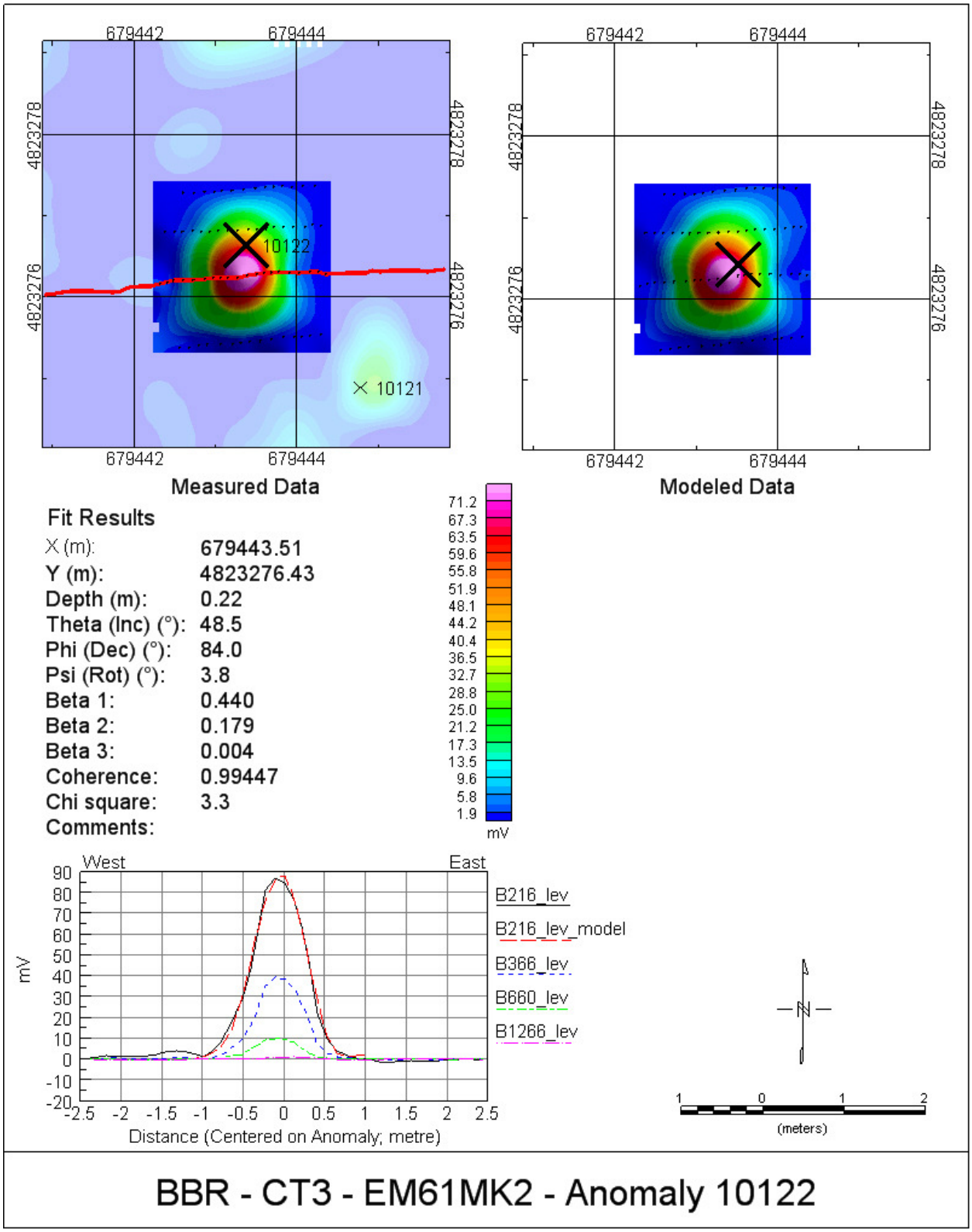

BBR - CT3 - EM61MK2 - Anomaly 10122

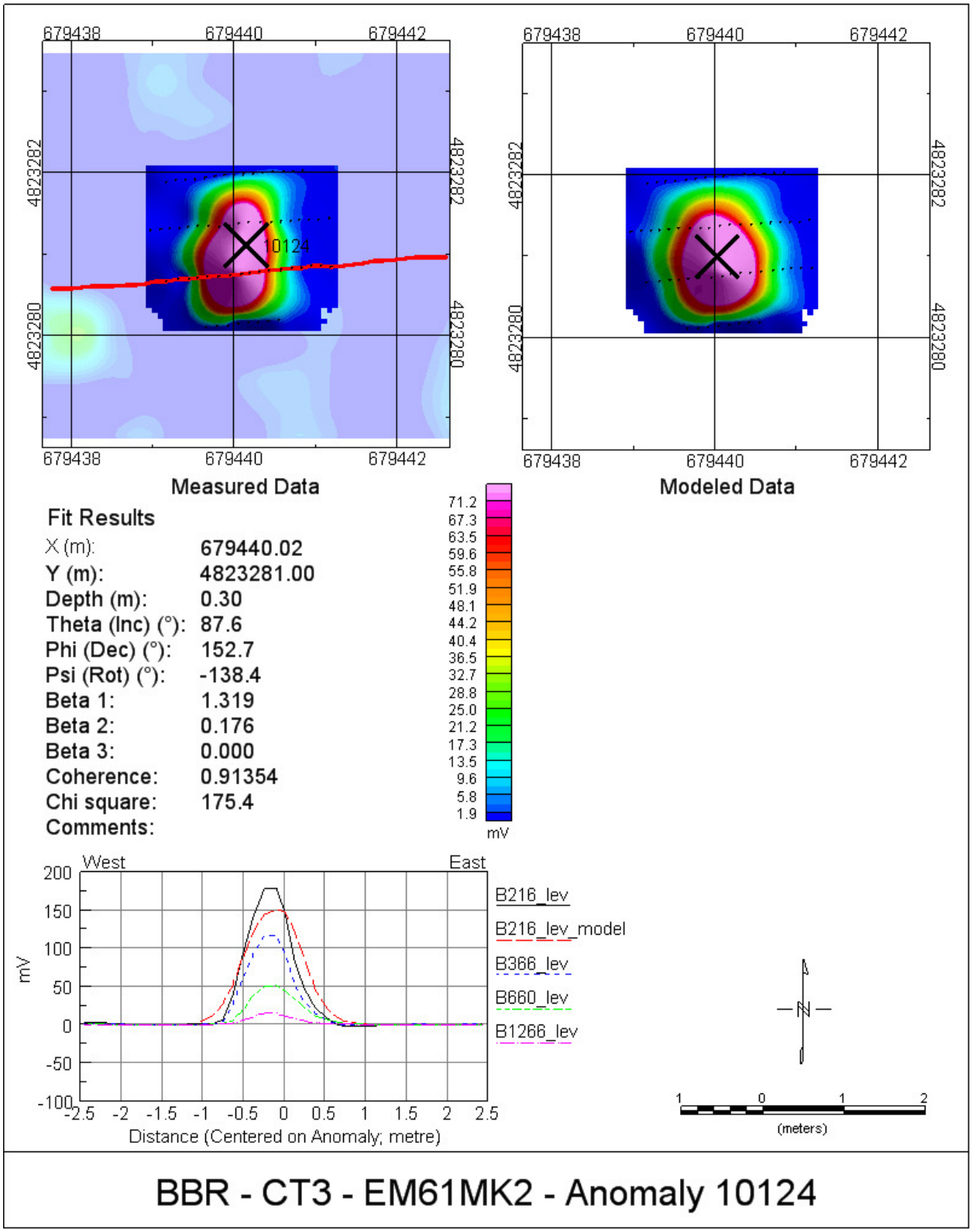

BBR - CT3 - EM61MK2 - Anomaly 10124

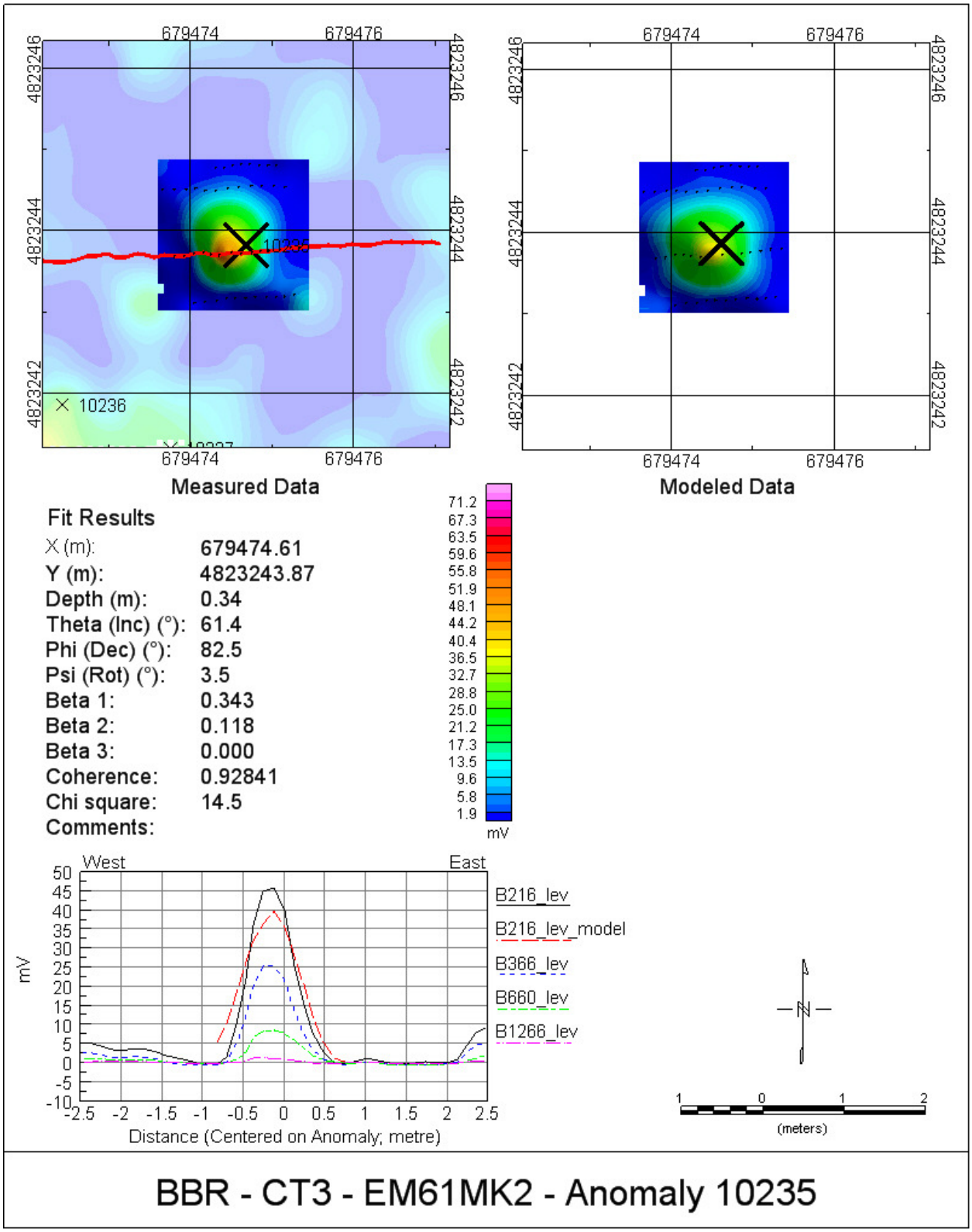

BBR - CT3 - EM61MK2 - Anomaly 10235

Appendix D – Towed Array EMI data for Cued Targets

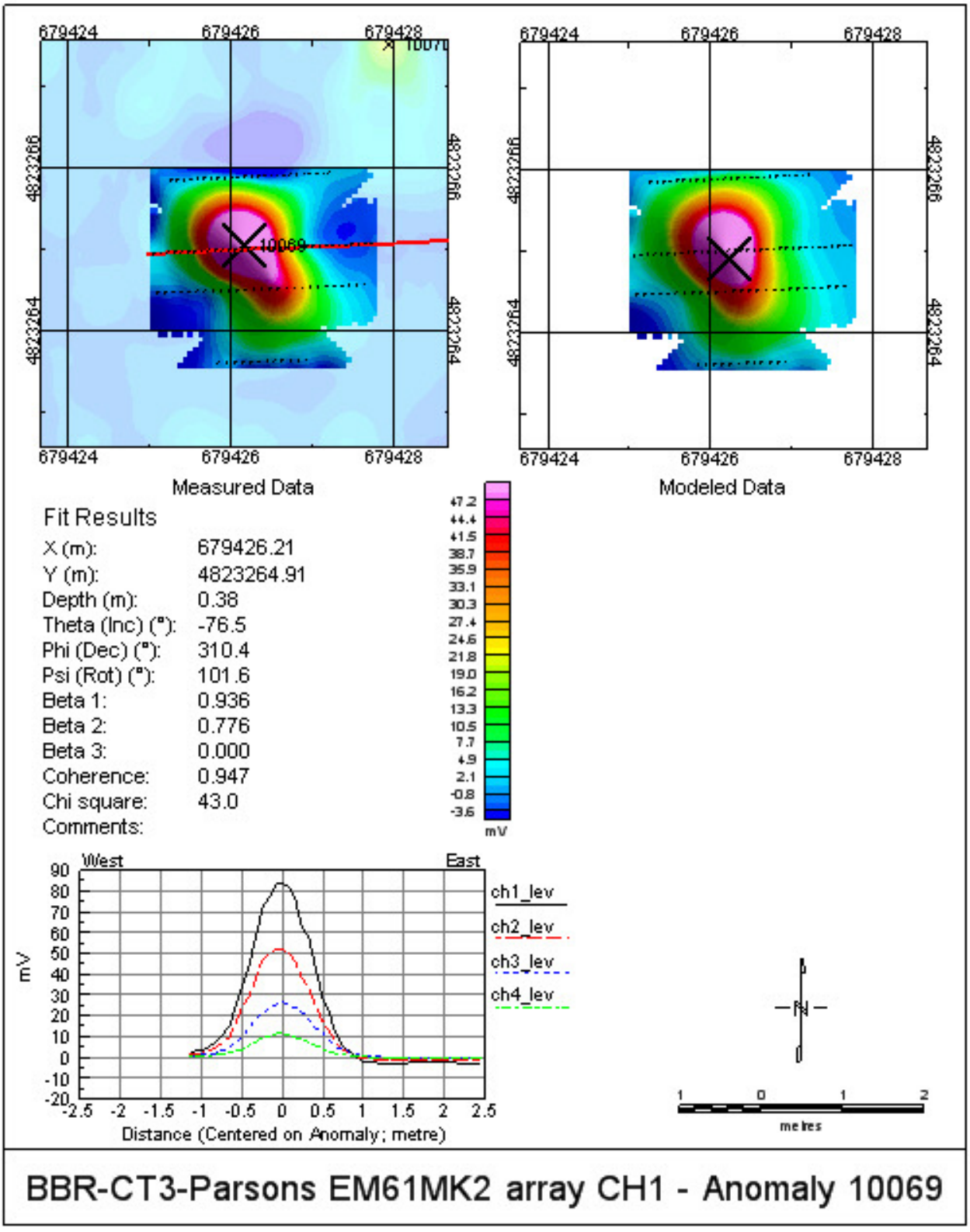

BBR-CT3-Parsons EM61MK2 array CH1 - Anomaly 10069

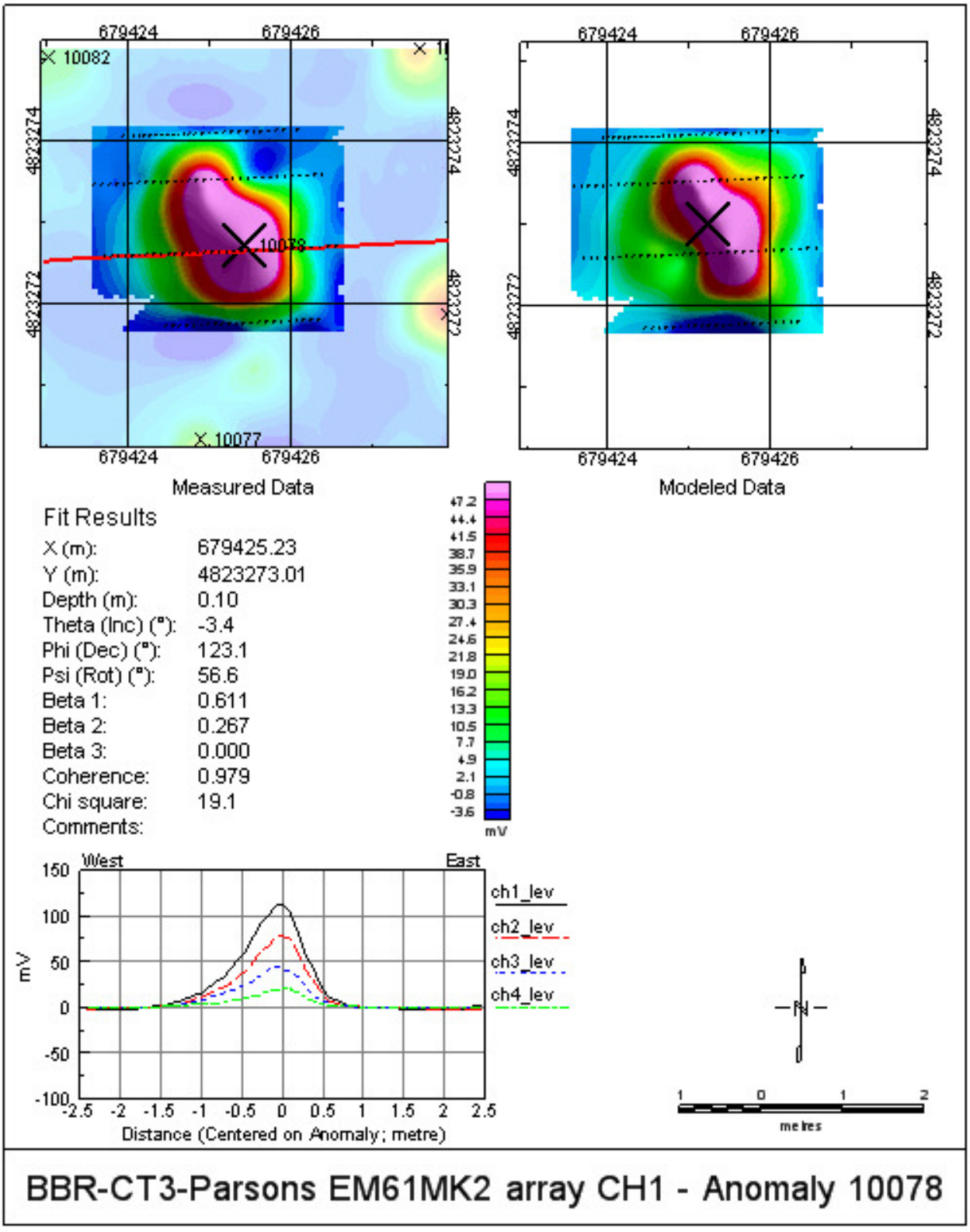

BBR-CT3-Parsons EM61MK2 array CH1 - Anomaly 10078

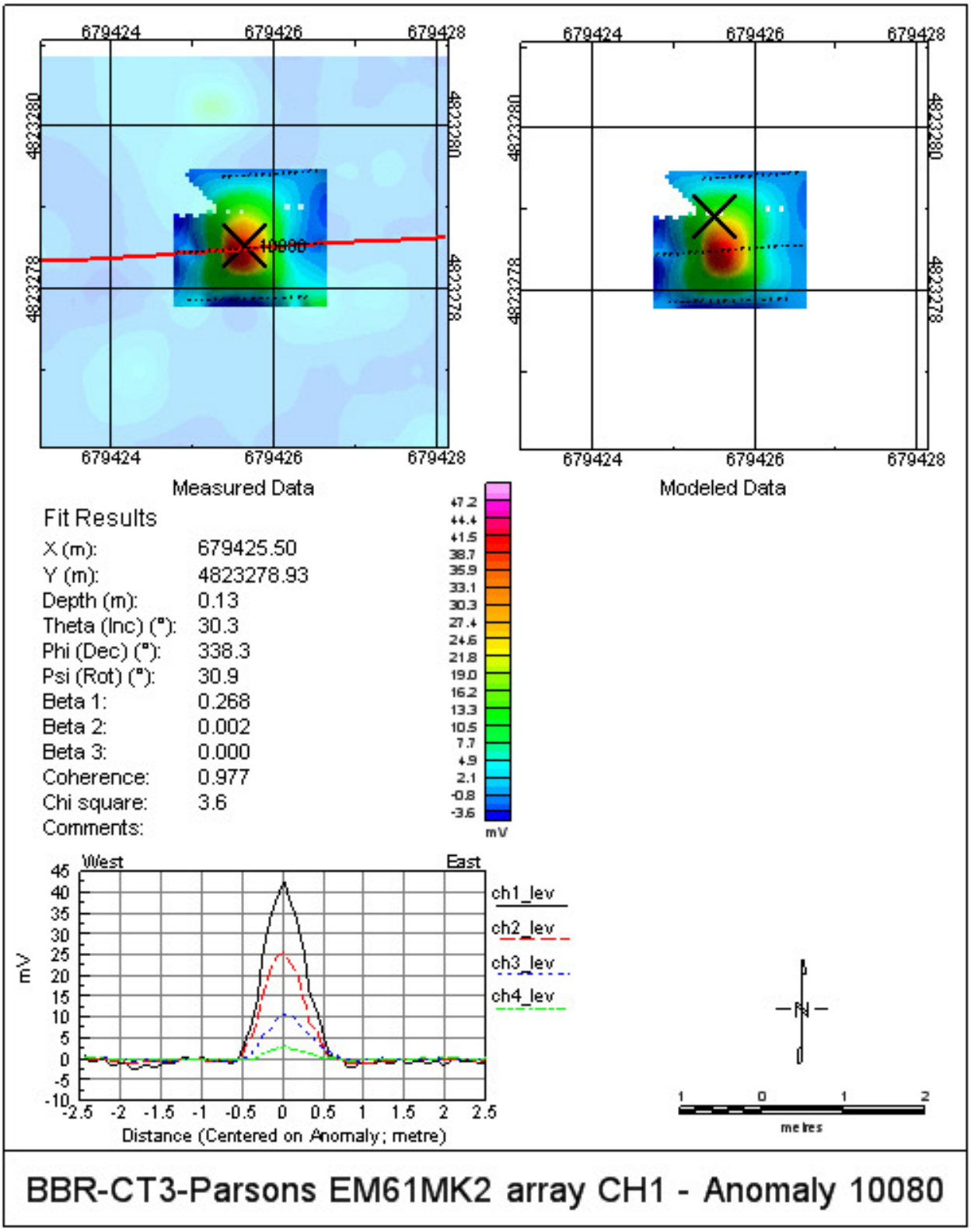
679424
679426
679428
4823280
4823278
10080
Measured Data
Modeled Data
Fit Results
X (m): 679425.50
Y (m): 4823278.93
Depth (m): 0.13
Theta (Inc) (°): 30.3
Phi (Dec) (°): 338.3
Psi (Rot) (°): 30.9
Beta 1: 0.268
Beta 2: 0.002
Beta 3: 0.000
Coherence: 0.977
Chi square: 3.6
Comments:
47.2
44.4
41.5
38.7
35.9
33.1
30.3
27.4
24.6
21.8
19.0
16.2
13.3
10.5
7.7
4.9
2.1
-0.8
-3.6
mV
West
East
ch1_lev
ch2_lev
ch3_lev
ch4_lev
mV
Distance (Centered on Anomaly; metre)
N
1 0 1 2
metres
BBR-CT3-Parsons EM61MK2 array CH1 - Anomaly 10080

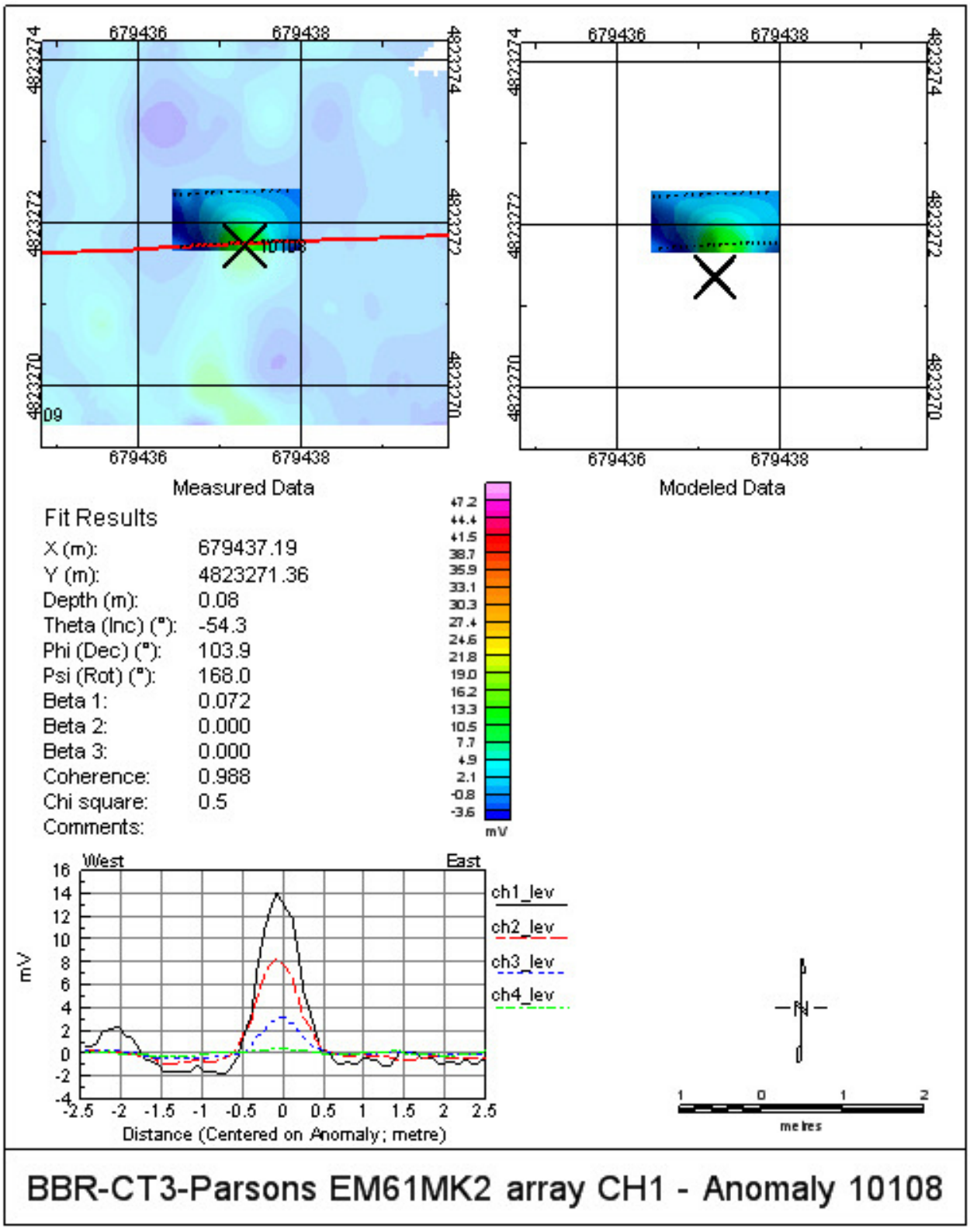

BBR-CT3-Parsons EM61MK2 array CH1 - Anomaly 10108

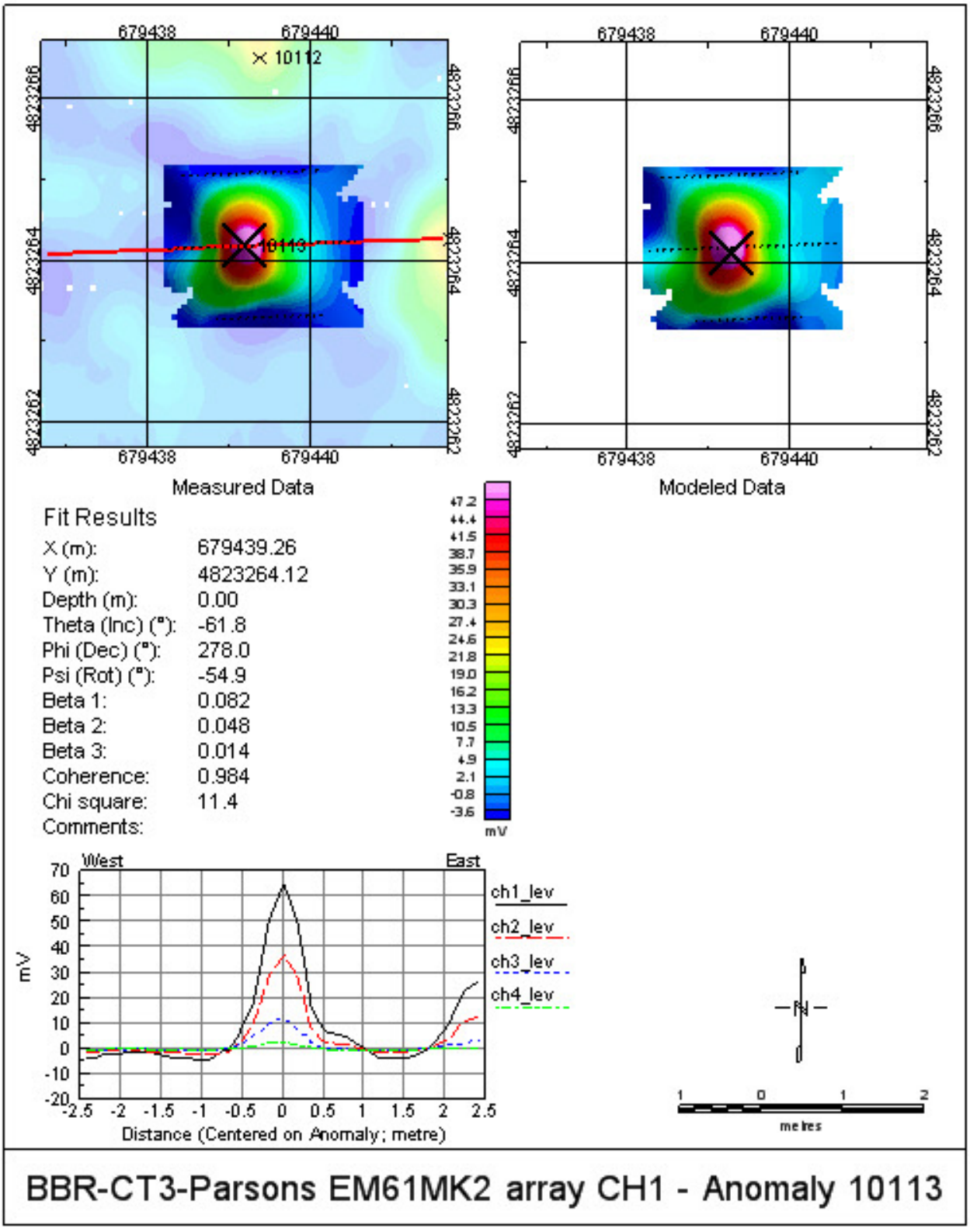

BBR-CT3-Parsons EM61MK2 array CH1 - Anomaly 10113

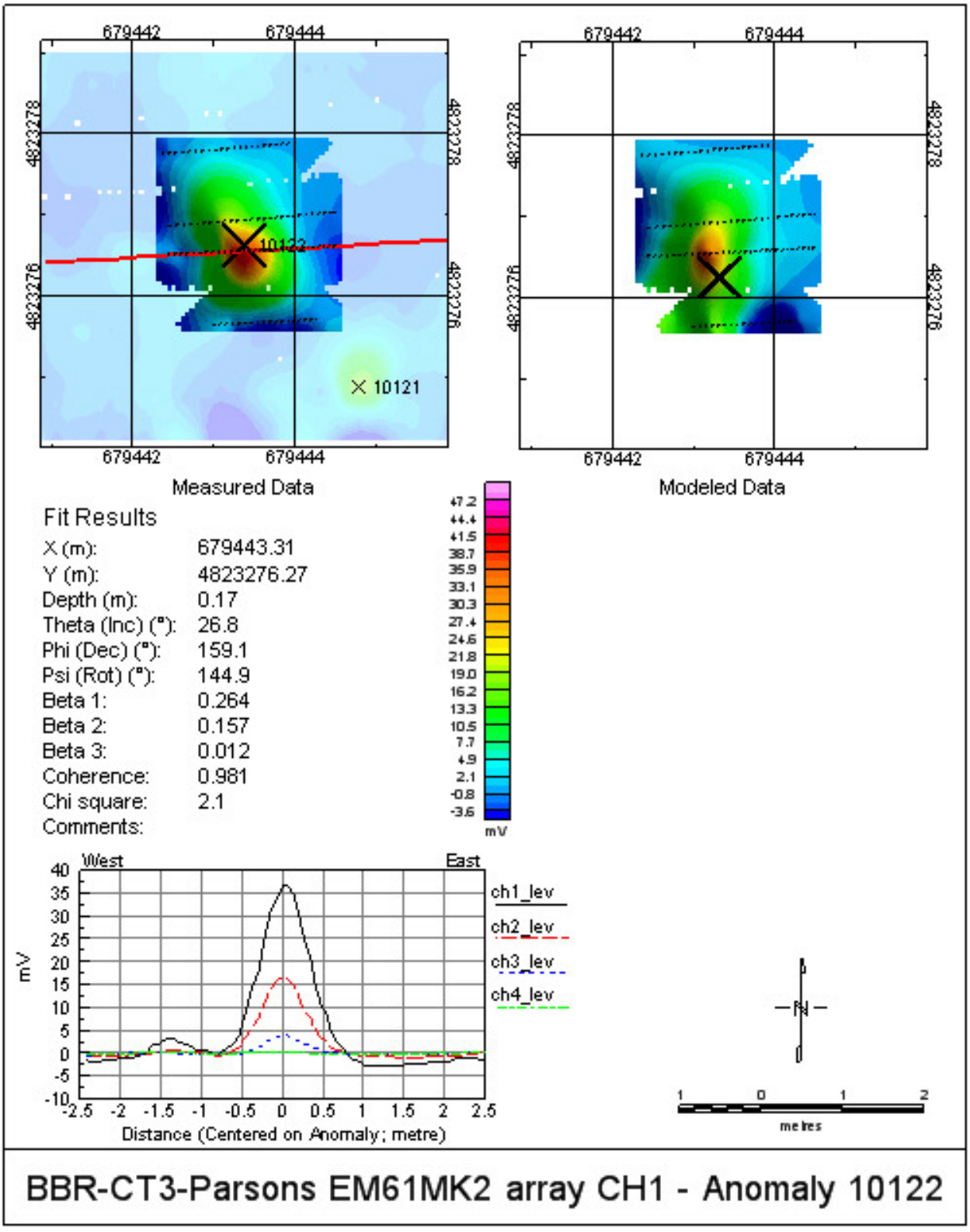

BBR-CT3-Parsons EM61MK2 array CH1 - Anomaly 10122

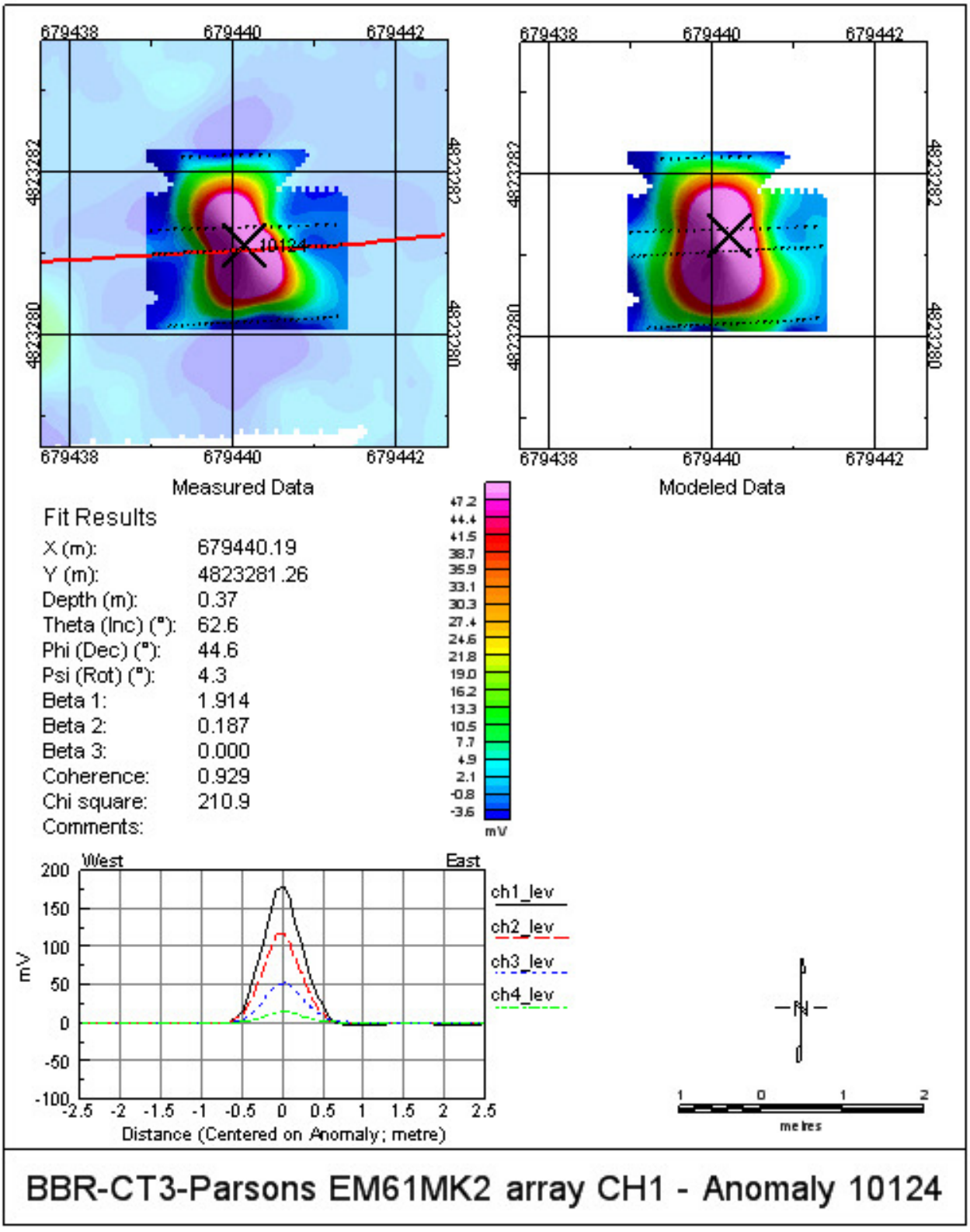

BBR-CT3-Parsons EM61MK2 array CH1 - Anomaly 10124

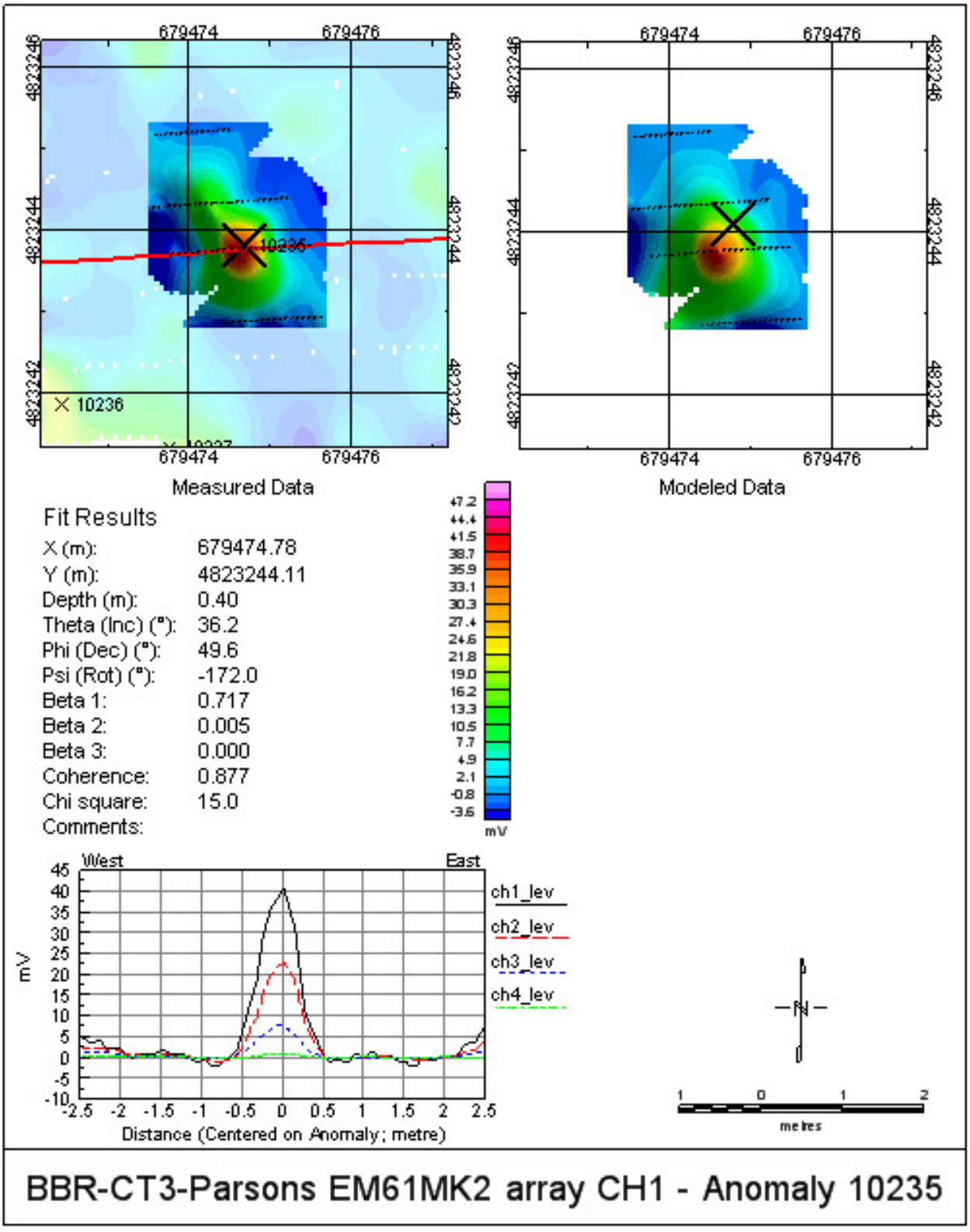

BBR-CT3-Parsons EM61MK2 array CH1 - Anomaly 10235